CANADIAN THESES

THÈSES CANADIENNES

NOTICE

The quality of this microfiche is heavily dependent upon the quality of the original thesis submitted for microfilming. Every effort has been made to ensure the highest quality of reproduction possible.

If pages are missing, contact the university which granted the degree.

Some pages may have indistinct print especially if the original pages were typed with a poor typewriter ribbon or if the university sent us an inferior photocopy.

Previously copyrighted materials (journal articles, published tests, etc.) are not filmed.

Reproduction in full or in part of this film is governed by the Canadian Copyright Act, R.S.C. 1970, c. C-30. Please read the authorization forms which accompany this thesis.

AVIS

La qualité de cette microfiche dépend grandement de la qualité de la thèse soumise au microfilmage. Nous avons tout fait pour assurer une qualité supérieure de reproduction.

S'il manque des pages, veuillez communiquer avec l'université qui a conféré le grade.

La qualité d'impression de certaines pages peut laisser à désirer, surtout si les pages originales ont été dactylographiées à l'aide d'un ruban usé ou si l'université nous a fait parvenir une photocopie de qualité inférieure.

Les documents qui font déjà l'objet d'un droit d'auteur (articles de revue, examens publiés, etc.) ne sont pas microfilmés.

La reproduction, même partielle, de ce microfilm est soumise à la Loi canadienne sur le droit d'auteur, SRC 1970, c. C-30. Veuillez prendre connaissance des formules d'autorisation qui accompagnent cette thèse.

THIS DISSERTATION
HAS BEEN MICROFILMED
EXACTLY AS RECEIVED

LA THÈSE A ÉTÉ
MICROFILMÉE TELLE QUE
NOUS L'AVONS REÇUE

Canadä

0-315-26848-4

PERMISSION TO MICROFILM — AUTORISATION DE MICROFILMER

• Please print or type — Ecrire en lettres moulées ou dactylographier

Full Name of Author — Nom complet de l'auteur

COSTAS   MACRIDES

Date of Birth — Date de naissance	Country of Birth — Lieu de naissance
December 15 1954	GREECE

Permanent Address — Résidence fixe

Department of Physics

Title of Thesis — Titre de la these

Interpretation of Seismic retraction profiles in
Saskatchewan

University — Université

of ALBERTA

Degree for which thesis was presented — Grade pour lequel cette thèse fut présentée

M.Sc.

Year this degree conferred — Année d'obtention de ce grade	Name of Supervisor — Nom du directeur de thèse
1983	Dr. E.R. Kanasewich

Permission is hereby granted to the NATIONAL LIBRARY OF CANADA to microfilm this thesis and to lend or sell copies of the film.

The author reserves other publication rights, and neither the thesis nor extensive extracts from it may be printed or otherwise reproduced without the author's written permission.

L'autorisation est, par la présente, accordée à la BIBLIOTHÈQUE NATIONALE DU CANADA de microfilmer cette thèse et de prêter ou de vendre des exemplaires du film

L'auteur se réserve les autres droits de publication; ni la thèse ni de longs extraits de celle-ci ne doivent être imprimés ou autrement reproduits sans l'autorisation écrite de l'auteur.

September 15 / 83	Macrides
Date	Signature

THE UNIVERSITY OF ALBERTA

INTERPRETATION OF SEISMIC REFRACTION PROFILES IN SOUTHERN

SASKATCHEWAN

by

COSTAS MACRIDES

A THESIS

SUBMITTED TO THE FACULTY OF GRADUATE STUDIES AND RESEARCH

IN PARTIAL FULFILMENT OF THE REQUIREMENTS FOR THE DEGREE

OF MASTER OF SCIENCE

IN

GEOPHYSICS

DEPARTMENT OF PHYSICS

EDMONTON, ALBERTA

FALL 1983

THE UNIVERSITY OF ALBERTA

RELEASE FORM

NAME OF AUTHOR   COSTAS MACRIDES

TITLE OF THESIS   INTERPRETATION OF SEISMIC REFRACTION

PROFILES IN SOUTHERN SASKATCHEWAN

DEGREE FOR WHICH THESIS WAS PRESENTED   MASTER OF SCIENCE

YEAR THIS DEGREE GRANTED   FALL 1983

Permission is hereby granted to THE UNIVERSITY OF

ALBERTA LIBRARY to reproduce single copies of this

thesis and to lend or sell such copies for private,

scholarly or scientific research purposes only.

The author reserves other publication rights, and

neither the thesis nor extensive extracts from it may

be printed or otherwise reproduced without the author's

written permission.

(SIGNED) ...*Macrides*.....

PERMANENT ADDRESS:

...*Department of Physic*...

...*University of Alberta*...

....

DATED *September 15*....19 *83*

THE UNIVERSITY OF ALBERTA

FACULTY OF GRADUATE STUDIES AND RESEARCH

The undersigned certify that they have read, and

recommend to the Faculty of Graduate Studies and Research,

for acceptance, a thesis entitled INTERPRETATION OF SEISMIC

REFRACTION PROFILES IN SOUTHERN SASKATCHEWAN submitted by

COSTAS MACRIDES in partial fulfilment of the requirements

for the degree of MASTER OF SCIENCE in GEOPHYSICS.

.....E..R...Karacuri.

Supervisor

..J.J..Krystaffe......

..J.J..Nernaka..

.......Eb..Chyly..

Date..August..22./83

ABSTRACT

Seismic refraction techniques were employed in crustal studies of South-Central Saskatchewan. A unique arrangement of the sources and receivers was set up to obtain three dimensional structure over a 300 km equilateral triangle. The interpretation of the data presented here is based on the three shot-reversed sides of the triangle.

The evaluation of the collected data was undertaken by use of several techniques including ray tracing, inversion of head waves and synthetic seismogram simulation. The derived models reveal a particularly complex many-layered structure of the crust below the study area. Layers are gently dipping the dip angle never being greater than 2.5°. Low velocity zones-probably associated with high conductivity material-have been detected below all three profiles. P-wave velocity in these layers is close to 6 km/s. Significant lateral heterogeneity is found below the southeasterly and northeasterly profiles (B and C). There is good evidence for a fault just west of line A. The fault strike is S.E. passing through the earthquake prone area of Bengough. Upper mantle velocity is practically invariable under the study area and close to an average value of 8.13 km/s. Depth of the Mohorovicic discontinuity varies from 36 to 45 km. The crust thins eastward and thickens southward.

ACKNOWLEDGEMENTS

LIST OF TABLES

LIST OF FIGURES

1. INTRODUCTION.

In August 1981 the CO-CRUST group conducted its third cooperative seismic survey in south-central Saskatchewan. The 1981 program consisted of four survey lines A,B,C and D .The location of the profiles is shown in figure 1. Refraction and wide-angle reflection techniques were employed. There were two main objectives for the experiment. The first aim was to obtain information about the structure of the earth's crust underlying the northcentral segment of the intracratonic Williston basin. In particular line A was placed close to the NACP conductivity zone in hope of obtaining some seismic expression of this anomalous area. Secondly the experiment tested a novel type of crustal refraction data gathering method. In this system, following a suggestion of E.R.Kanasewich, three profiles(lines A,B and C)were arranged in an equilateral triangular form so that three dimensional information was obtained by the combination of inline reversed shots and also by the broadside recordings from opposite corners of the triangle. This thesis deals with the interpretation of the three in-line recordings of the triangle. The analysis of the collected seismic data was undertaken by the use of three different methods: 1)Inversion of first arriving head wave information,2)Ray tracing of wide angle reflected energy, and 3) The interpretation of amplitude information using synthetic seismograms. Future analysis of the overlapping broadside data in the central portion of the triangle will

1
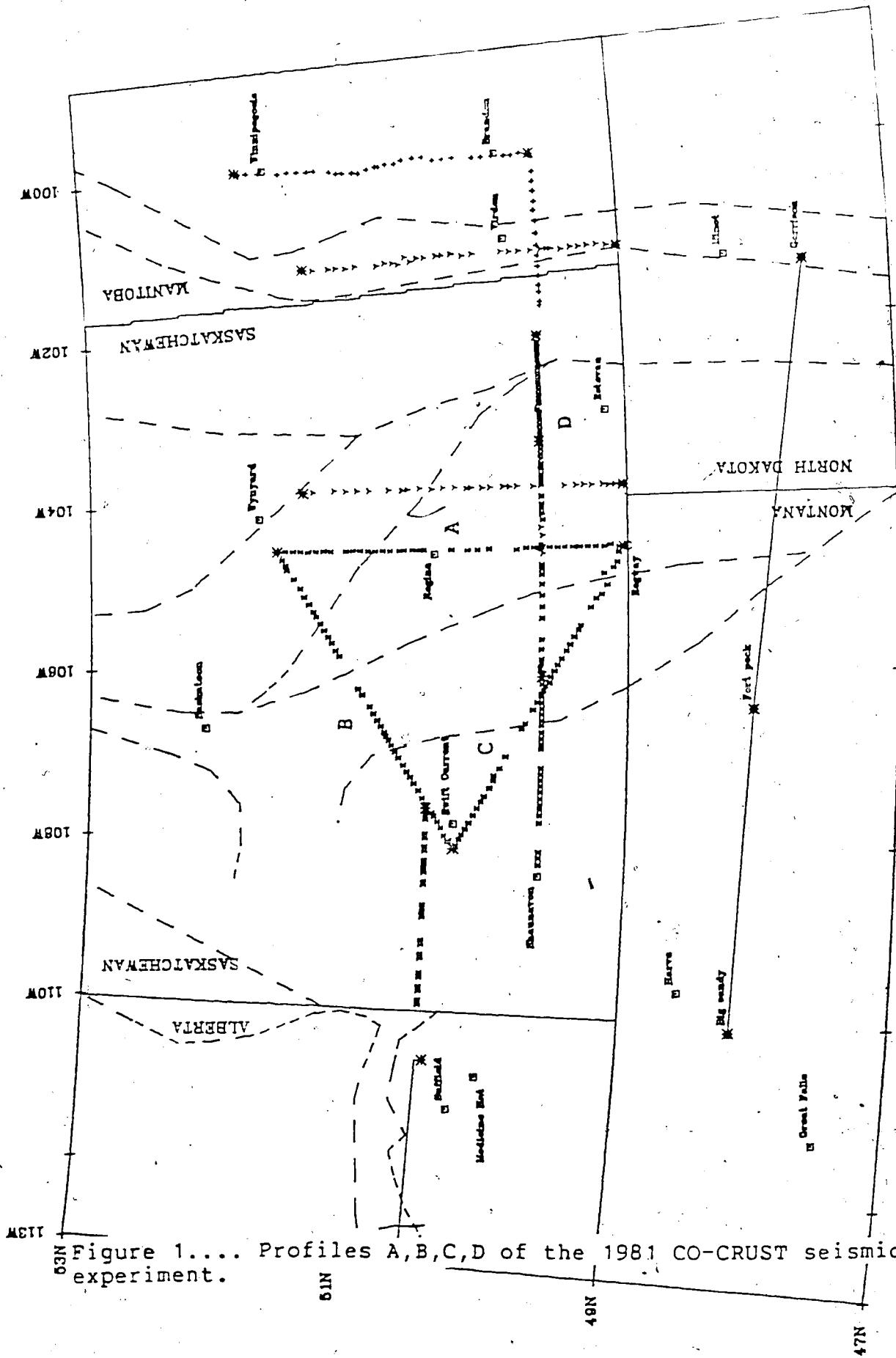
Figure 1.... Profiles A,B,C,D of the 1981 CO-CRUST seismic experiment.

be based on the models presented here.

The inferred crustal models are compared with previous seismic studies in eastern and western Saskatchewan . The operational and theoretical aspects of the work are discussed.

2. GEOLOGY AND GEOPHYSICS OF THE STUDY AREA

2.1 Geology of the study area

Geologically Canada is divided into a number of regions, (figure 2). The area of the 1981 experiment is the central-south Saskatchewan. It is placed entirely within the Interior Platform which is the part of the North American craton that subsided slightly in the past and now is covered with Phanerozoic sedimentary rocks. To the north and east the craton crops out forming the Precambrian Canadian shield which is the largest continuously exposed area of Precambrian rocks in the world. To the west of the Interior Platform the craton is bordered by the Cordilleran orogen. The southern boundary of the western Canada sedimentary basin can be defined only in an arbitrary manner. If all of the Williston basin is included, the boundary is probably best drawn by the Sioux uplift in southwestern Minnesota to the Black Hills and thence to the Little Rocky mountains and westward to the Lewis thrust.

By far the greater part of the basin is floored by rocks which were intruded or metamorphosed 1800 million years ago. The span of 1200 m.y. prior to Cambrian time permitted deep erosion and the development of a marked degree of tectonic stability within the interior plains area.

Contours drawn on the surface of the Precambrian indicate the existence of three basins and two arches in the
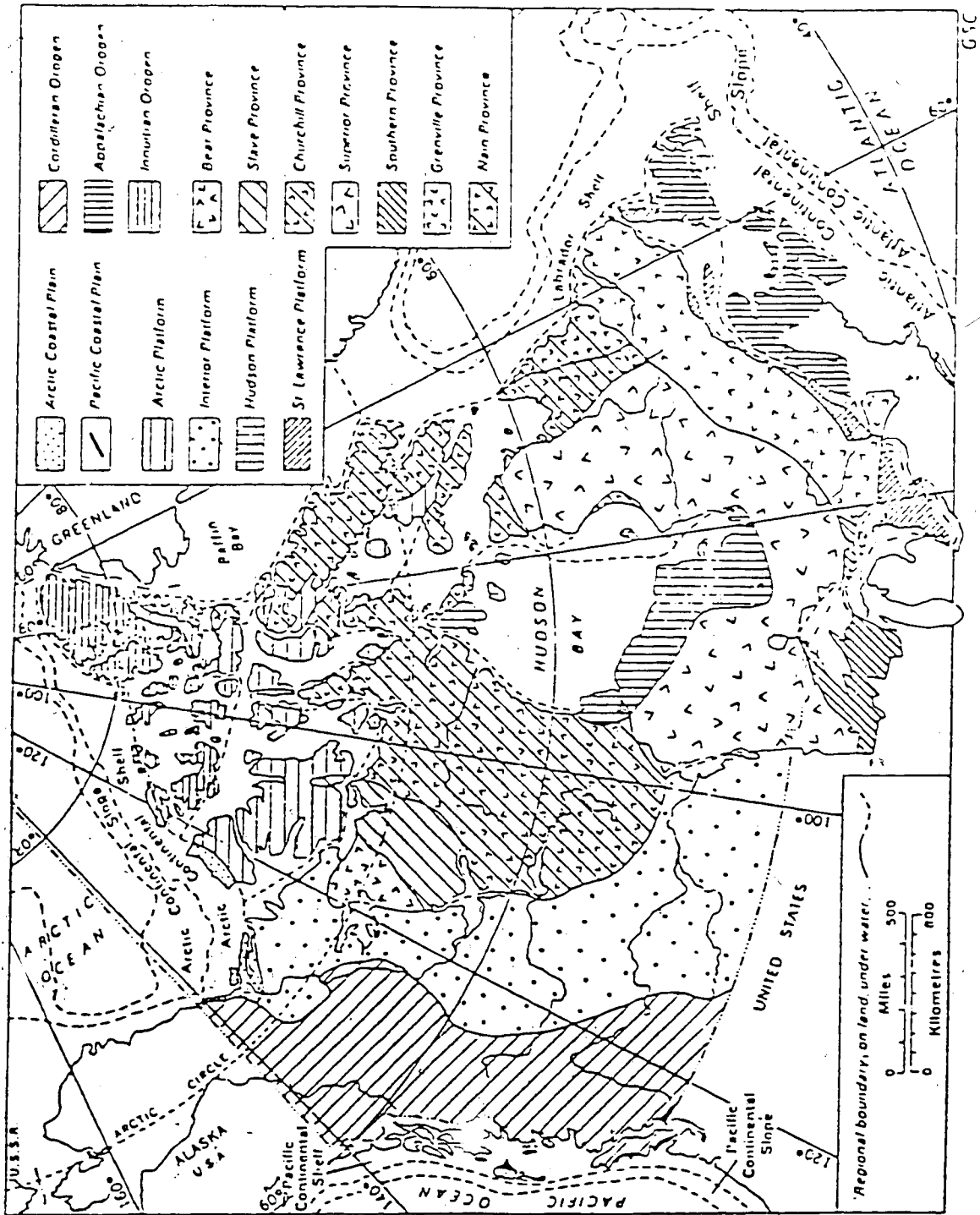
Figure 2.... Structural provinces in Canada (from Geology
and Economic minerals of Canada, 1970).

Interior Plains area, between latitudes 49 and 60°. From northwest to southeast the basement features have been named: 1)Northern Alberta basin, 2)Peace River arch, 3)central Alberta basin,4)Sweetgrass arch and 5)Williston basin. It is in this latter area that the 1981 experiment was entirely placed. The landscape of the Williston basin is simple. Near, surface sediments of Cretaceous age are essentially flat lying and have an average elevation of a few hundred meters above sea level.The older and gently rolling landscape has been buried by deposits of glacial till, sand and gravel. The Phanerozoic sedimentary section is up to 3.0 km thick near Southern Saskatchwean. The sediments thin northward to the exposed craton of northern Saskatchewan, (figure·3).

This difference is due to varied basin subsidence and sedimentation in different regions.Subsidence was accentuated at various times throughout the Phanerozoic.Basin sedimentation was locally affected by movements of structural regions or blocks of the Precambrian basement delimited by lineaments as well as by solution of massive halite beds which also resulted in the collapse of overlying strata. The base of the stratigraphic column is a succesion of early Paleozoic clastics followed by Ordovician to Mississipian carbonates and evaporites and Jurassic to Pleistocene clastics.The clastic rocks of the Cambrian lie unconformably on the basement, figure 4.
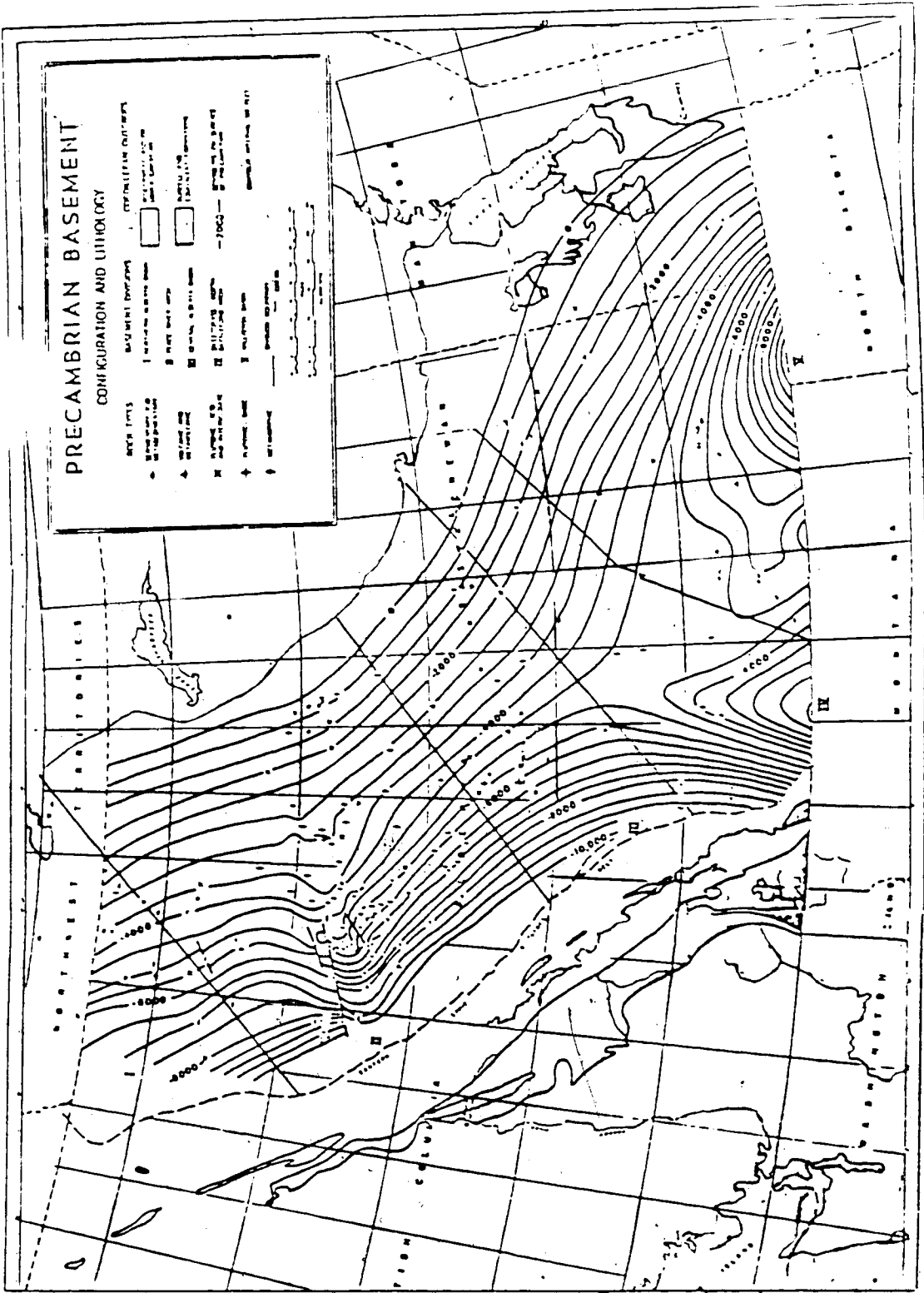
Figure 3.... Basement configuration in western Canada (from Geologic history of Canada, 1965).
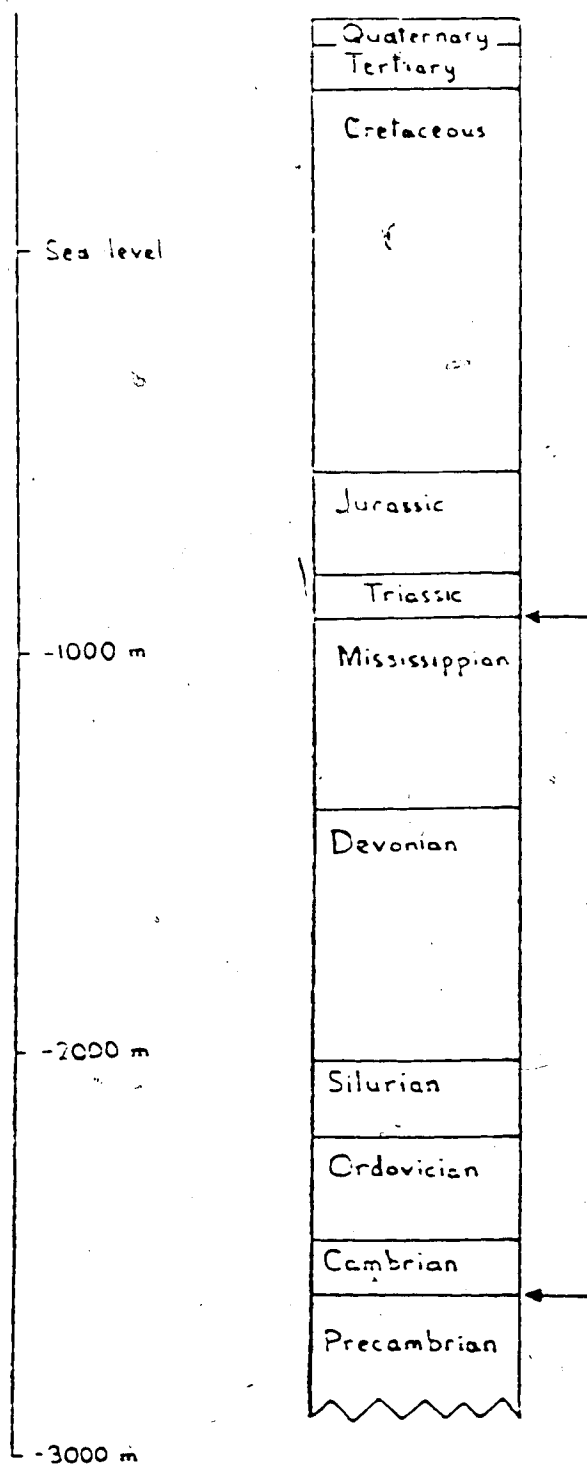
Figure 4.... Reference geological column for southern Saskatchewan indicating order of geological systems. Arrows indicate major unconformities.

Geologic information on the Precambrian comes from studies of the exposed shield (Bell,1971) and studies from core samples(Burwash and Culbert,1976). The basement under the Interior Plains appears to be a south-western continuation of the exposed Precambrian shield. In particular, the composition of the basement under the Williston basin shows a high concentration of metamorphosed and volcanic and metavolcanic rocks.Percentage of sedimentary rocks is about 35%.

2.2 Previous seismic studies

Previous crustal seismic studies in Saskatchewan include the works of Chandra and Cumming(1972) and Green and co-workers (1980). Their interpretation deals with the Suffield-Swift Current profile and the Weyburn-Brandon profile respectively. Their results are illustrated in figure 5. Both works indicate a relatively thick multilayered crust at the margin of the Williston Basin. The Riel discontinuity (Clowes,Kanasewich and Cumming,1968B) of tesent in both models. The Weyb   andon profile has been reinterpreted by Moon and L La   (1981),figure 6. Their model does not show evidence f   Riel discontinuity. Instead they introduced a positiv   ity gradient in the lower crust. There is also the Lc   rofile (B) of the CO-CRUST 1979 experiment which   s been interpreted by Kazmierczak, (1980), figure 7.Finally the   reversed line C of the 1979 survey was interpreted by Shahriar
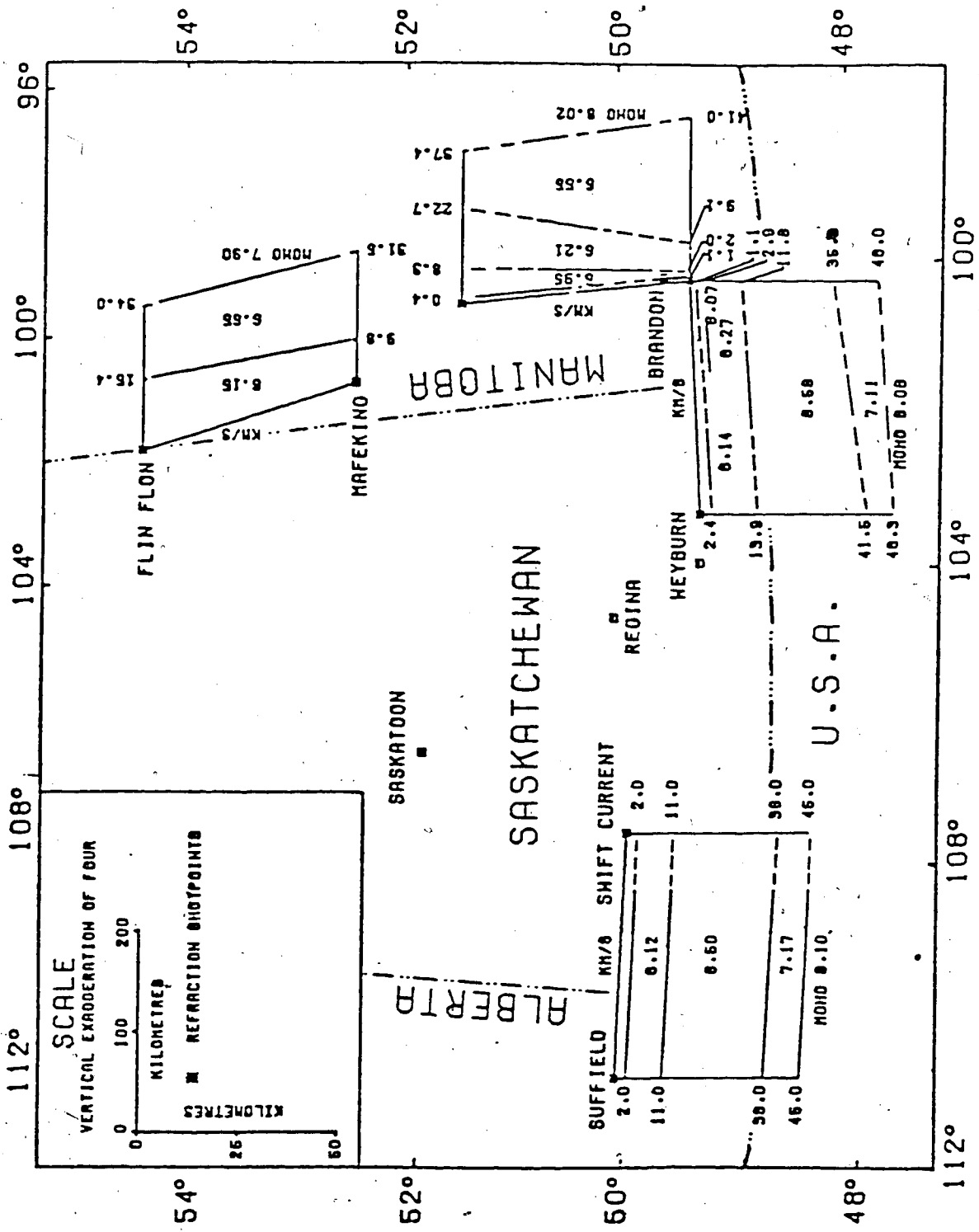
Figure 5.... Crustal models from refraction experiments in Manitoba, Southern Saskatchewan and Southern Alberta
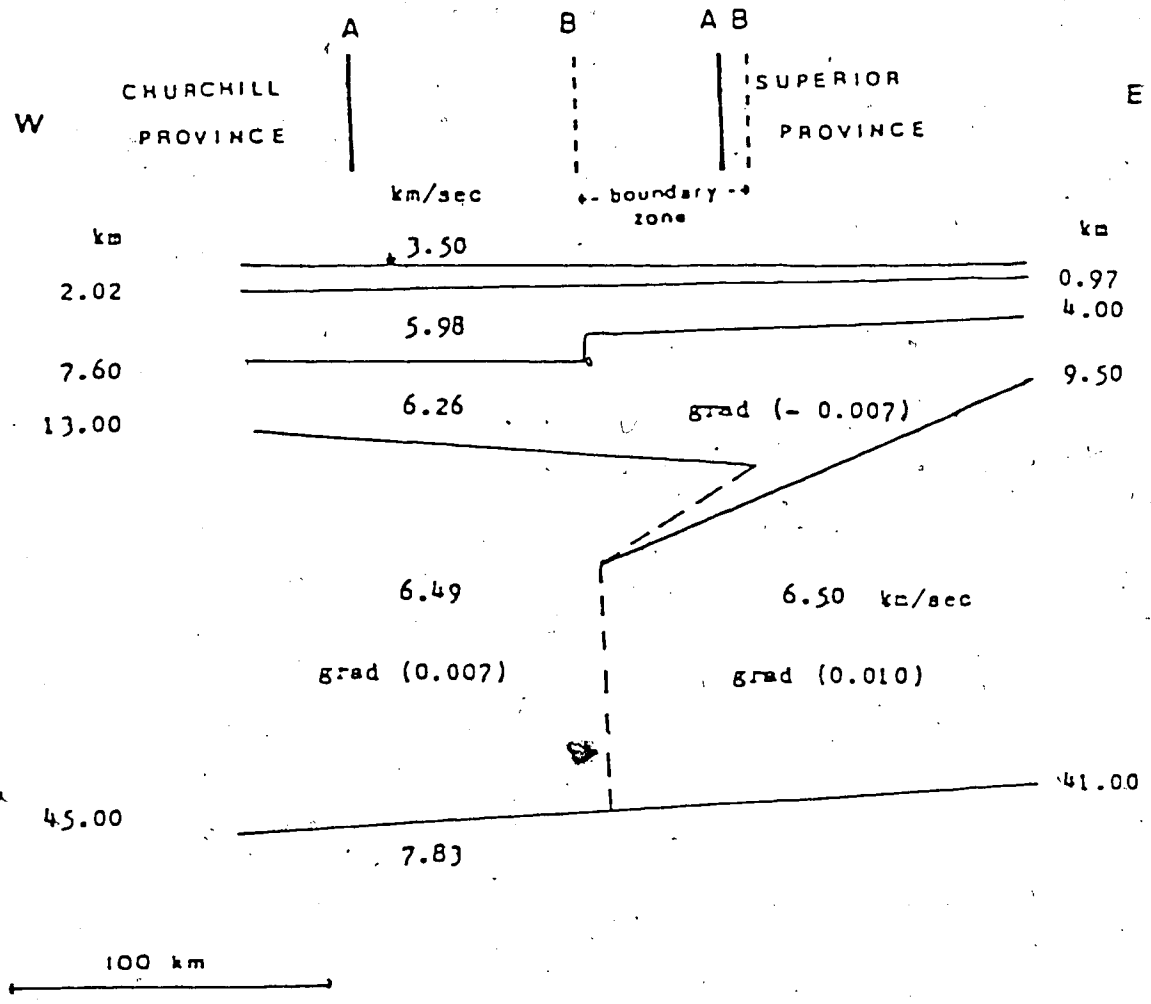
Figure 6.... Crustal model from CO-CRUST 1977 east-west refraction profile

Figure 7.... Crustal models from CO-CRUST 1979 refraction experiment

(1982).The derived horizontal model is illustrated in table 1.The profile runs east-west at a latitude of 49 ° ,38', from Limerick (longitude 106°, 44') to Carlyle (longitude 102°, 5.8'). Hence it crosses our line A and therefore it will be a useful reference for comparison. The shot point was at the west end of the profile which was shot reversed (as line D) during the 1981 survey.

Furthermore,combined refraction and reflection interpretations revealed the existence of a major crustal fault within the Churchill province (Green et al. 1976,b,Kazmierczac,1980), at a longitude of 103 °. There is a variation in crustal thickness across the fault of at least 5 km,the upthrown block being at its west side.

Layer	Velocity km/sec	Thickness km	Depth km
1	3.2	2.8	0.0
2	6.0	2.3	2.8
3	6.2	6.0	5.0
4	6.1	3.0	11.0
5	6.5	5.0	14.0
6	6.7	6.0	19.0
7	6.1	4.0	25.0
8	6.7	15.5	29.0
9	8.1	—	44.5

Table 1.

Horizontal model for the CO-CRUST C-1979 profile

(after M.Shahriar,1982)

3. DATA ACQUISITION AND PROCESSING

3.1 Data acquisition and description of profiles .

The north -south line,line A,was located in the central region of the crustal midcontinental conductivity zone. This anomalous area was first described by Camfield and Gough(1977).The northeasterly line,line B,was placed between Wynyard and Swift Current.The south-easterly line,line C, extends from Swift Current to Regway at the Canadian-U.S. border.The total lengths of the lines were 287.9 km, 288.6 km and 288.4 km respectively. Ideally,the experiment would cover the triangle ABC by only three shots. However one immediately realizes the difficulty concerning the availability of 180 individual stations' which would be required for such an experiment, let alone the huge cost of the operation. Only 45 stations were available,adequate to cover only one profile at a time.Hence three shots were required for each line(two inline shots plus the broadside shot),i.e. a total of 9 shots were detonated for the triangle. All recording sites were selected along roads such that no location deviates from the staight line more than ± 1km.The average separation between recording sites was 6.5 km.Ideally the spacing would be around 1 Km (close to the wavelength of the seismic energy). Elevations,latitudes and longitudes of all recording sites and shot locations were taken from 1:50,000 topographic maps.The accuracy of the

----

'for an average separation of 5 km.

coordinates is in the range of ± 0.0005° i.e. ± 35 m. Shot point to receiver distances were calculated using a geodetic computer program by supplying the geographical coordinates as input data.Time of shots,receiver coordinates and elevations as well as instrumentation and shot point information were compiled by Dr.Hajnal of the Department of Geological Sciences of the University of Saskatchewan. All recording systems were pre-programmed to a set of specific time windows. The digital interval of the data was 0.01667s (60 Hz).Consequently the Nyqyist frequency was 30 Hz.The University of Alberta recorded with the "University of Toronto digital event recording system".Vertical as well as N-S and E-W horizontal component of motion were recorded.In addition,the absolute time signal(WWVB) was incorporated as a fourth channel in our magnetic tape data (see figure 8).This was of particular importance in order to check the accuracy of the times of the first data samples for each station.In addition to the above set of equipment we also recorded into a linear array, consisting of 12 TI-36,2 Hz vertical component geophones with spacing of 268 m.Two traces of the array were included in the major line information.

All 1981 refraction data were compiled in digital form on a 9-track, 1600 B.P.I.(bytes per inch) magnetic tape. Each block of data,-a total of 24 blocks per channel-in the original master tape contained 5 seconds of data and occupied 4800 bytes of memory.The logical record length was
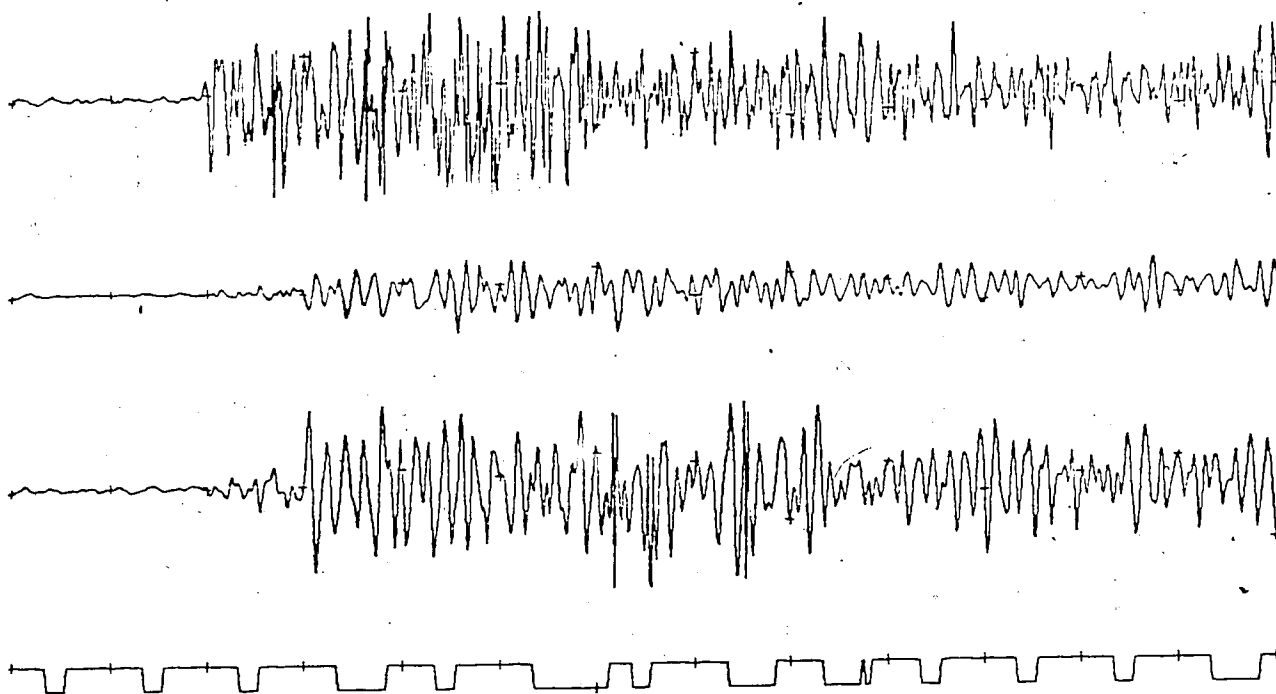
Figure 8.... An example of the U. of A. original
four-channel records.

80 bytes, hence the format by which each block was written was 60*(5E16.6).The total set of the recorded data occupied 436 files on the magnetic tape.Each file was preceded by its header information which consisted of ten card images,containing detailed information about the recording station.We decided,for our data processing purposes,to reformat the data and we copied them into a new tape in which they were written in integer *2 form, each block consisting of 1200 data samples(hence a total of 6 blocks/channel). The logical record length was 20 bytes,hence the format of the new tape was 120*(10F8.0).

3.2 Presentation of the data

The first step towards the evalution of seismic refraction data is the display of the records.For this purpose form of record sections is generally chosen.A rec section consists of seismic traces on a time-distance graph.The simplest way is to plot travel time versus distance using shot instant and location as the zero reference. Such a presentation requires a large page size or an inconveniently small time scale. The other form of display uses a reduced travel time instead of time. The reduced travel time t' is defined as $t'=t-x/V$ where t is the time from shot detonation,x is the offset distance and V is the reduction velocity. Such a presentation has the effect of rotating all the travel time branches clockwise around their point of intersection with the t axis,the amount of

rotation being inversely proportional to the reduction
velocity V.The result is better time resolution over smaller
space.V was chosen to be equal to 6.5 km/sec for the data in
this work. The significance of V is that if this velocity is
close to the apparent velocity of the waves of interest it
will produce a display showing the head wave phases all
arriving at the same reduced time.Hence this kind of display
facilitates the correlation process.

Since we planned to process only the P-wave phases, all
our record sections show only the traces for vertical
component seismometers. It must be mentioned that no
elevation corrections were applied to the data for two
reasons. 1)Such corrections would require the knowledge of
near surface velocities in detail.2)The amount of correction
would be insignificant (.03 sec maximum) since the
differences between station elevations was small (less than
60 meters).

3.3 Power spectral analysis

A seismic trace is a function of time,$f(t)$,representing
the velocity of the ground at the site of the sensor.Its
Fourier transform $f(w)$,yields the phase and amplitude
spectrum of the ground velocity.In many cases however it is
more appropriate to consider the power spectrum of the
signal.The power spectral estimate is equal to the smoothed
square of the amplitude spectrum.

The technique we applied for our power spectral
estimates was as follows.The periodogram was computed by use

of a discrete fast Fourier transform.An example is shown in figure 9.Clearly the periodogram needs to be smoothed and for this purpose we applied the Daniell (or box-car) window in the frequency domain according to the equation:

$$P(W) = \frac{N'}{N} \frac{1}{2m+1} \sum_{j=-m}^{m} F(W-J)F^*(W-J)$$

W=0,1,2,...N'/2.

The Daniell window was chosen because 1)It gives non negative estimates and 2)It gives equal weight over the entire range of its frequency bandwidth. N'(the full length of the time series) was equal to 512,while N was 360 (=6s).The time series was padded with zeros for $361 \le j \le 512$.The parameter m which determines the resolution was taken equal to 3.The effect of the application of the Daniell window on the periodogram of figure 5 can be seen in figure 10, which shows our spectral estimate for trace (24,1,1).The station was at a distance of 145.5 km from the shot.In figure 11 and figure 12 one can see the power spectral estimates for the traces(10,1,1) and (36,1,1) at offsets of 70.7km and 265.9 km respectively. By comparing the three spectra, one can see clearly the displacement of the seismic energy towards lower frequencies as we move further away from the shot.This is expected of course if we recall that the amplitude A(x,t) of a one dimensional plane wave is given,apart from a geometrical spreading term,by the formula A(x,t)= $A_o$exp[i(k(w) + ia(w))x-wt] where x is the distance the seismic wave has travelled and a,the
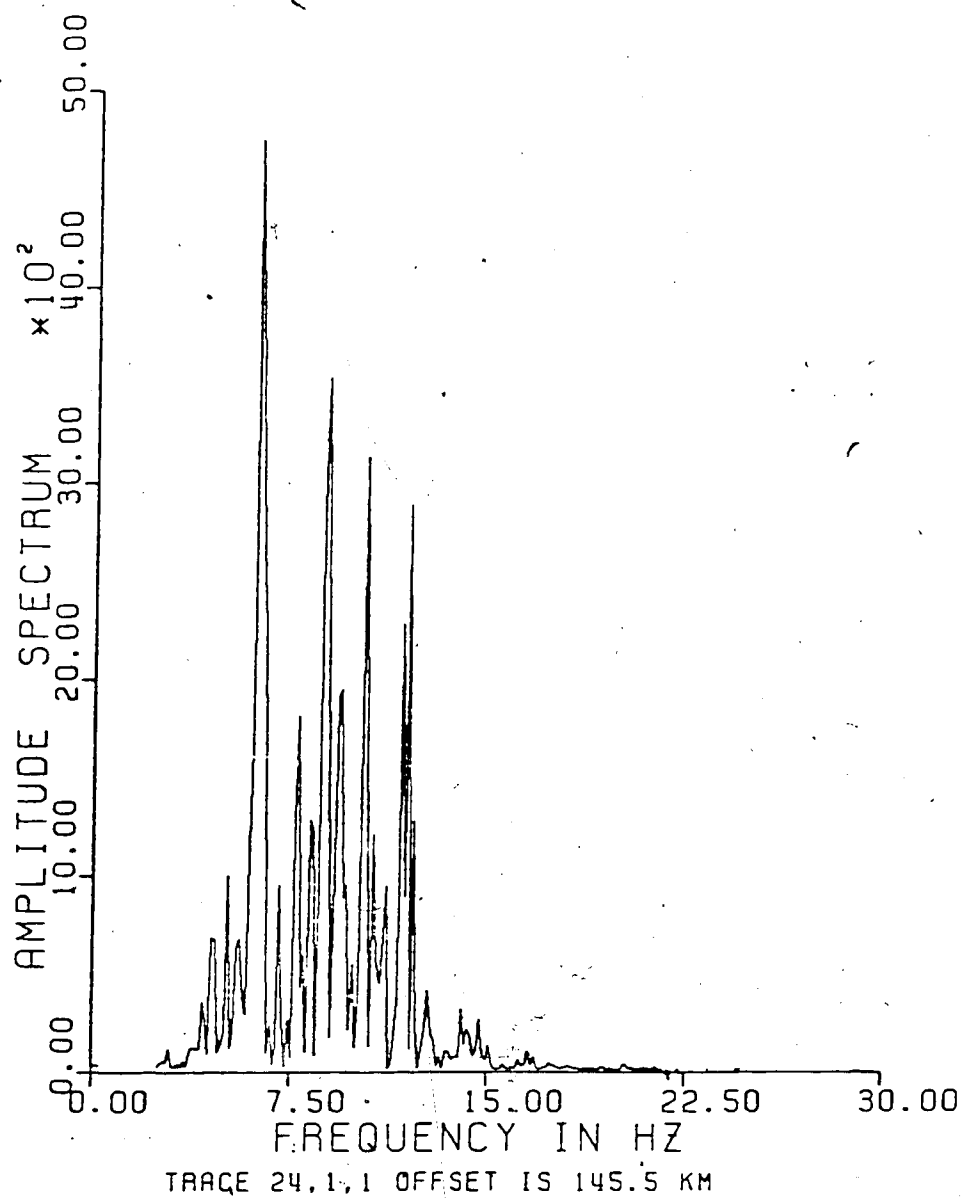
Figure 9.... Periodogram of the seismic energy for record
(24,1,1).
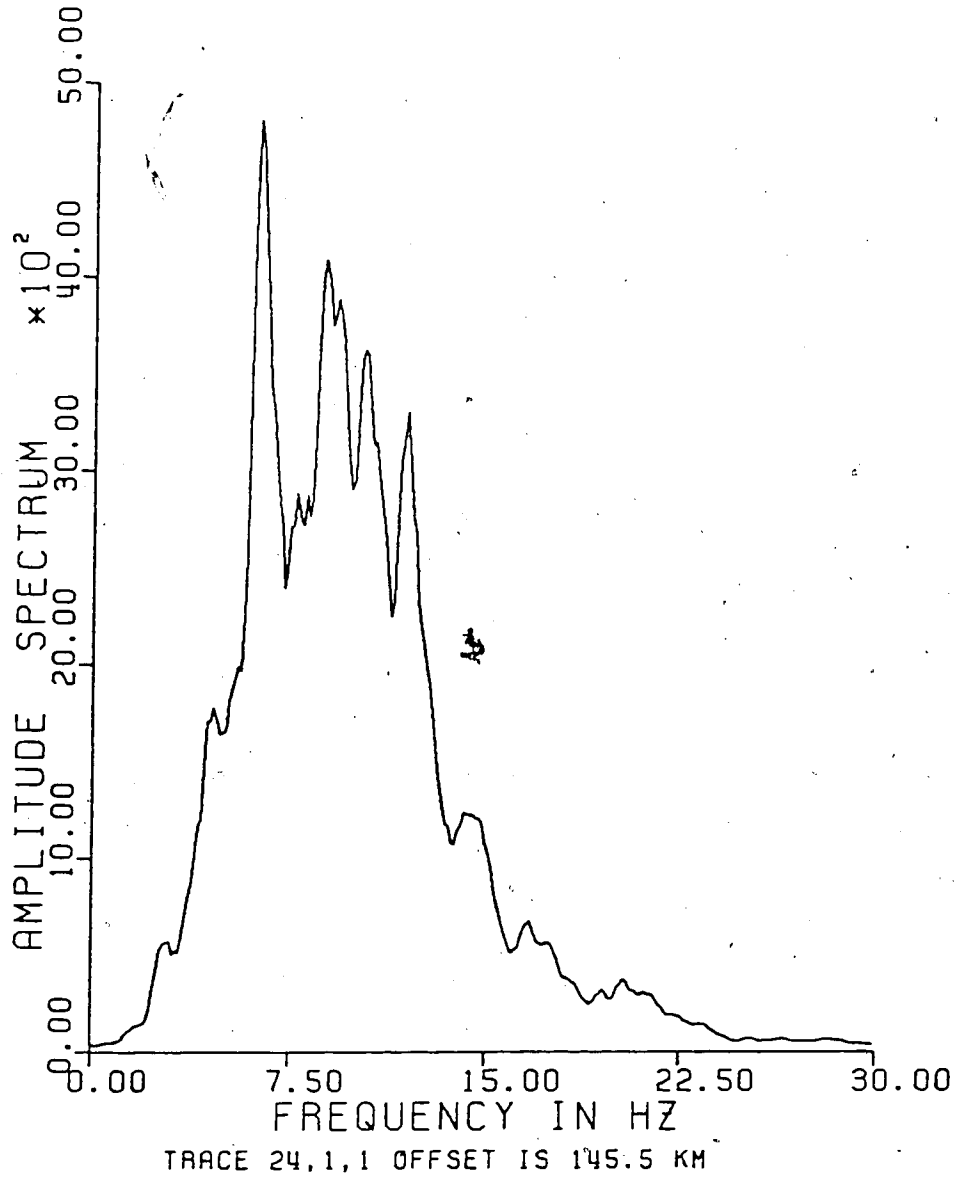
Figure 10.... Power spectral estimate for record 24,1,1
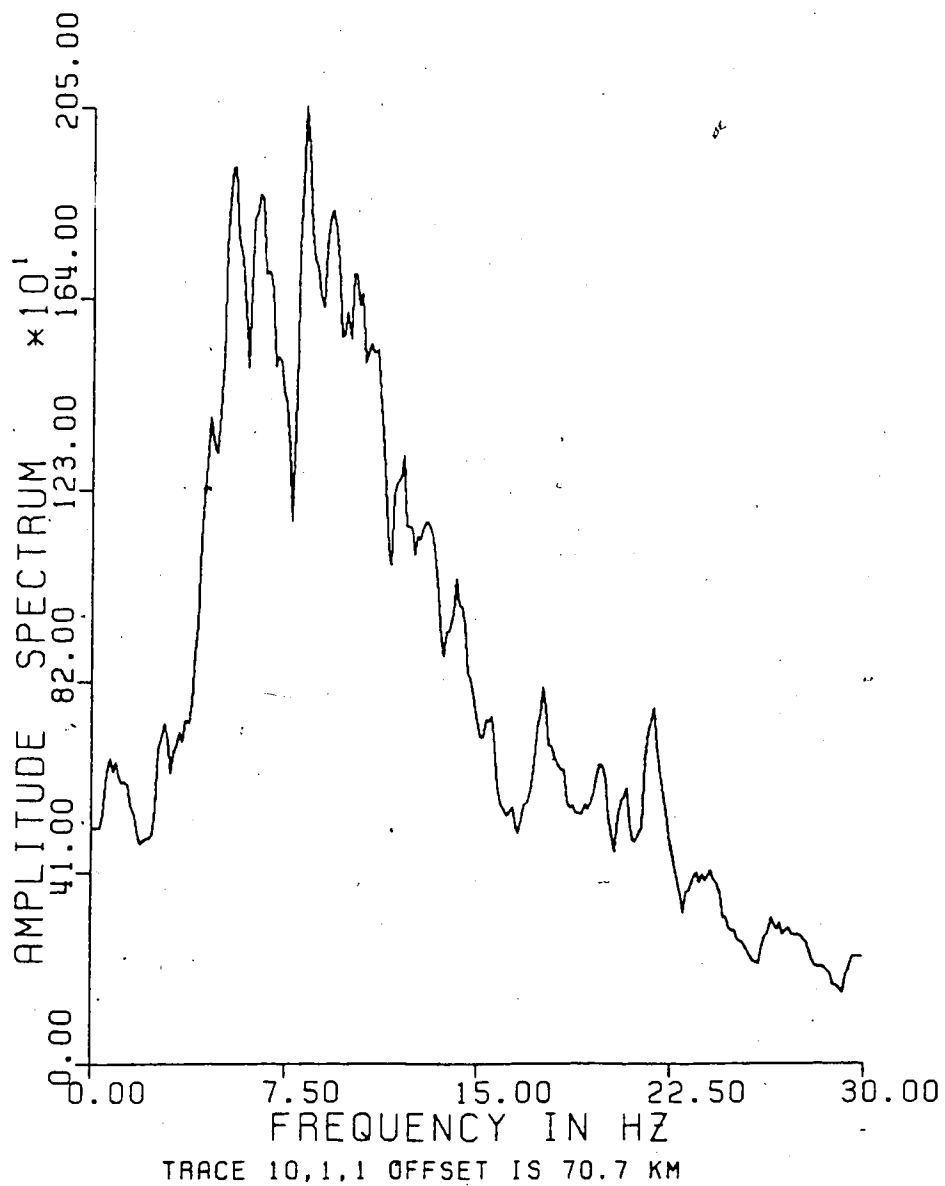
Figure 11.... Spectral estimate for record 10,1,1
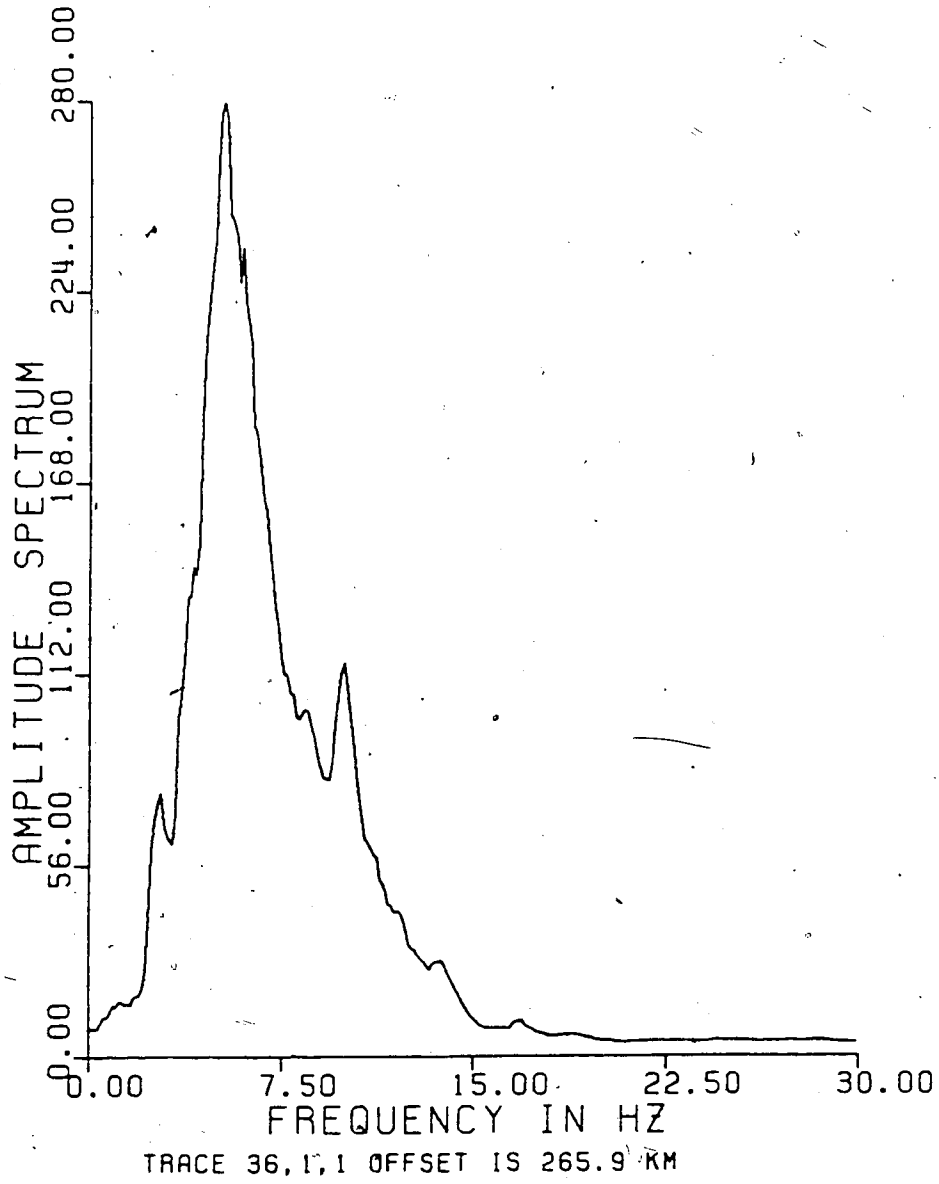
Figure 12.... Spectral estimate for record 36,1;1

attenuation coefficient, is proportional to the frequency of the wave.Thus, at large distances from the shot,high frequencies will be greatly attenuated.

It is of interest at this point to see the power spectrum characteristics of the background noise of the records.This will be useful later when bandpass filtering will be applied on the records.Thus, power spectra of the noise for several traces were computed;figure 13 and figure 14 show two typical examples of such spectral estimates.Careful comparison of the computed power spectra leads to the following conclusions:

1. Tests on noise show that the energy of the background noise of the records is concentrated between 1.5 and 6 Hz.

2. In nearly all cases the energy of the noise is decreasing beyond 15 Hz.

3. Spectral estimates of the signals themselves (after the onset of the seismic energy)- figures 10,11,12 show that the significant energy is always between 1 and 17 Hz.

The above conclusions suggest that a band of 5-17 Hz is the appropriate one when bandpass filtering is to be applied on the records.

3.4 Filtering

Broadly speaking, a filter is a device or a physical process that operates on a time history and changes the time history in some manner.The principal use of filtering in seismic data reduction is frequency smoothing of the data
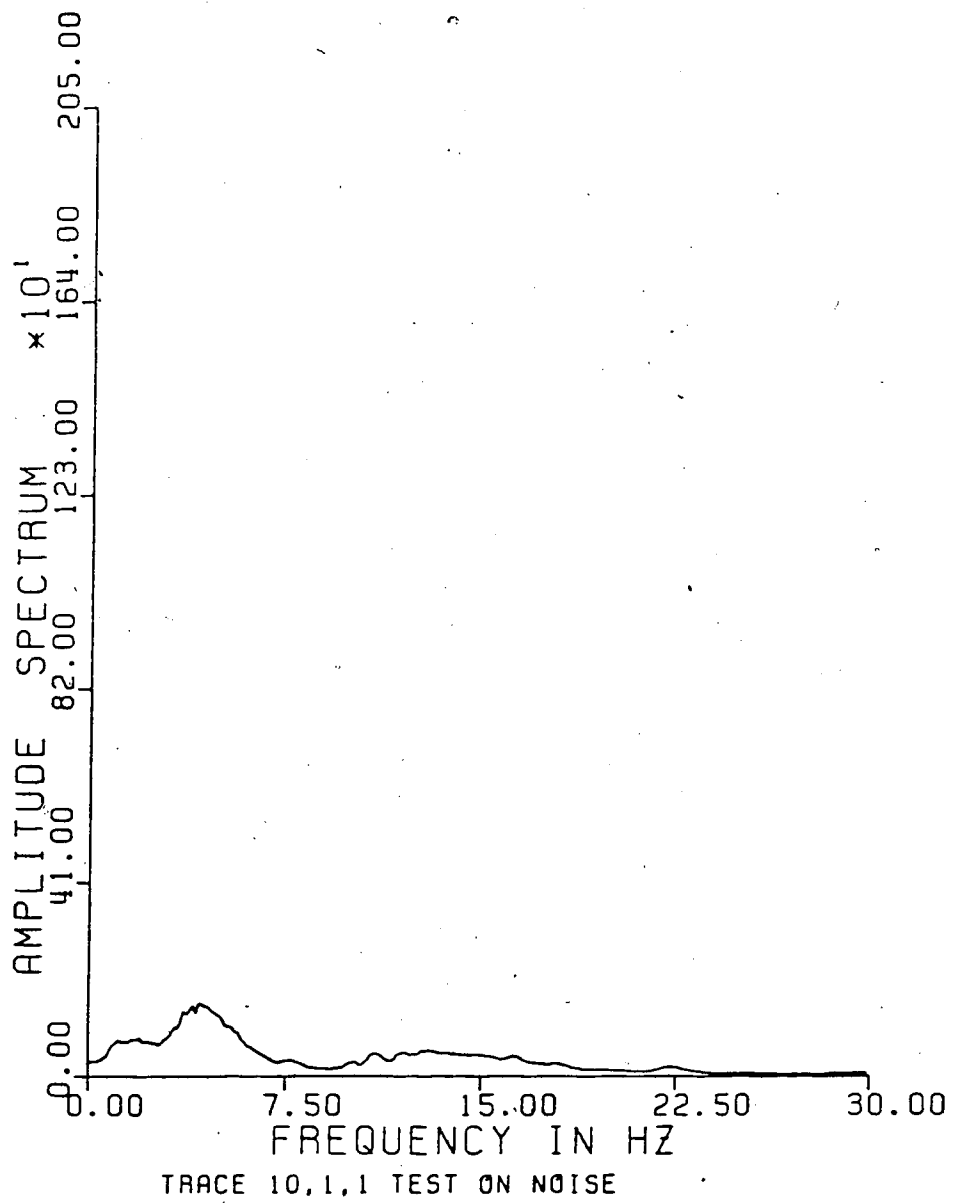
Figure 13..... Spectral estimate of the noise of record 10,1,1
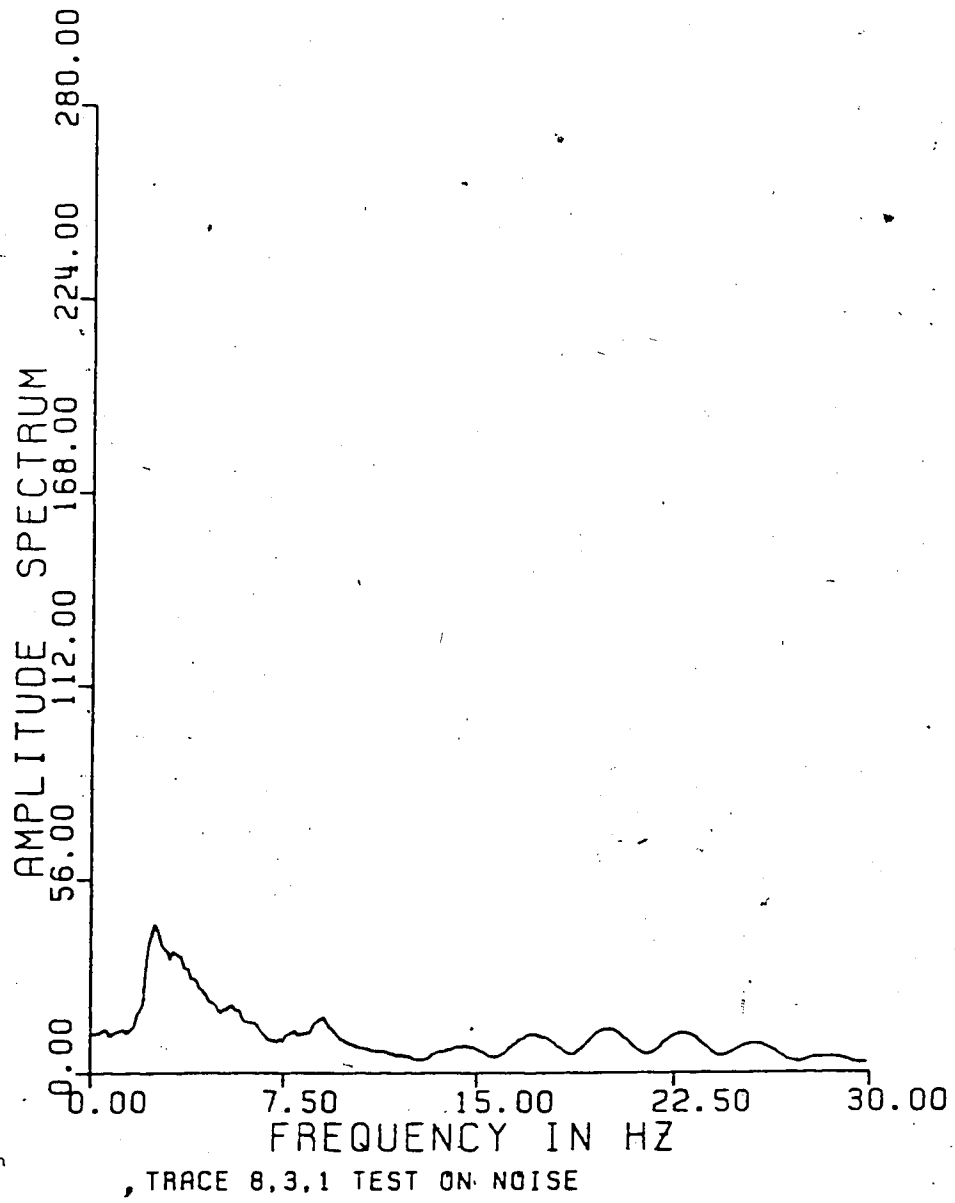
Figure 14.... Test on noise for trace 8,3,1

under analysis. This means that the filter is designed to pass signal frequencies in a desired band and to attenuate all other unwanted frequencies, outside the band. Digital recursive filters allow the greatest flexibility in frequency smoothing and in this study a recursive zero-phase bandpass Butterworth filter will be useful. A detailed analysis of the eight-pole bandpass Butterworth filter can be found in Kanasewich (1981). A FORTRAN program for such a filter was written by D. Ganley in 1977 during his graduate studies at the University of Alberta. As an example of the effectiveness of the filter, figure 15 compares a record of unfiltered data with the same record after filtering with two different bands, 5-17 Hz and 7-13 Hz . The improvement of the quality of the record is clearly visible. However care must be exercised in timing the onset of first energy with data filtered by a zero phase shift filter. Finally a band of 5-17 Hz was decided for our records following the conclusions of the power spectral analysis discussed in the previous section.

3.5 Despiking the data

As a general comment on the original data, the noise level was rather low, and the first breaks of the seismic energy quite clear and distinct from the noise background. However, a significant problem with the University of Toronto recorders was their small dynamic range leading to a saturation or spiking of the data. On the records, the

UNFILTERED DATA.TRACE 10.1.1

FILTERED DATA.BAND 5-17 HZ
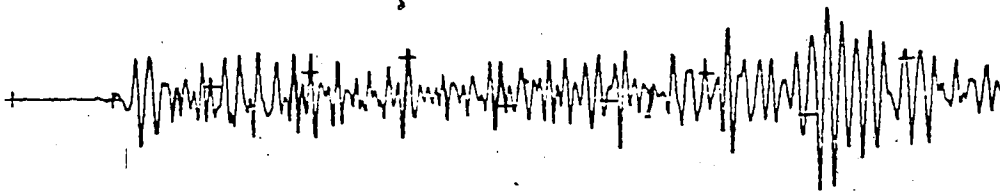
FILTERED DATA.BAND 7-13 HZ

15.00   17.00   19.00   21.00   23.00   25.00
                              TIME (SEC)

Figure 15.... Bandpass filtering by the Butterworth
eight-pole filter

appearance was that of a series of spikes, whenever the amplitude of the signal was large.

These rapid and high amplitude variations are not attributable to a physical process but rather to saturation effects, either saturation of the digitizer or saturation of the amplifiers. As a matter of fact the high sensitivity required to obtain good signals on early-arriving head waves made it very difficult to adjust the gains of the amplifiers during the experiment.

A computer program was written which attempts to obtain the correct sign of the signals while making no attempt at obtaining the correct amplitude.

The program works as follows: The data are passed through several tests and accesses to these tests decided upon the operation to be applied, which generally consists of a proper alteration of the sign and the amplitude of the samples. The program makes use of several empirical parameters, which were decided after careful examination of a large number of spikes and which concern minimum amplitude of a spike, differences in amplitudes between adjacent samples, etc.In figure 16 are shown: a) Top of the page:record 32, shot 6,vertical and horizontal components (original data), b) The same record after application of the despiking operation and c) The same despiked record after application of the Butterworth filter band 5-17 Hz.A flow chart of the despiking program is shown in figure 17. Very little use was made of heavily spiked areas so the

1024 UNITS/IN F11.8174
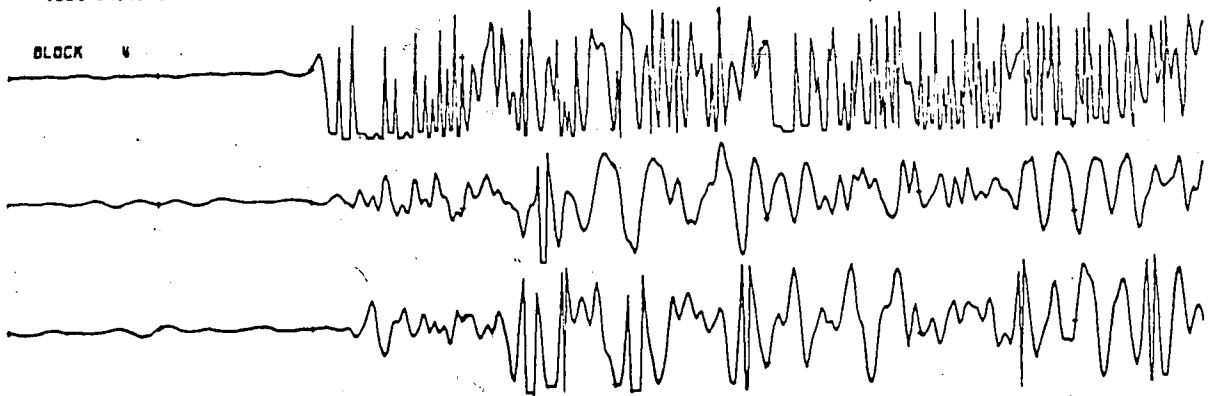
BLOCK 4

1024 UNITS/IN F11.8174 DESPIKE

BLOCK 4
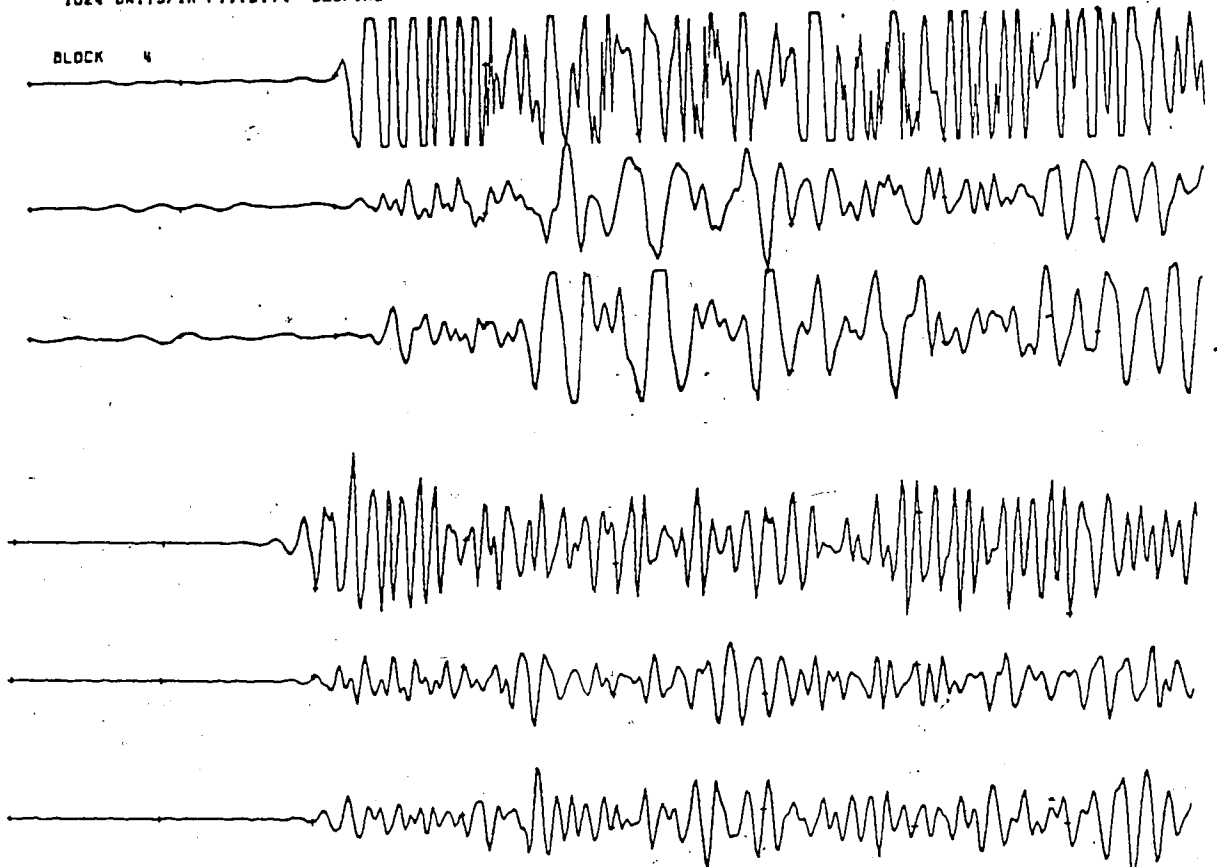
Figure 16.... Successive application of the despiking and
filtering operations on the original data

DESPIKER PROGRAM
ID = A = ORIGINAL DATA   IDLA = ID(J) - ID(J-1)   AMAX = 410

IT = B = FINAL DATA   IDLZ = ID(J) - IT(J-1)   AMIN = 10

IF |ID(J)| < AMAX

IF |IDLA| < AMIN

IF |IDLA| < ID(J)+200

IF IG1 < 0

IT(J) = IGS × |ID(J)|

IT(J) = ID(J)

IT(J) = IGS × 511

IF |IDLZ| < ID(J)

IF IG1 < 0

IT(J) = IGS × 51

IT(J) = IGA × (-511)

IF IG2 > 0

IT(J) = IGAA × (-511)

IT(J) = ID(J)

IGAA = IGR
IGR = IGS
IGS = SIGN OF IT

IG2 = IG1
IG1 = IG0
IG0 = 1 NO SPIKE

IGAA = IGR
IGR = IGS
IGS = SIGN OF IT

IG2 = IG1
IG1 = IG0
IG0 = -1 SPIKE

SIGN FLAGS

SPIKE FLAGS

IF IT(J) < 510

IT(J) = IT(J)

IF IT(J) < 510

IT(J) = IT(J)

IF IT(J+1) > -511

IF IT(J+1) < -511

IT(J) < 495

IT(J+1) = -511

IF IT(J+2) = -511

IF IT(J+2) > 0

IT(J+2) < 50

IT(J+1) = ID(J+1)

IT(J+2) = ID(J+2)

FINAL OUTPUT

Figure 17....
Flow chart of the despiking operation.

interpretation does not depend critically on reliability of these data.

3.6 Normalization

The concept of normalization is quite important in order to obtain usable amplitude information from the seismic section. Different seismometer responses ,coupling between the seismometers and the ground and different gain settings,are all factors that may cause considerable amplitude differences from trace to trace. The purpose of normalization is to minimize the effect of these factors.

It is expected theoretically that the average power of the records should decrease monotonically with distance.Thus,multiplication factors' for each trace were calculated in order to make the power values of the traces decrease with distance in a linear fashion according to the equation POWER(J)=POWER(1)-B*DIST(J). J is the number of the station, increasing with distance and DIST(J) its offset. The range within which the power values will vary,between the first and the last trace of the section, can be easily controlled by proper adjustment of the slope B.In figure 18,(record section of line A,shot 1),maximum amplitude values are the same for all the traces,while figure 19 shows the same section after application of the above technique of normalization. The numbers at the end of the traces are the calculated amplification factors of the traces. It can be seen that a considerable improvement in relative amplitude information has been achieved.
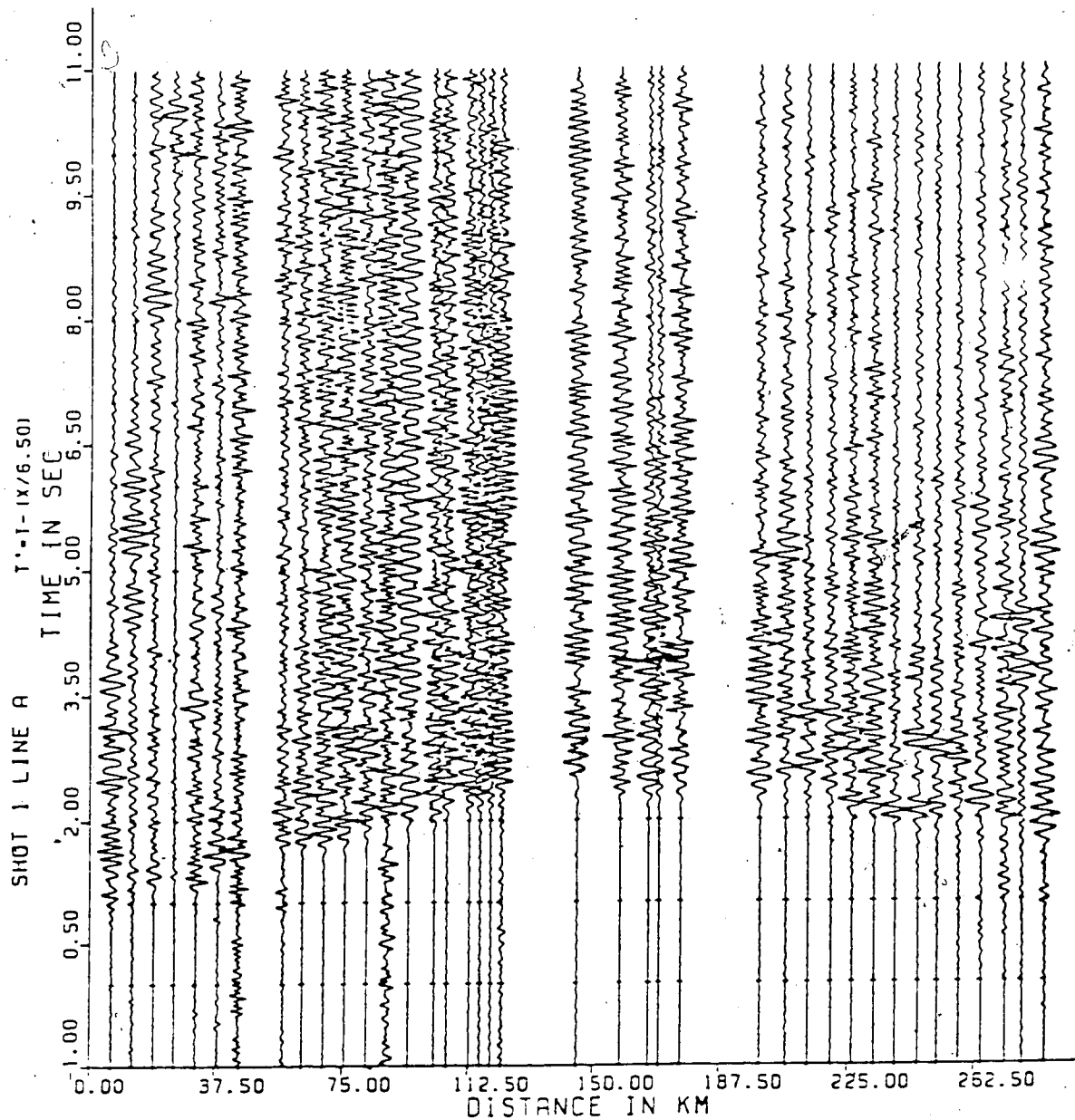
Figure 18.... Record section for shot 1.Maximum amplitude values are the same from trace to trace.
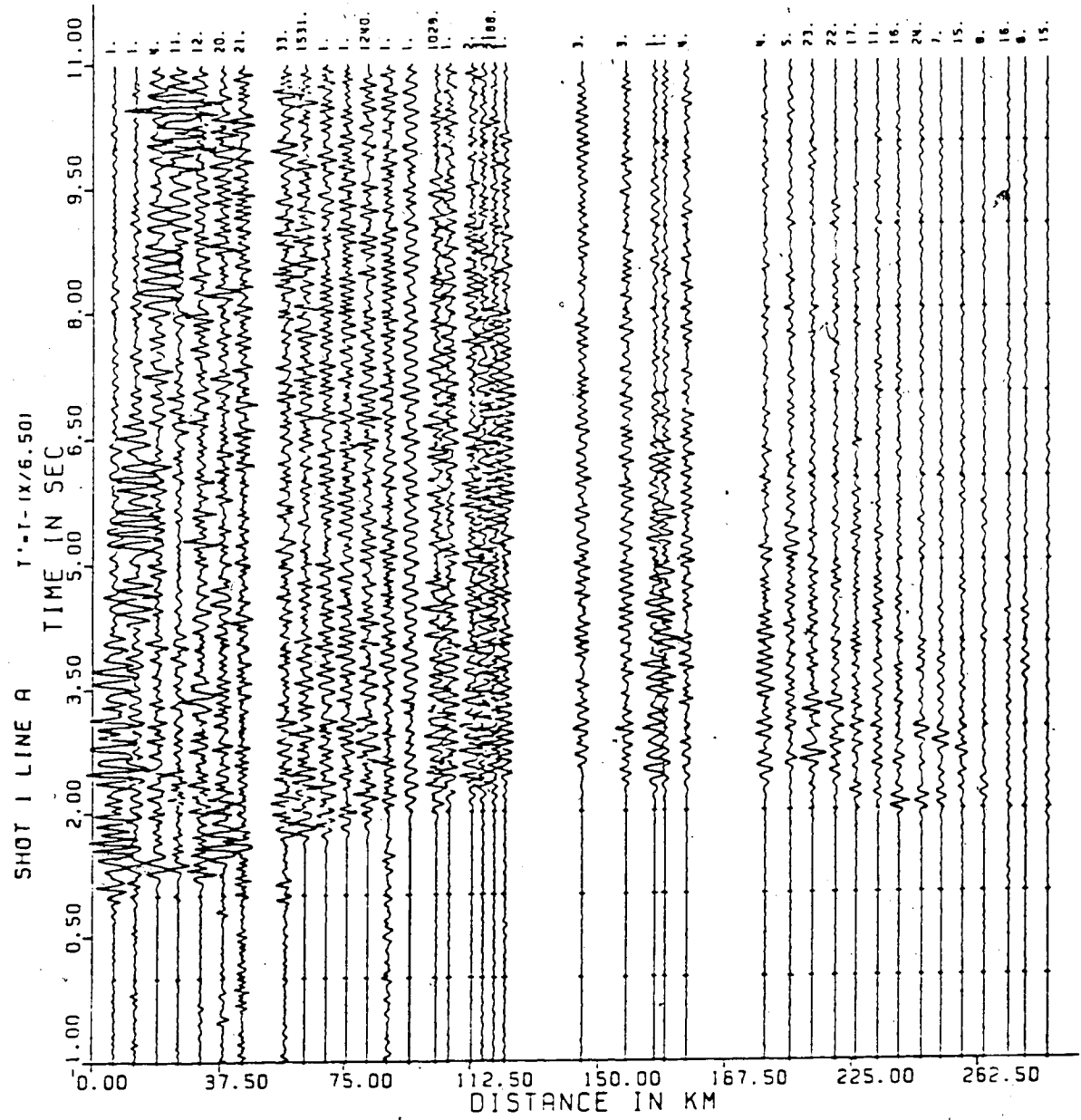
Figure 19.... Record section, shot 1,after normalization.

4. SEISMOLOGY AND THE EARTH'S CRUST

4.1 The main crustal wave groups

In a layered elastic isotropic medium which is a first order valid approximation for the earth's crust, two kinds of body waves can exist: compressional P-waves and transverse, or shear S-waves. There are four main P-wave phases usually observed in seismic crustal studies: Pg, P*, Pm and Pn.

a) The Pg phase is a wave penetrating into the upper part of the basement and is generally observable up to a distance of 60-100 km. It has a velocity between 5.5 and 6.4 km/s. In a continuous profile it will comprise several prograde segments of travel time branches with the velocity increasing with distance. This splitting nature of the Pg group will not be detected if the spacing of the recording stations is too large (>10 km.) The g stands for "granitic" layer.

b) The P* phase is a P-wave refracted through an intermediate layer in the crust with a velocity near 6.5 km/s. The upper boundary of this layer has been called Conrad discontinuity in Europe. The P* phase is often the most prominent first arriving event in crustal seismic sections.

c) The Pm is a wave reflected at the crust/mantle transition or boundary. It is a retrograde branch on a time-distance presentation which shows that a strong velocity discontinuity exists between the crust and the

mantle.The Pm curve is generally well expressed by large amplitudes in the range of the critical point (where the angle of incidenceis i=arcsin(V(Pg)/V(Pm))).

d). The Pn waves are diffracted from the top of the mantle. They have a linear relationship on a prograde branch on a graph of arrival time versus distance from the shot. At sufficient distances(between 150-300 km) the Pn is the first arrival wave,the amplitude being usually very small and its frequency significantly lower than the Pm. Its velocity is between 7.8 and 8.3 km/s. The Pn phase has long been interpreted as a head wave.The observed amplitude,however,is usually greater than that predicted for head waves, implying that the velocity change at the MOHO is not exactly step-like but it has a finite gradient within a transition zone.Currently,instead of interpreting the Pn as a head wave, a more likely explanation is given in terms of guided waves within a high Q layer several tens of kilometers in thickness at the top of the mantle. Anisotropy of the Pn velocity has been reported by several authors(Hess ,1964,Rait et al.,1969) in an oceanic setting.

4.2 The composition of the crust

The great value of seismic velocity structures is that they may allow us to make an interpretation about the tectonic history of the region and of the lithology at various depths.Laboratory measurements of seismic velocities in rocks under a wide range of confining pressures,pore

pressures and temperature conditions simulating those in the crust can be compared with velocities derived from seismic crustal records to infer information about the kinds of rocks present at various depths.Jeffrey's (1937) early hypothesis that the crust varies from the top to the bottom between an acidic and intermediate composition is probably a still valid approximation. However, modern work has refined this oversimplified picture.

Recent results from geological and geophysical studies can be summarized as follows. Crustal refraction surveys encountering Precambrian crystalline basement rocks usually measure upper crust velocities from 5.8 to 6.1 km/s which are typical of light granitic rocks and metamorphosed sediments. The upper crust, below the sedimentary cover,consists of layered metamorphic rocks such as gneisses and schists,often penetrated by granitic intrusions.The grade of metamorphism increases with depth. In the shallow or middle crustal refraction sections one also has slightly higher velocities which range from 6.1 to 6.4 km/s.These are often attributed to migmatitic rocks which are believed to comprise most of the middle crust and on a larger scale they may behave as intrusions into the overlying cover of metamorphic rocks(Haller,1958,Smithson et al. 1975). Seismic velocities from the lower crust are most often in the range between 6.5-6.9 km/s.These velocities are too low for gabbroic rocks and there is strong evidence that they are associated with a lower crust predominantly composed of

granulite facies rocks (Smithson,Shive and Brown ,1977).However,lower crustal velocities in the range of 7-7.5 km/s have been reported in several seismic studies showing that parts of the lower crust are truly gabbroic. Upper mantle velocities in the range of 7.8-8.4 km/s are certainly attributed to ultramafic rocks and most probably to dunite.

Numerous attempts have been made recently(Burke and Dewey,1973, Gibb and Walcott,1971) to explain the development of the Precambrian through plate tectonics.The plate tectonics hypothesis implies a complex series of events affecting continents including rifting, continent-continent collision and continent-arc collision.Horizontal movements of lithospheric plates predominate.Surely such processes must lead to distinctive geophysical signatures.The first most obvious feature that we would expect is fused continental blocks of different composition and therefore of different physical properties. In fact, the lateral variation or blocks that have been suggested for continental crustal structure(Kosminskaya and Zverev,1968;Smithson and Brown,1977) may be, in part, a vestige of Precambrian plate tectonic processes.We would expect continental blocks of different composition to have different thicknesses since Precambrian areas should be approaching isostatic equilibrium.Discontinuities of great variability and structural complexity should be located between these blocks.

Plate tectonics theory would explain the gently folded blocks generally identified in the lower crust as part of an early succession marked by horizontal tectonic movement whereas the more steeply dipping zones often detected in the upper crust are a later development during a lock-up stage promoted by collision.

4.3 Low velocity zones

Low velocity zones in the upper and middle crust have been postulated by Landisman and Mueller(1966) in north Germany,Pennsylvania ,Central Japan and east Montana,and in regions of the Canadian Shield by Braile(1977).According to Snell's law,no seismic rays originating from a near surface source can be returned to the surface from within a low velocity zone.Hence,an interpretation of the seismic data based on the first arrivals alone will give no evidence of the LVZ. Furthermore, one obtains depths greater than the true ones for all the lower boundaries. To recognize the existence of such a zone one needs to identify the reflections from the top and the bottom of the LVZ in a high quality crustal seismic section. The use of synthetic seismograms for this purpose is of great help.

A satisfactory explanation for the existence of velocity inversions in the crust has not yet been reached.It is however an apparently common feature of the crust, its presence being observed in geologic sections that have undergone vastly different histories. This suggests that the

controlling factor is not a compositional variation of the crustal section but rather a variation of the physical parameters that affect seismic velocities.Whether this is in the form of a high temperature gradient regime or in the form of a decrease of the effective pressure because of an increase of the pore pressure exerted by pore fluids in the rock remains problematic.

4.4 The crust-mantle boundary

Until rather recently, the Mohorovicic discontinuity,the crust mantle boundary, was generally considered to be a first order discontinuity where the compressional wave velocity increases discontinuously from a value of around 7 km/s to a value between 7.8 and 8.6 km/s. Although this simple model is still widely used, studies with synthetic seismograms(Fuchs,1969)combined with observations of near vertical reflections from the Moho(Clowes,Kanasewich and Cumming, 1969) suggest a gradational change in velocity rather than a first order discontinuity.To explain the observed amplitudes,the change in velocity must be accomplished within less than 1km. An even more complicated model has been proposed by Clowes and Kanasewich (1970) and Meissner(1973) who suggest that the crust/mantle transition zone is a many layered complex of alternating high and low-velocity laminae having a total thickness of a few kilometers.Such a sandwich-like struct re would explain satisfactorily the composite nature of th

reflections from the moho, that are often identified in field records. It can also explain the anisotropy as well as the amplitudes of the Pn waves.

4.5 Theoretical travel times for a multilayered medium

A seismic head wave is a diffracted wave, propagating along an interface between a lower and a higher constant velocity layer. It can often be used to determine the depth of the interface as well as the velocity of propagation of the elastic waves along the higher velocity layer. The first step in solving the problem of a multilayered case is to attempt the forward problem. For a completely defined model it is a straightforward procedure to compute the theoretical travel times of the seismic rays travelling through the medium. With the assumption of plane layering and velocity increasing with depth one can use the travel time observations from field records in a direct inversion to determine a preliminary model. The travel time calculations are approached by applying geometrical optics theory to the seismic rays, assuming a multilayered earth in which the elastic wave velocity increases monotonically with depth, in a stepwise fasion and remaining constant within each layer:

$$\alpha_1 < \alpha_2 \cdots < \alpha_{n-1} < \alpha_n \qquad (1)$$

n is the number of layers including the half space. The free surface interface is the horizontal surface upon which the source and receivers are situated. The layers may have arbitrarily dips. For an updip source, the travel time of the

n^2 layered arbitrarily dipping model is:

$$T_{Un} = \frac{x \sin D_1}{\alpha_1} + \sum_{\ell=1}^{n-1} \frac{ZU_\ell}{\alpha_\ell} [\cos D_\ell + \cos U_\ell] = b_{Dn}x + I_{Un} \qquad (2)$$

This will give the travel time for a head wave travelling at the top of the n'th layer. For the downdip source the equation is (Adachi, 1954):

$$T_{Dn} = \frac{x \sin U_1}{\alpha_1} + \sum_{\ell=1}^{n-1} \frac{Z_{D\ell}}{\alpha_\ell} [\cos D_\ell + \cos U_\ell] = b_{Un}x + I_{Dn} \qquad (3)$$

Zul and Zdl are the updip and downdip thicknesses of the l'th layer respectively. The updip and downdip rays, incident on the l+1 interface, are defined by the angles Dl and Ul with respect to the vertical direction while $\delta_{\ell,n}$ and $v_{\ell,n}$ are the corresponding angles with spect to the vertical , to the interfaces.

$$D_\ell = \delta_{\ell,n} + \theta_{\ell+1} \qquad (4)$$

$$U_\ell = v_{\ell,n} - \theta_{\ell+1} \qquad (5)$$

where $\theta_{\ell+1}$ is the dip angle of the (1+1)'th interface. The critical refraction at interface n occurs when

$$\frac{\sin\delta_{n-1,n}}{\alpha_{n-1}} = \frac{1}{\alpha_n} = \frac{\sin v_{n-1,n}}{\alpha_{n-1}} \qquad (6)$$

hence $\delta_{n-} \quad _{n-1}$. The other angles of incidence are calculated from the use of snell's law of refraction. The calculation starts from $\delta_{n-1,n}$ and proceeds upwards.

$$\left. \begin{array}{c} \dfrac{\sin\delta_{n-2,n}}{\alpha_{n-2}} = \dfrac{\sin(D_{n-1} - \theta_{n-1})}{\alpha_{n-1}} \\[3mm] \dfrac{\sin v_{n-2,n}}{\alpha_{n-2}} = \dfrac{\sin(U_{n-1} + \theta_{n-1})}{\alpha_{n-1}} \end{array} \right\} \qquad 7$$

$$\frac{\sin \delta_{1,n}}{\alpha_1} = \frac{\sin(D_2 - \theta_2)}{\alpha_2}$$

$$\left. \frac{\sin \upsilon_{1,n}}{\alpha_1} = \frac{\sin(U_2 + \theta_2)}{\alpha_2} \right\} \quad 8$$

Equations 2 thru 8 have been programmed for a digital computer using FORTRAN language. The computation proceeds recursively startin~ from n=2, until the last layer of the model is encountered. The case of a source burried at some depth within the first layer is also taken into account by the program. The program will be useful later to test the accuracy of the derived models. Figure 20 shows a ray diagram for a three layer model illustrating the geometrical parameters involved in the computations. From eq. (2) and (3), the slopes of the travel times curves are b_{Un} and b_{Dn}. These are the inverse of the apparent velocities. Clearly

$$b_{Dn} = \frac{1}{v_{Dn}} < \alpha_n \quad \text{and} \quad b_{Un} = \frac{1}{v_{Un}} > \alpha_n .$$

With field observations ..e process is rather in reverse order. From the apparent velocities one can find

$$\delta_{1,n} = -\theta_2 + \sin^{-1} \frac{\alpha_1}{v_{Dn}} \qquad 9$$

$$\upsilon_{1,n} = \theta_2 + \sin^{-1} \frac{\alpha_1}{v_{Un}} \qquad 10$$

The other angles of incidence can be found now using equations 7,8 again but in reverse order starting from $\delta_{1,n}$, $\upsilon_{1,n}$ and proceeding downwards. Then from eq. 6,7,4,5 it is found that the critical angle of incidence at the interface n and its dip θ_n are given (for n≥3) by:
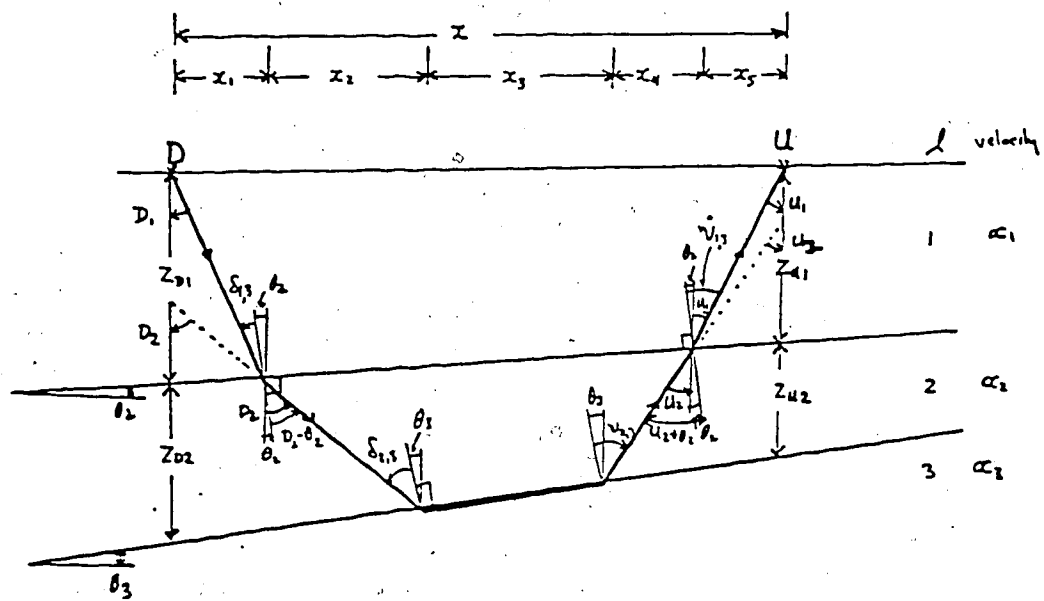
Figure 20.... Ray diagram of a three layer model.

$$\delta_{n-1,n} = \frac{1}{2}\left[\sin^{-1}\frac{\alpha_{n-1}}{\alpha_{n-2}}\sin(\delta_{n-2,n}) + \sin^{-1}\left(\frac{\alpha_{n-1}}{\alpha_{n-2}}\sin(v_{n-2,n})\right)\right]$$

$$(11)$$

$$\theta_n = \theta_{n-1} + \frac{1}{2}\left[\sin^{-1}\left(\frac{\alpha_{n-1}}{\alpha_{n-2}}\sin(\delta_{n-2,n})\right) - \sin^{-1}\left(\frac{\alpha_{n-1}}{\alpha_{n-2}}\sin(v_{n-2,n})\right)\right]$$

For n=2 the equations are: $\qquad\qquad$ (12)

$$\delta_{1,2} = \frac{1}{2}\left[\sin^{-1}\left(\frac{\alpha_1}{v_{D2}}\right) + \sin^{-1}\left(\frac{\alpha_1}{v_{U2}}\right)\right] \qquad (11a)$$

$$\theta_2 = \sin^{-1}\left(\frac{\alpha_1}{v_{D2}}\right) - \sin^{-1}\left(\frac{\alpha_1}{v_{U2}}\right) \qquad (12a)$$

α_1 is given by the direct wave. The velocity in the n'th layer is obtained by Snell's law:

$$\alpha_n = \frac{\alpha_{n-1}}{\sin\delta_{n-1,n}} \qquad (13)$$

The thickness of the n-1 layer is obtained from the intercept times Idn and Iun and the relations (2) and (3)

$$z_{D,n-1} = \frac{\alpha_{n-1}\left[I_{Dn} - \sum_{\ell=1}^{n-2}\frac{z_{D,\ell}}{\alpha_\ell}(\cos D_\ell + \cos v_\ell)\right]}{\cos D_{n-1} + \cos v_{n-1}} \qquad (14)$$

$$z_{v,n-1} = \frac{\alpha_{n-1}\left[I_{vn} - \sum_{\ell=1}^{n-2}\frac{z_{U,\ell}}{\alpha_\ell}(\cos D_\ell + \cos v_\ell)\right]}{\cos D_{n-1} + \cos v_{n-1}} \qquad (15)$$

Equations 9 thru 15 were also programmed in a recursive manner to solve the problem of the multilayer dipping model. The program will receive as input, information from the actual seismic records (apparent velocities and intercept times) and will give the depths, dip angles and true velocities of the various layers. It is interesting to

notice that with one source alone,there is insufficient information to solve the problem of the n-layer case, there being $3(n-1)$ unknowns and only $2(n-1)$ supplied by the data.

4.6 The t^2-x^2 method

In a layer over a half space, the arrival time of reflected energy depends not only on the reflector's depth h and the velocity v above the reflector,but also on the offset distance x.The equation,for a single layer over a non-dipping halfspace,relating the arrival time t with x,v is:

$$t^2=x^2/v^2+4h^2/v^2 \qquad (16)$$

If the reflecting interface is dipping by an angle θ an extra term $\dfrac{4hx\sin\theta}{v^2}$ should be added to the right side of the equation.However for small dip angles (less than 1°) and for small offsets this term becomes negligible. Hence, if we plot t^2 versus x^2 we get a straight line of slope $1/v^2$ from which we can determine the velocity v above the reflector. From the intercept with the t^2 axis we can determine the corresponding depth of the interface. For an l layered sequence above the reflection it can be shown that the velocity v is related with a root mean square velocity v for the layered sequence.

Once the RMS velocities v_1 and v_2 have been determined for two successive reflectors, the interval velocity Vi can be found from Dix (1955) formula:

$$Vi=v_2^2t_2-v_1^2t_1/t_2-t_1 \qquad (17)$$

Where t1,t2 are the intercept times of the successive reflection branches. The method assumes straight ray paths in the overburden and the existence of a first order discontinuity as a reflecting horizon.

For an accurate calculation of the depths and the interval velocities one has to confine oneself to the subcritical region of the reflection branches. Supercritical reflections are affected by refraction and will give a larger depth for the reflector as well as larger velocity. Also, at large offsets the effect of dip may not be negligible.Nevertheless, if the full length of the retrograde branch is used using both subcritical and supercritical reflections then a reduction of 10% for the calculated depths is recommended by Giese(1976) and a correction of 3% for the average velocities may be applied as well.For subcritical reflections,no correction is needed.As we will see in the interpretation of the data,the T^2-X^2 method proved to be of considerable help in determining the depths of reflectors which do not show up as refractors and also in revealing information about velocity inversions within the crust.

4.7 Synthetic seismograms

While the general velocity structure of the earth's crust can be inferred from studies of the travel times of seismic waves, detailed velocity structure including identification of velocity gradients within layers and

recognition of low velocity zones, can best be determined by a combined interpretation of the travel times and amplitudes of refracted and reflected waves.

Several methods have been used recently to compute theoretical seismograms and they have been so far developed that synthetic body wave seismograms can be calculated for models which are as complicated as those estimated from modern travel-time inversions. The main methods are the reflectivity method(Fuchs and Mueller,1971),the asymptotic ray theory(Hron and Kanasewich,1971) the generalized ray method(Wiggins and Helmerger,1974), disc ray theory (Wiggins and Madrid, 1974,Wiggins, 1977) and the WKBJ seismogram,(Chapman,1978,.Dey-Sarkar and Chapman 1978) which is used in this work.

Chapman's method requires a model consisting of plane,laterally homogeneous and isotropic layers (or spherical shells) overlying a half space. Vertical velocity gradients are approximated by a large number of thin homogeneous layers having small velocity contrasts. Layers are considered to be perfectly elastic so that no attenuation effects are considered.Shear wave velocities were calculated assuming a Poisson's ratio of 0.25 and densities are computed from $\rho = 0.252 + 0.3788 V_p$(Birch,1954). Synthetic vertical component seismograms were computed at 10 km distance intervals and displayed in record sections using a reducing velocity of 6.5 km/sec.Synthetic and observed record sections are plotted on the same scale so that by

supefimposing one section. on the other, detailed characteristics of the observed sections can be compared with the theoretical seismograms as a means of interpretation.

4.8 Ray tracing

The physical basis for ray tracing and travel time calculation for arbitrary two-dimensional models is Huyghen's principle and Snell's law.The following simple method of ray tracing was applied in this work; First, a convenient system of cartesian coordinates is chosen and the equations of the interfaces of the model are defined. Then,starting from the source of the seismic energy and a given ray parameter,the equation of the ray incident at the top of the second layer is derermined. By successively applying Snell's law for this ray, the equations of its refracted and reflected segments up to the desired depth are defined until the ray returns to the earth's surface.Subsequently, the system of linear equations for the ray segments and of the interfaces it has encountered are solved to find the coordinates of the points of intersection. Once these coordinates are known it is easy to compute the travel time of.the ray by summing up the travel time increments amd also to produce a ray diagram using a computer graphics system. The computation is repeated for a large number of ray parameters and for various levels of maximum penetration. Positive or negative velocity gradients

can be satisfactorily approximated by an arbitrary number of thin constant velocity layers. Interfaces can be arbitrarily dipping and possibility of low velocity zones is not excluded. The program also computes the times and offsets of the critical reflections.

4.9 Correlation

Correlation is the first step and perhaps the most important one in the interpretation of seismic data. The term correlation in seismic interpretation implies the identification of the same phase on different seismic traces in the time-distance domain. Such an identification of the seismic phases is based on the following criteria.

1) Coherency of the events: arrivals of elastic energy from the same seismic phase will have a distinctive similarity in appearance from one recording location to another. Clearly, the amplitudes must decrease with distance and the shape of the wavelet will change due to preferential absorption of higher frequencies at larger offsets.

2) The apparent velocities must show values within a physically realizable range.

3) The travel time branches must be of sufficient length to be identified uniquely.

It may be noticed that the criteria for correlation are different in reflection and refraction seismology. In reflection seismology, correlation of the reflected phases

on the time sections is very directly related to the depth
of the reflector. This is not as direct in the
interpretation of refracted rays. Phase correlation is most
successful if closely spaced detectors, are used and the
spacing between them being usually less than 100 m in
reflection studies. In retraction studies however,the
spacing of geophones is often a few kilometers.

To pick up the first arrival of wave energy on our
records we used large scale plots (two inches per second,
2.5 inches for peak-to-peak large amplitudes). The records
were not filtered. (Filtering may disturb considerably the
onset time of the first arrivals). Generally the background
noise level was low and the first breaks could easily be
read with an uncertainty smaller than ±0.05 sec.

5. RESULTS AND INTERPRETATION

5.1 Interpretation of line A

Low noise levels and clear first arrivals events permit a quite accurate correlation of the initial waves from both the north and the south shot sources of line A.Five linear travel time segments were interpreted for each shot.The method of least squares was applied to determine their slopes (which are the inverse of the apparent velocities) and their intercept and reciprocal times.It is then noticed,comparing the two sections, that considerable differences in intercept times and apparent velocities exist.The intercept times and apparent velocities of the northern source are considerably lower than those of the southern source.The two sets of seismic observations for line A are shown in figure 21 and figure 22 .The travel times are plotted with a reduction velocity of 6.5 km/s.

It should be noted that the average velocity for the sedimentary layer using direct waves was observed at only one location.Calculation of $v(1)$ from this single arrival time would be highly unreliable because there is a rapid increase of seismic velocity through the Mesozoic and Paleozoic sedimentary rocks causing significant curvature on the travel time branch of the first arriving refracted waves to be recorded.Instead,a pseudoaverage $v(1)$ velocity was computed using the drill-hole information on depths to the Precambrian crystalline basement. As a consequence of
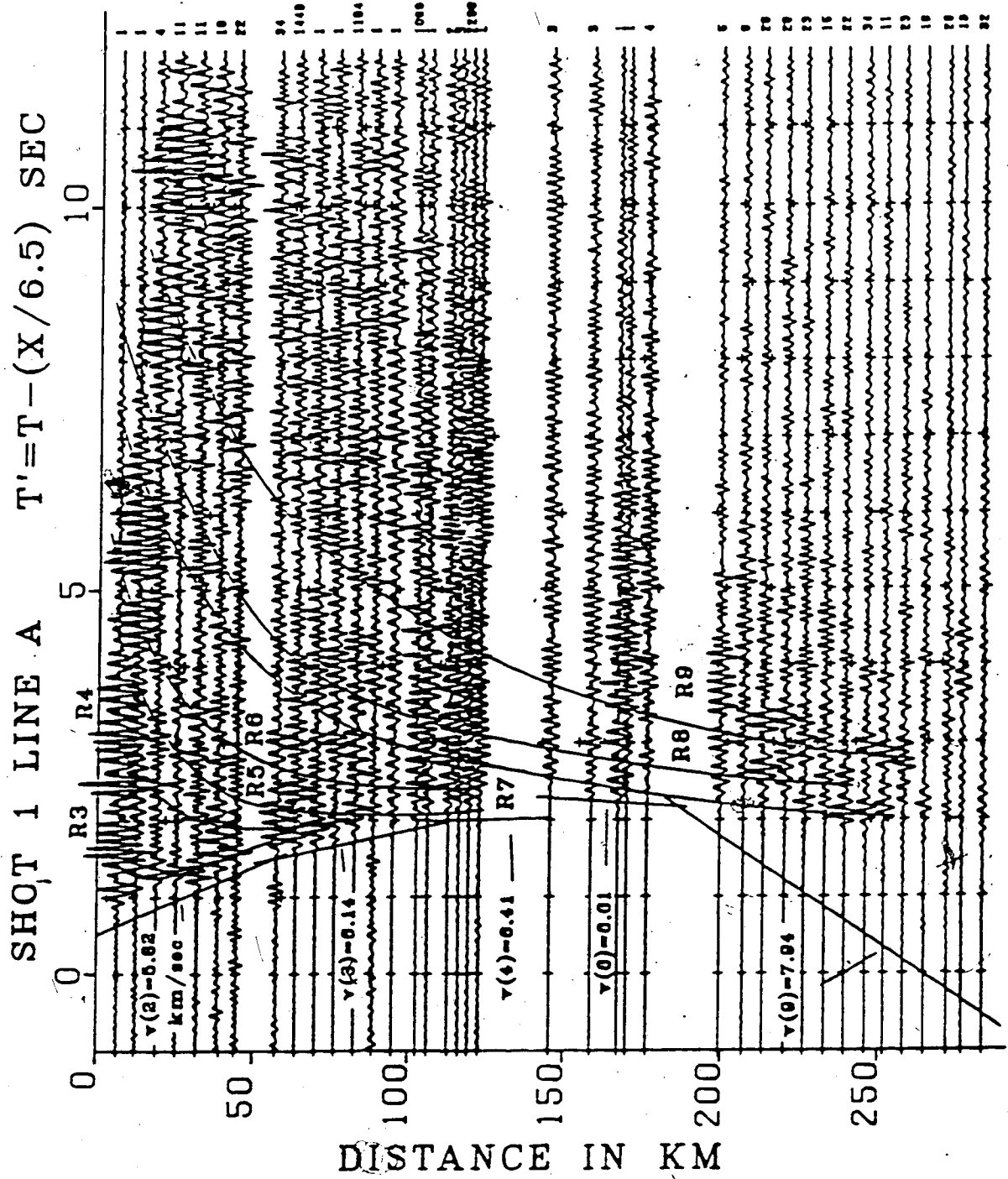
Figure 21.... Record section for line A, shot 1
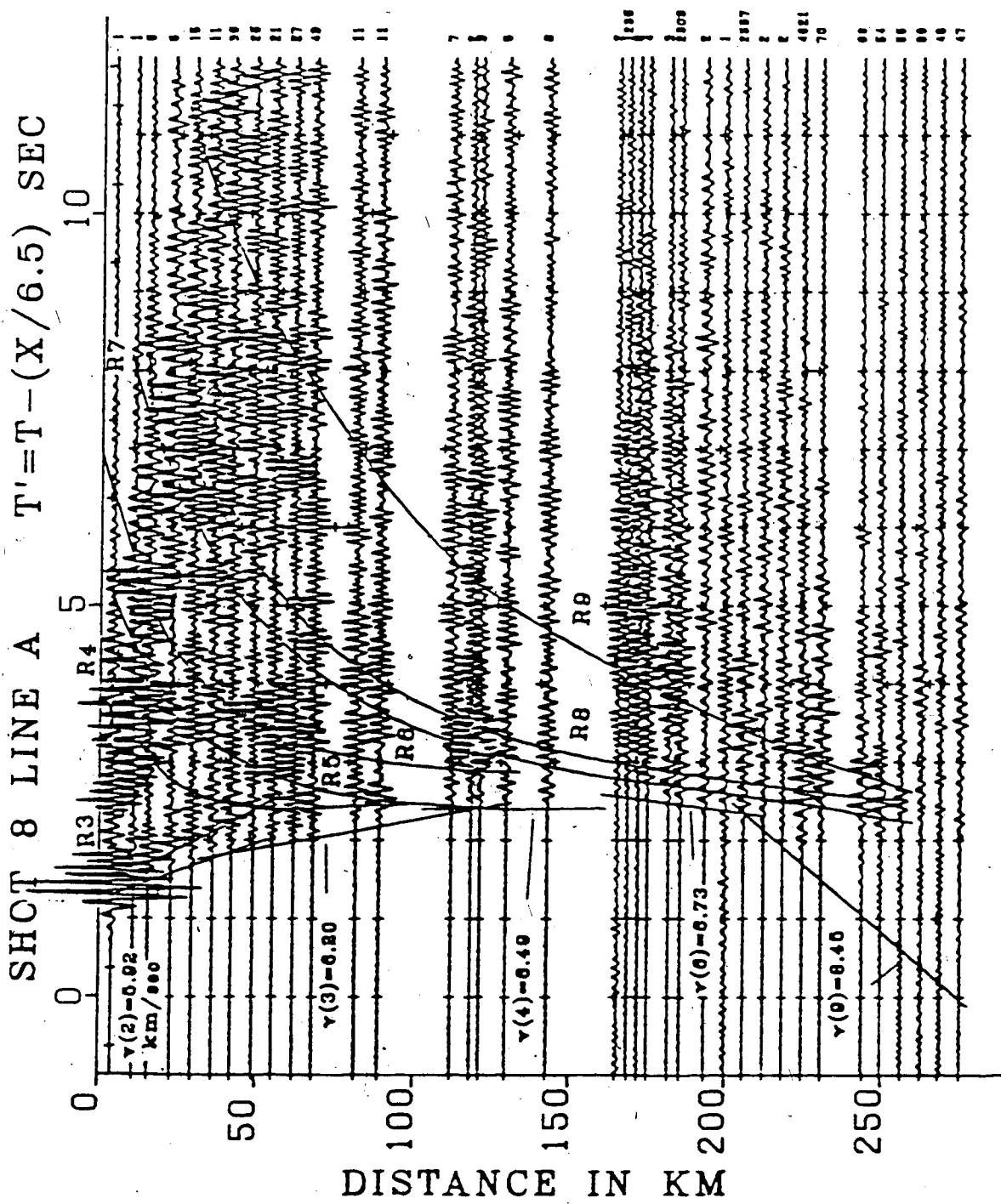
Figure 22.... Record section for shot 8.

reciprocity , the extrapolated time of any ray travelling
from shot point to shot point must be the same when shooting
in either direction. As can be seen in table 2, good
agreement between reciprocal times is observed for line A.
Small corrections to the first arrival times, were applied
to make the reciprocal times ▓▓▓▓▓ and to avoid any
inconsistencies in the inversion ▓▓ time corrections
were always smaller than the ▓▓▓▓its of the first
arrival times(table 2, columns 8 and 9). The available set
of first arrivals data of line A is reliable and is suitable
for the first inversion scheme described in section 4.5. The
result of this first inversion showing depths,dips and model
velocities of the layers is shown in table 2. Subsequently,
the programmed Adachi's equations are used to calculate the
travel times of the head waves of the derived model and
compare them with the observed times. It can be seen (table
2) that agreement is very good and that the only notable
discrepancy is between the observed and calculated head wave
times from the basement below the south shot. It is clear
that the calculated arrivals of this event- assuming
$v(1)=3.30$ km/s - are delayed by about 0.1s with respect to
the observed times. The discrepancy could be removed either
by reducing the depth of the basement or by in creasing the
average velocity $v(1)$ below shot 8 .Since a depth of the
basement at 3 km, is correct according to drilled well
information we must accept the second alternative and by
modelling we find that the average

TABLE 2

First Inversion Model For Line A
(V(1)=3.3km/sec)

The headers of the columns are defined as follows:

I – Interface.
S – Shot number.
N – Number of records used in least squares.
Rt_0 – Record t_0 (sec).
Mt_0 – Model t_0 (sec).
Depth – Depth of the interface (km).
V app – Apparent velocity (km/sec).
RRT – Record Reciprocal Time (sec).
    – Model Reciprocal Time (sec).
    True velocity (km/sec).
    – Dip of interface (degrees).

I	S	N	Rt_0	Mt_0	DEPTH	V app	RRT	MRT	Vtr	DIP
2	1	3	0.62±0.03	0.65	1.3±0.1	5.82±0.04	50.04	50.07	5.87	0.33
	8	3	1.31±0.03	1.40	3.0±0.1	5.93±0.04	50.11	50.07		
3	1	6	1.03±0.04	1.03	4.9±0.3	6.14±0.04	47.91	47.94	6.17	-0.16
	8	7	1.47±0.04	1.55	3.9±0.3	6.20±0.04	47.92	47.94		
4	1	5	1.81±0.06	1.81	11.5±0.5	6.41±0.04	46.71	46.74	6.45	0.10
	8	4	2.41±0.06	2.43	12.5±0.5	6.49±0.04	46.79	46.74		
5	1	4	2.64±0.08	2.64	18.6±0.6	6.62±0.04	46.16	46.20	6.67	0.80
	8	4	3.45±0.08	3.46	21.1±0.6	6.73±0.04	46.25	46.20		
6	1	8	7.43±0.10	7.44	36.5±1.0	7.94±0.04	43.77	43.83	8.15±06	2.10
	8	3	9.90±0.14	9.98	47.8±1.5	8.40±0.07	44.00	43.83		

sedimentary velocity under shot 8 must be 3.5 km/s, in contrast with 3.3 km/s below the north shot . As will be seen later, this conclusion is in agreement with the results of the interpretation of line C which also suggests a higher average sedimentary velocity at the south end of the profile. The final result of our first inversion model , based entirely on head waves arrival times, is shown in figure 23, illustrating a model of the earth's crust below line A, consisting of five layers over a half space.

Clearly , this model quite satisfactorily reproduces the observed first arrival times but its uniqueness is questionable. For instance, low velocity zones, if present in the section , cannot be detected by analysis of head waves alone since no head wave is possible from the top of the low velocity layer. Hence, further modelling , analysis of secondary arrivals , ray tracing and synthetic seismogram simulation were carried out in order to investigate the uniqueness of the initial model .

Quite prominent bursts of energy occur at various places on both record sections of line A . These secondary arrivals were correlated and analysed as reflected energy using the T^2-X^2 method as described in section 4.6 to obtain depths of the reflectors and interval velocities using Dix's formula. It must be mentioned that even after application of the 5-17 Hz bandpass filter , the reflections were partly obscured in the record sections. A filter of 6-14 Hz made the reflections much clearer to observe. The reflections

LINE A, INITIAL MODEL

S
SHOT8

N
SHOT1

3.50   KM/SEC

5.87

6.17

6.45

6.67

36.5

M O H O

8.15

47.8

1.3   KM

4.9

11.5

18.6

1.0

12.6

21.2

VERTICAL EXAGGERATION OF FOUR   50.000 KM
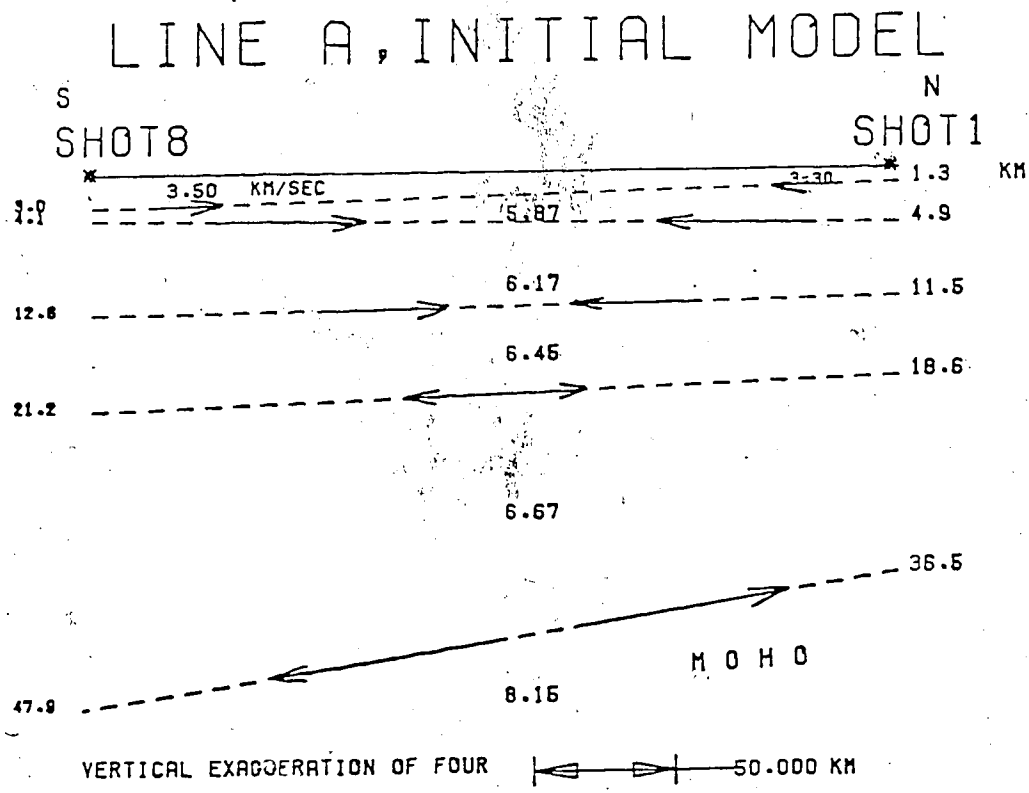
Figure 23.... First inversion model for line A

from the basement could not be identified in the records except only on the first trace of shot 1 (at t'=1s). However, the next two reflection branches (R3 and R4 in figures 21,22) are quite prominent in both sections, within the first 70 km. The depths of the reflectors, according to the T^2-X^2 method, are at 5.3 and 11.8 km below shot 1 and 5.9 and 12.8 km below shot 8. The interval velocity is 6.02 km/s for shot 1 and 6.07 km/s for shot 8. The next step was to compute the synthetic seismograms for these first three layers of our model. Agreement between observed and synthetic travel times and amplitudes of these two reflection branches is excellent for the following depths of the interfaces: 4.9 and 11.6 km below shot 1 and 4.1 and 12.1 km below shot 8, with $v2 = 5.87$ km/s, $v3 = 6.17$ km/s. These values were incorporated in the final model.

Continuing our interpretation we notice that the fourth travel time linear branch in both sections is considerably delayed with respect to the previous linear segment and as a result of this a notable break exists in the continuity of the first arrivals travel times. On the other hand the weak phases observed in both sections at offsets between 10 and 130km can be interpreted as reflections from an interface at 16.0 km, the corresponding head wave travel time branch from this interface being absent. These features provide a good hint on the existence of a low velocity layer in the upper crust below line A. Careful examination of the seismograms

shows that,in fact,the weak phases are the continuation of a quite prominent reflection branch,R5, clearly observed at shorter distances. The reflection branch corresponding to the delayed head wave arrivals is also identified and these two reflection branches are analyzed using the T^2-X^2 method. The results are: depths of reflectors at 16.3 km and 19.9 km below shot 1 and 17.8 km, 21.4 km below shot 8. Interval velocities are v(4)=6.33 km/s and v(5)=6.10 km/s which shows the presence of a thin low velocity layer situated on the top of the fifth layer of our initial model. Comparison of the synthetic and observed reflection branches at the boundaries of the low velocity zone indicates some disagreement concerning the amplitudes of the near vertical reflections: Synthetic amplitudes are much greater than the observed ones. To remove this discrepancy we decided to make the velocity contrasts at the top and the bottom of the low velocity zone gradational rather than first order discontinuities. This has negligible effect on the wide angle reflections amplitudes while reducing considerably the amplitudes of the near vertical reflections. The depths of the low velocity layer and its interval velocity as determined by the synthetic modelling are shown in fig 4 of the final model. The layer is slightly dipping to the south dip=0.4°.

Continuing our modelling towards greater depths, we notice quite prominent supercritical reflections, observable in both sections of line A, arriving later than the

reflections from the bottom of the LVZ are earlier than the
Pm branch. In fact, correlation of these events can be
continued without great difficulty toward shorter offsets,
establishing two new reflection branches R7 and R8 for each
record section of line A. No head waves arrivals
corresponding to these reflection branches can be
identified. The T^2-X^2 method yields the following depths of
the reflectors: 26 km, 28.9 km below shot 1 and 29.5 km,
33.5 km below shot 8. The interval velocity of the layer
bounded by these two interfaces is 6.03km/s indicating a
second low velocity below line A, this time in the lower
crust. This layer is embedded within the fifth layer of our
initial model which has an interval velocity of 6.67
km/s. Synthetic seismogram amplitudes however suggest that
these velocity contrasts, 6 km/s for LVZ2 and 6.63 km s
above and below the layer, are probably incorrect as they
give rise to very large amplitudes at near vertical
reflections from the top and the bottom of the low velocity
zone On the other hand, our ray tracing calculations
indicate that a velocity greater than 6.0 km/s would not fit
the observed times for the reflections at the bottom of the
low velocity layer. One then would be tempted to increase
the dip of the base of the LVZ2, which would give good fit
for one side of the profile but not for the other. Hence, we
insist on the velocity of 6.0km s for LVZ2 and we choose to
take the following two steps in order to reduce the
synthetic amplitudes of the near vertical reflections:

')Substitute the first order velocity discontinuity at the top of LVZ2 by a gradational velocity change (as in LVZ1)/ 2) Reduce the velocity contrast at the bottom of LVZ2 by considering a velocity of 6.5 km/s below the zone instead of 6.67 km/s and introduce an average velocity gradient of 0.05 km/s km in the lower crust, 0.045 under the north shot and 0.055 under the south shot. The result of these modifications is to obtain acceptable reflection amplitudes for LVZ2 and also to reduce considerably the synthetic amplitudes of near vertical reflections from the "Moho" which otherwise would be quite large in disagreement with the ovserved amplitudes.

Concluding our interpretation of line A we model the reflections from the Mohorovicic discontinuity. It must be mentioned that the Pn arrivals were of very small amplitude but due to the practically zero noise level they were quite unambiguously correlated, giving quite accurate intercept times and apparent velocities. Hence the results of the initial model showing that the Moho is dipping to the south by about 2.0 degrees must be reliable. However, the calculated depths must be slightly greater than the correct ones because of the absence of low velocity layers in the initial model.

Corr tion of the Pn arrivals is difficult both record sections of the profile. Unfortunately, because of the malfunction of some of our recording instruments, we have missed most of the reliable information for the

critical region of the Pm branch. However we were able to pick the reflections from the Moho mainly guided by rather clear supercritical and subcritical reflections. It is of interest at this point, in order to model these reflections, to consider the results of the ray tracing to take into proper account the true attitudes of the interfaces and especially the relatively steep dip angle of the moho discontinuity. (The synthetic seismogram program considers horizontal interfaces). In fact it is shown for the reflections from the Moho that there is a discrepancy as large as 1s between horizontal and true dipping model travel times for larger offsets. (At zero offset the two travel time branches will coincide). The ray tracing, inluding the previously mentioned velocity gradient in the lower crust gives depth of the moho at 35.3 km below shot 1 and 46.1 km below shot 8. For the purposes of the synthetic amplitude calculation of a horizontal Moho , the interface is positioned at the depths of the critically reflecting segments of the dipping interface. There is a notable disagreement between synthetic and observed amplitudes for the near vertical reflections. In fact, as one can see in the seismograms, extremely low amplitudes are observed in the first 25 km from the shot , for t > 7.0s, practically undistinguishable from noise. These extremely weak near vertical reflections can possibly be explained by roughness of the moho discontinuity. Also, synthetic amplitudes for

----

The T-Z method gives depth of the moho at 38.5 km below shot 1 and 48.5 km below shot 8.

the Pm critical region of shot 1 are quite large while no similar high amplitudes are observed in the record section of this shot. It is quite possible however that we would have observed them, had the recording at offsets between 120 and 150 km been successful.figure 24 and figure 25 show the final model of line A in cross section and in profile form respectively, while figure 26 shows the ray diagram for shot 1; figure 27 shows the travel time reflection branches as calculated by the ray tracing program;figure 28 and figure 29 show the synthetic seismograms for the final model.

Two alternative solutions

For modelling gravity data and for purposes of comparison with other continental crustal sections, it is convenient to have a simple one or two layer model of the crust. This model with a constant velocity or a simple gradient in the crust can be used to describe an area which laterally is very heterogeneous.

1) Starting from our final model for line A we would like to compute an alternative equivalent model (A1) consisting only of two layers over the half space: The sedimentary cover and an average structure for the crust with constant velocity. We invert the reversed Pn arrivals assuming a one layer crust to find and average velocity (below the sedimentary cover) of 6.4 km/s,or, we can calculate weighting factors for the detailed velocity structure of the final model, in which case we find v crust=

LINE A FINAL MODEL
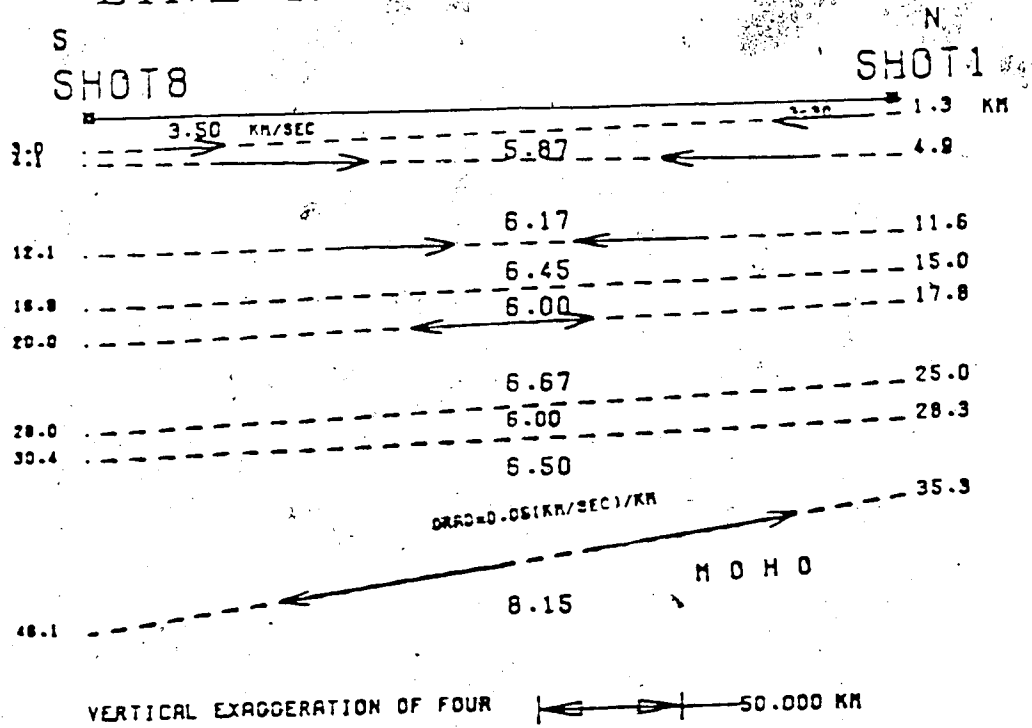
Figure 24.... Final model line A. Solid lines indicate where head waves or refracted rays provide direct evidence for an interface.
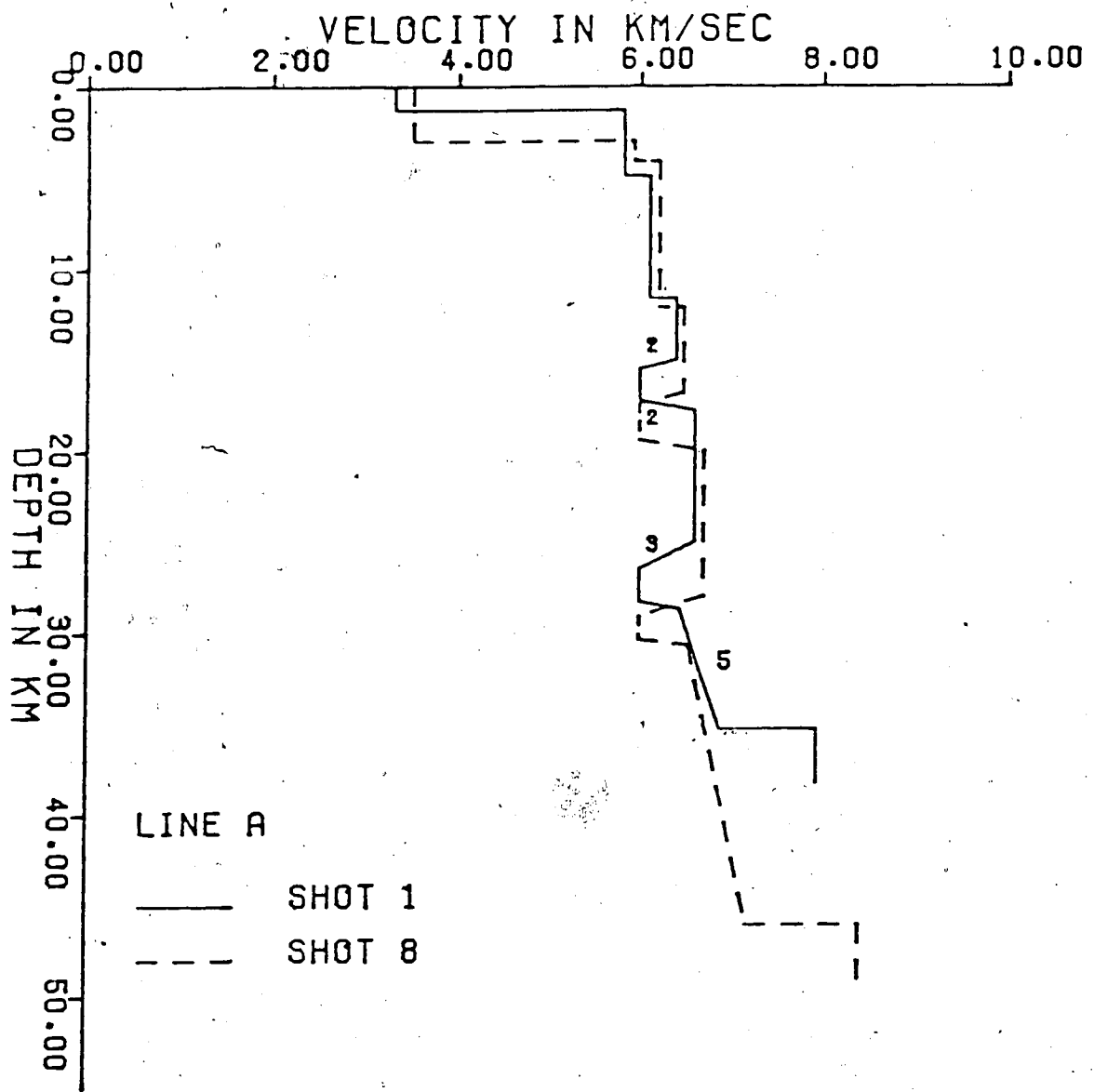
Figure/25.... Final model in profile form for line A.The
numbers near the segments of the velocity-depth function are
the numbers of layers used for the approximation of the
velocity gradients.

RAY TRACING FOR LINE A SHOT 1

M O H O
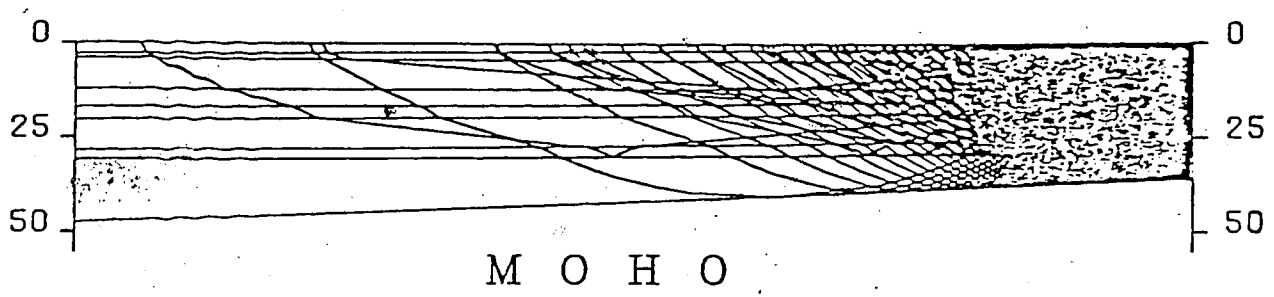
Figure 26.... Ray diagram ,line A shot 1
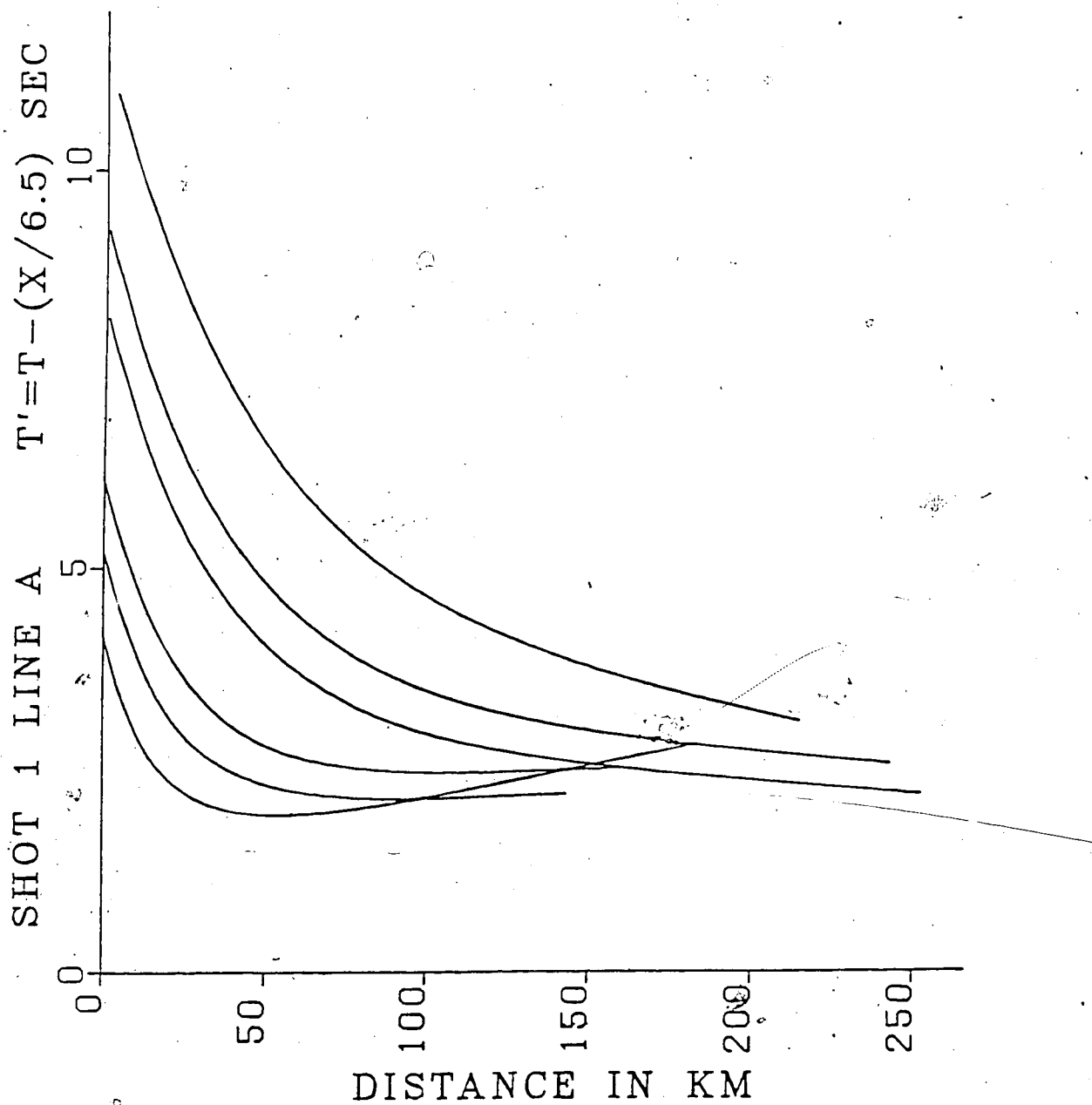
Figure 27.... Theoretical reflection travel-time branches performed by ray tracing, shot 1.

SHOT 1 LINE A
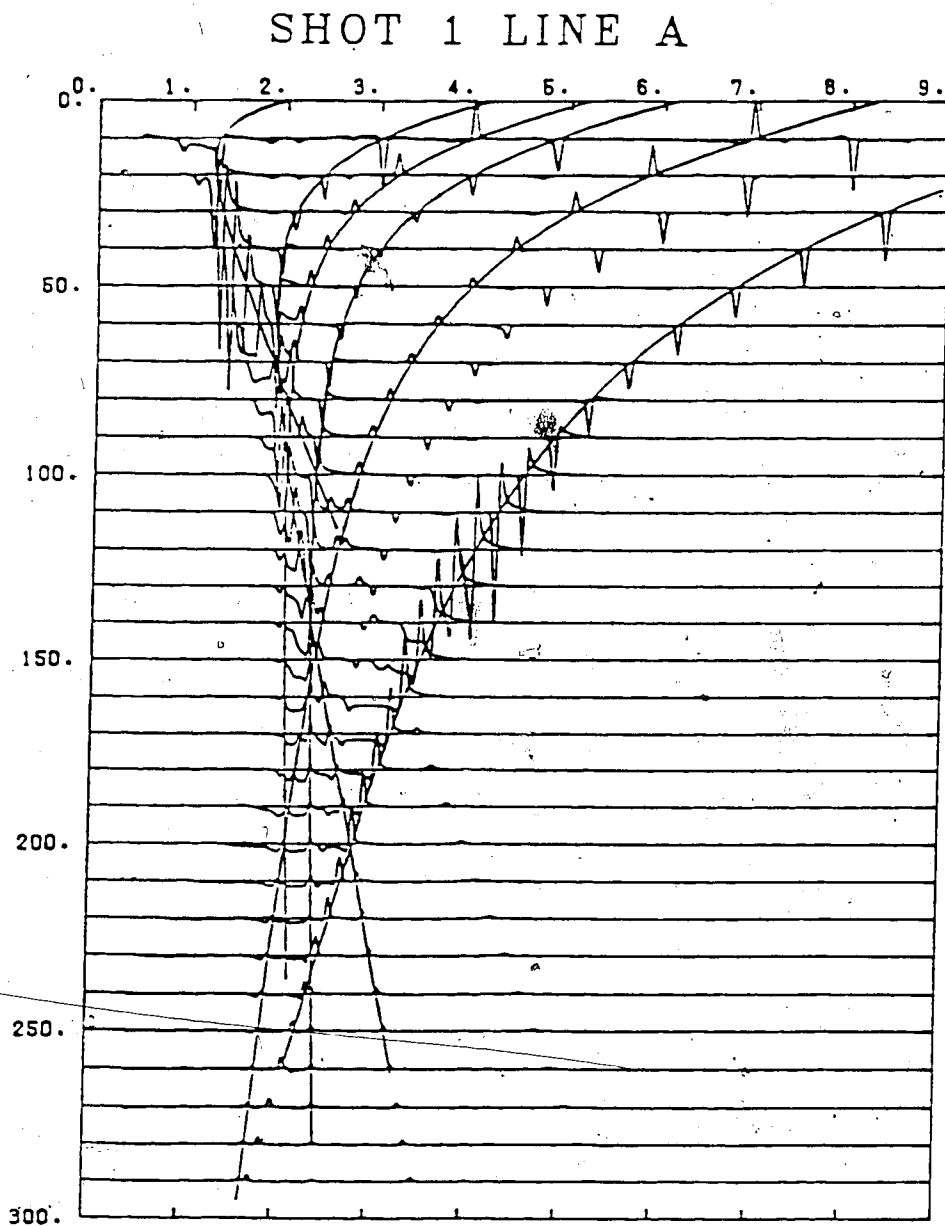
Figure 28.... Synthetic vertical component seismograms for the final model A shot 1

SHOT 8 LINE A
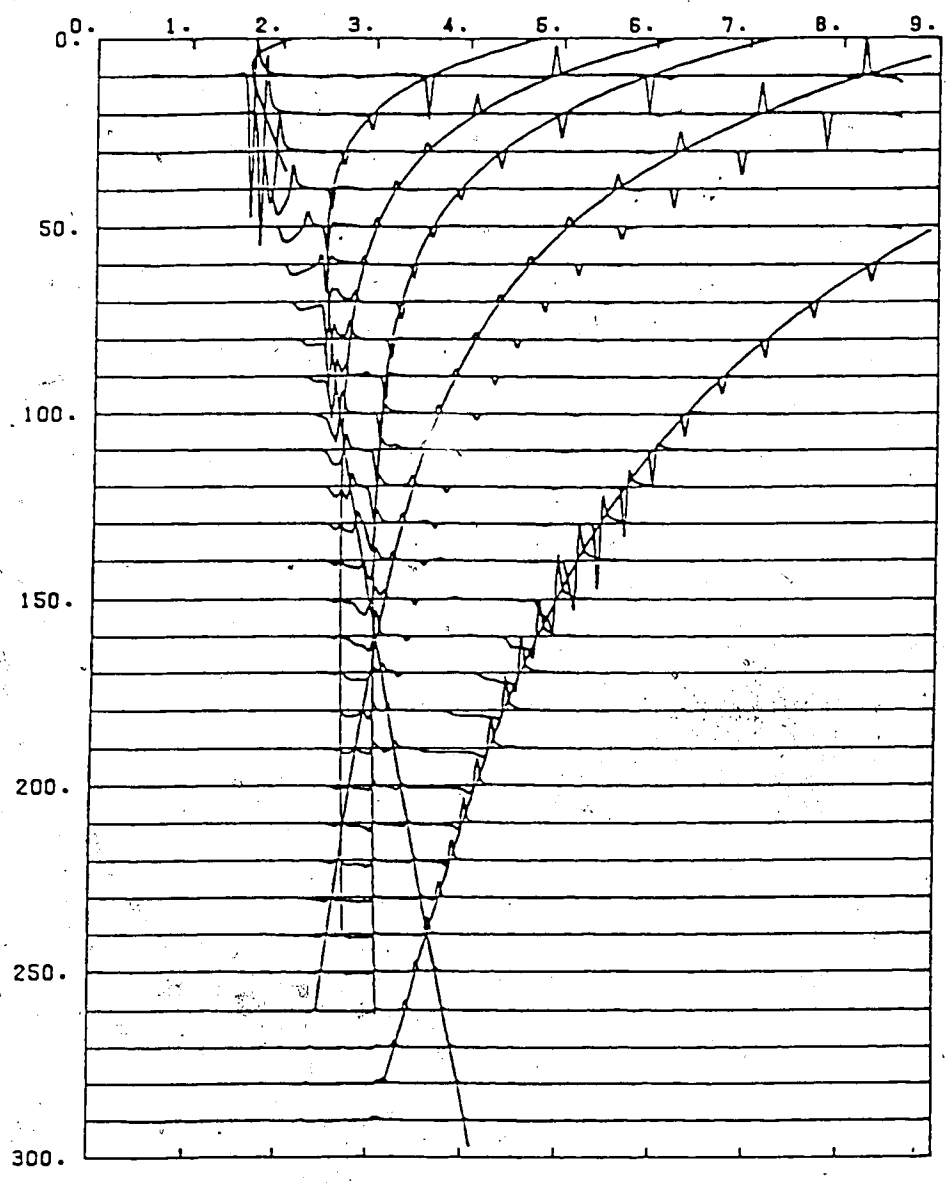
Figure 29.... Synthetic section shot 8

6.36 km/sec for shot 1 and 6.53 km/sec for shot 8.

2)Finally we would like to compute a model (A2) of a constant velocity gradient k within the crust. The velocity function will be $V(z)=V_0+k(z-z_0)$. where z_0 is the depth of the basement and $V_0=5.87$km/sec. Then the one way vertical travel time t for a ray travelling through this velocity structure will be $t = \frac{1}{k} \ell_n \frac{V_0+kZ_{max}}{V_0+kZ_0}$ where Zmax is the depth of the Moho. Then $k= \frac{V_0}{Z_{max}} (e^{kt}-1)$ This equation is solved by the aid of the computer in an iterative manner to find the best value of k that will fit the observed travel time $t=(Zmax-Z_0)/Vcrust$. The result is k=0.0262 sec^{-1}, Vm (=velocity at the vase of the crust)= 6.76 km/sec for shot 1 and k=0.0276 sec^{-1}, Vm = 7.06 km/sec for shot 8.figure 30 shows the two alternative models in profile form.

5.2 Interpretation of line B

Very low noise level and clear first breaks are observed on both record sections of line B which are shown in figure 31 and figure 32. An exception are the Pn arrivals of shot 3 which are severely disturbed by noise.Correlation of these events became possible,although still somewhat ambiguous, after application of a 5-12 Hz bandpass filter.Correlation of the first breaks yields five linear travel time segments for shot 4 and six for shot 3.Their apparent velocities as well as intercepts and reciprocal times were determined (table 3).It is noticed immediately

TABLE 3

First Inversion Model For Line B.
(V(1)=3 4km/sec)

The headers of the columns are defined as follows:
I – Interface.
S – Shot number.
N – Number of records used in least squares.
Rt_0 – Record t_0 (sec).
Mt_0 – Model t_0 (sec).
Depth – Depth of the interface (km).
V app – Apparent velocity (km/sec).
RRT – Record Reciprocal Time (sec).
MRT – Model Reciprocal Time (sec).
Vtr – True velocity (km/sec).
DIP – Dip of interface (degrees).

| I	S	N	Rt_0	Mt_0	DEPTH	V app	RRT	MRT	Vtr	DIP
2	3	3	0.59±0.03	0.59	1.3±0.1	5.66±0.04	51.70	51.90		0.18
	4	3	1.06±0.03	1.10	2.2±0.1	5.76±0.04	51.40	51.90	5.70	
3	3	5	0.83±0.04	0.82	3.3±0.3	6.00±0.04	48.50	48.70	6.00	0.14
	4	5	1.28±0.04	1.32	4.0±0.3	6.10±0.04	48.90	48.70	6.10	
		3	1.25±0.05	1.25	7.0±0.5	6.21±0.04	47.70	47.70	6.21	0.0
		3	1.81±0.05	1.80	8.7±0.5	6.37±0.04	47.10	47.20	6.37	0.0
5	3	7	1.65±0.07	1.64	12.0±0.6	6.36±0.04	47.20	47.20	6.36	0.0
	4	9	2.52±0.04	2.52	15.8±0.4	6.62±0.03	46.30	46.30	6.62	0.0
6	3	4	3.89±0.09	3.87	26.9±1.1	6.80±0.05	46.10	46.13	6.80	0.0
	4	–	––	––	––	––	––	––	––	–
7	3	3	8.52±0.30	8.56	46.5±2.0	7.90±0.20	45.12	45.06	7.90	0.0
	4	5	9.90±0.10	9.93	49.0±1.3	8.36±0.05	44.54	44.50	8.36	0.0

Figure 30.... Constant velocity and constant velocity
gradient model for line A
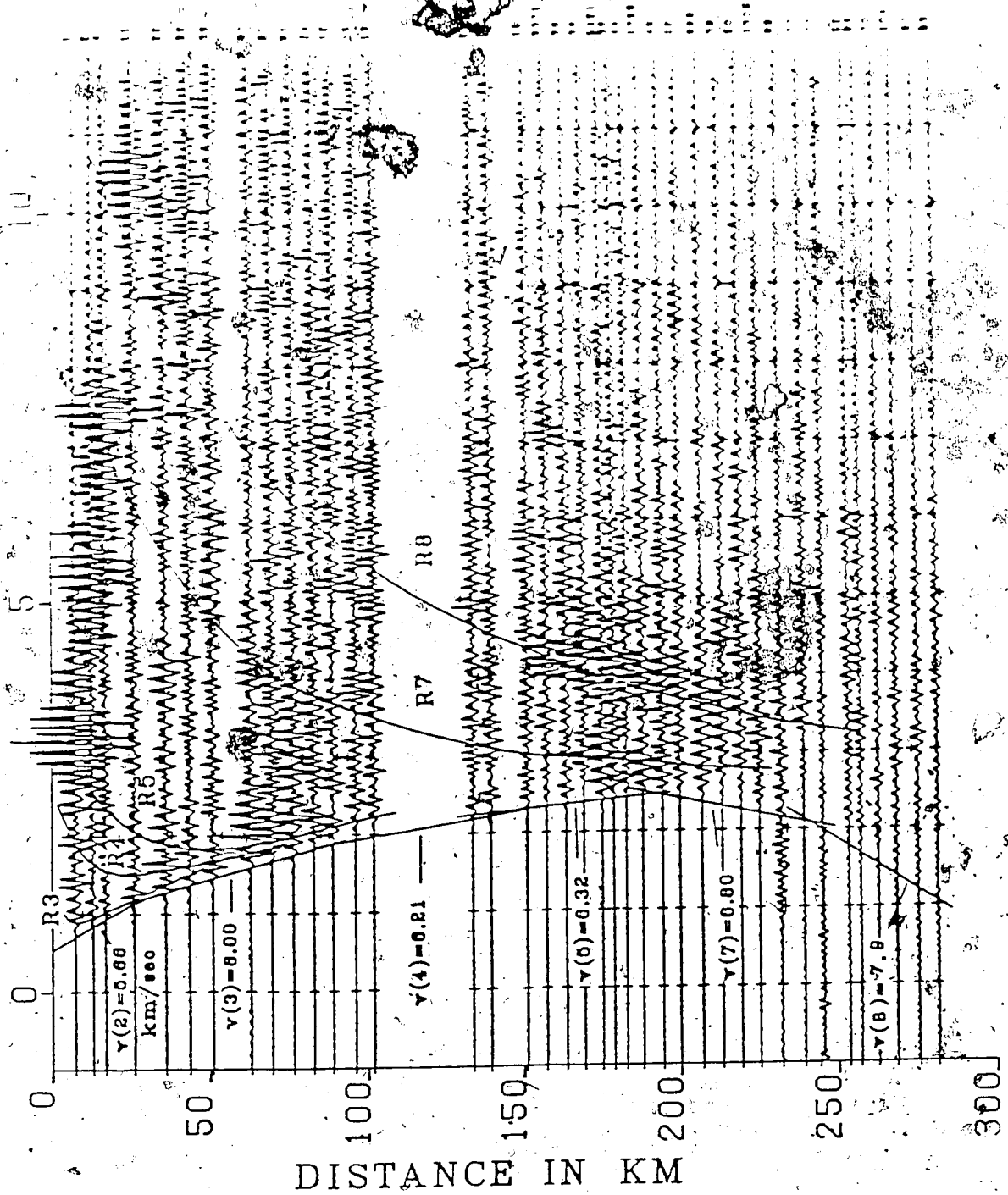
Figure 31.... Record section of line   shot 3
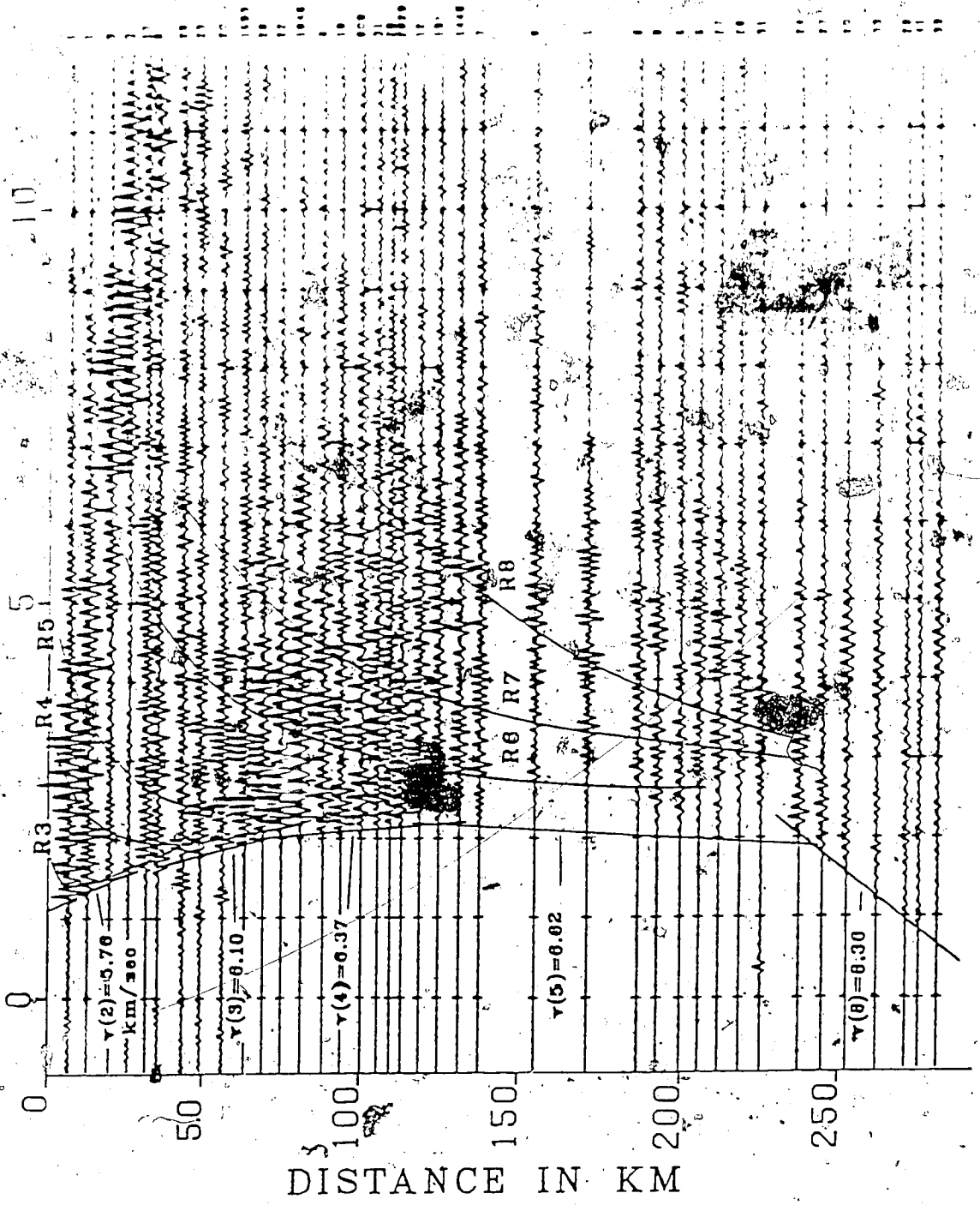
Figure 32.... Record section shot 4.

that unlike line A agreement of reciprocal times is poor except from the fir two interfaces and the reciprocal times of the SW shot are inconsistently lower than those of the NE shot.

For the purposes of creating a first inversion model and because of these discrepancies in the reciprocal times, the two sets of data were treated as independent sections,assuming that apparent velocities are true velocities their differences being entirely due to lateral heterogeneity and not to the dips of the interfaces which all but the first two will be considered horizontal.The first inversion scheme outlined in line A was used to yield the depths of the interfaces from the intercept times. The result is the initial model shown in fig.1 and table 3. The model successfully duplicates the observed head wave times but considerable effort was expended in determining the extent to which this initial velocity structure satisfied other information.

Reflected phases in line B are quite clear and certainly not of the complexity observed in line A. Furthermore, very prominent critical reflections are observed on the records almost for all the reflection branches.These critical reflections provide an additional useful constraint for our modelling,since the distances and times of the critical reflections as calculated for the derived model can be compared with the observed ones.

Analysis of the first reflection branch gives depths of the interface at 3.3 km below shot 3 and 4.0 km km below shot 4, in agreement with the results of the initial model. Interval velocity is 5.70 km s. Average velocity of the sedimentary layer is 3.40 km s which gives correct depth of the basement at both ends of the profile. The second reflection branch is clearly observed in both sections within the first 70 km. The critical reflection of this branch is observed at x=37 km, t'=1.5s, for shot 3. It is not so well defined however for shot 4. Depth of the interface is 6.9 km below shot 3 and 9.1 km below shot 4, as determined by the ray tracing calculations which also suggest that a slight lateral velocity heterogeneity (6.02 km/s vs. 6.10 km/s) must be introduced in this layer in order to fit satisfactorily the observed times. The calculated critical distance is Xcritical=36 km ,T'critical=1.5s for shot 3, and Xcritical=47 km ,T'critical=1.96s for shot 4. These figures are in good agreement with the observed ones.

Critical reflections are very prominent for the next reflection branch in both record sections. They are observed at Xcrit.=63 km T'crit.=1.90s for shot 3 and Xcrit=71 km, T'crit.=2.20s for shot 4. According to the ray tracing travel time calculations the depth of the reflector is at 11.2 km below shot 3 and 13.9 km below shot 4. The calculated values for the critical reflections are: Xcrit.=62 km, T'crit=1.90s for shot 3 and Xcrit=70 km

,T'crit=2.24s for shot 4, in good agreement with the observed values.It is noticed however that the depth of the interface below shot 4, as determined by the reflection arrivals-13.9 km- is in notable disagreement with the depth as determined by the head wave arrivals -15.8 km-. To explain this discrepancy we must first keep in mind that the reflecting segments of the interface that give rise to the observed retrograde branch (shot 4) are confined within the first 50 km ,while the head wave first arrivals information comes approximately from the middle of the interface (see arrows in figure 33). Hence it is suggested that the interface is broken the position of the fault shown in figure 34,justified by the fact that no break in the travel time branch of the head waves is observed in the records. The head wave first arrivals (shot 4) are coming from the downthrown block of the fault giving rise to a greater intercept time which is translated to a depth of 15.8 km. The throw of the fault is about 1.5 km. Interval velocity is 6.23 km/s at the NE side of the profile and 6.30 km/s for the SW. Continuing our modelling and after careful examination of the seismograms we notice the following. One additional reflection branch (R7) arriving before Pm can be identified for shot 3. The head wave travel time segment corresponding to this branch has an apparent velocity of 6.80 km/s. On the other hand, two reflection branches R6 and R7,arriving before Pm can be identified for shot 4 while head wave arrivals corresponding to these reflections are

INITIAL MODEL

SW   NE
SHOT4   SHOT3

```
0.0  ×————————————————————————×  1.3 KM
2.2  ——3.40 KM/SEC——————————  3.40——  
4.0  ——5.70——————————————→  5.70——  3.3
                                    6.00——  7.0
8.7  ———6.10——————————→         
                                    6.21——  12.0
                        ←————————————
15.8 ——6.37——————————————→

                                    6.36

                        ←——————————————  26.9

                              6.80

6.62
```

```
        ←————— 46.5KM
     7.90  KM/SEC    49.0——————→
                        8.36 KM/SEC
                    M O H O
VERTICAL EXAGGERATION OF FOUR  |←——|——→|——50.000 KM
```
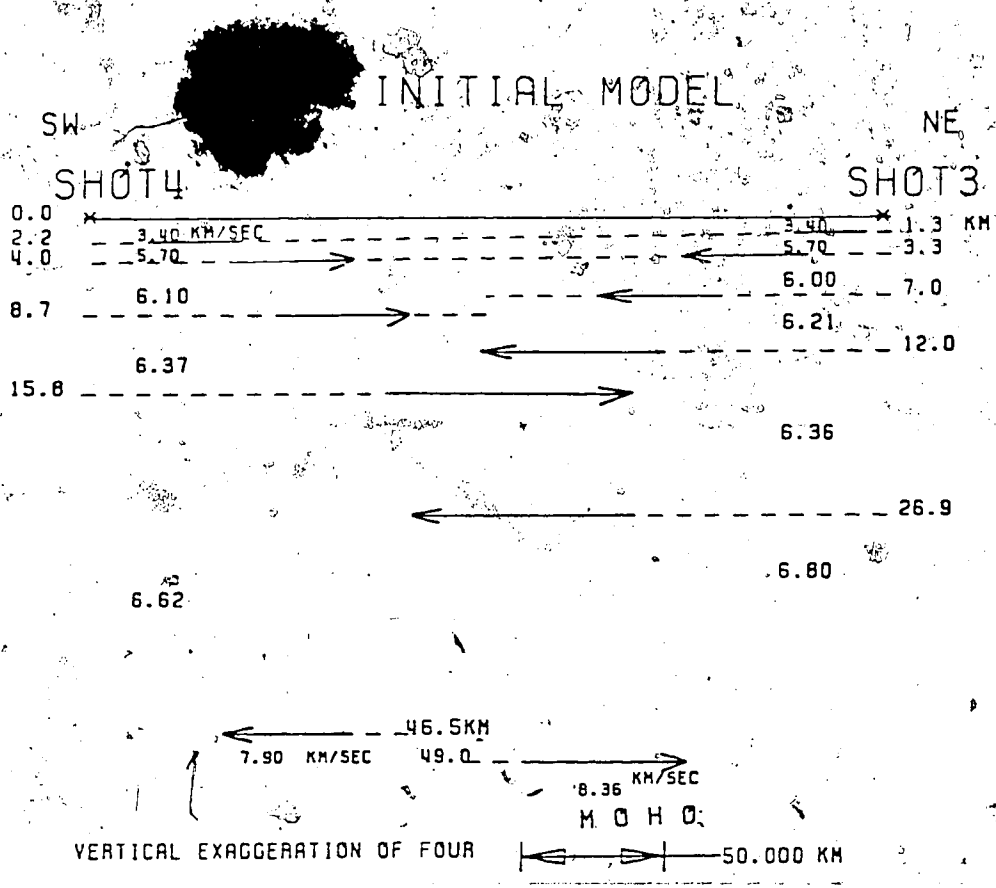
Figure 33.... First inversion model line B.

LINE B, FINAL MODEL

SW   .NE

SHOT4   SHOT3

2.2   3.40 KM/SEC   1.3 KM

4.0   5.70   3.3

6.10   02   6.9

9.1   6.23   11.4

6.30

13.9

6.48   6.44

24.7

6.00

31.0   28.4

6.77

40.0

6.87   44.5

47.0

47   M O H O

8.15

VERTICAL EXAGGERATION OF FOUR |◁——▷|——50.000 KM

Figure 34.... Final model line B   .Solid lines indicate where head waves provide direct evidence for an interface.

absent in the records. Consequently these two reflection branches are analyzed by the T^2-X^2 method which gives depths of the interfaces at 26 and 32 km respectively (shot 4). The interval velocity was 6.05 km/s while interval velocity between R5 and R6 was 6.50 km/s. Hence , R6, R7 are the reflections from the top and the bottom of a low velocity zone situated in the middle crust below line B. However, absence of R6 for shot 3 shows that this zone is absent under the NE portion of the profile. This represents a significant lateral heterogeneity in our model. Absence of head wave arrivals from the interface at 28.4 km for shot 4 is explained by the presence of the LVZ which sufficiently delays these events not allowing them to appear as first arrivals. Due to their weak amplitudes they could not be detected as secondary arrivals in our records.

Concluding our interpretation we would like to map the Moho discontinuity of the crust below line B. This was not an easy task since reliable information from the Moho was limited. Although Pn arrivals for shot 4 were quite clear, Pn for shot 3 were very ambiguous. The Pm group was well defined for shot 3 but not so well for shot 4 especially for the subcritical region where amplitudes were very low. However, the critical reflection was very clearly observed at Xcrit=130 km, T'crit 5.40s .

We start from the initial model of a horizontal moho as shown in the first inversion model, fig 33: Depth of 49 km below shot 3 and depth of 46.5 km below shot 4. We would

like now to repeat the initial inversion of the Pn arrivals
to include the effect of the low velocity layer. We
calculate the extra time the rays are spending within the
low velocity zone to conclude that the depths of the moho
must be reduced by 0.5 km. Then the new depths will be:48.5
km and 46 km respectively.

The next step is to calculate the true dip of the
interface. We invert the reliable Pn arrivals of shot 4
assuming VMoho=8.15 km/s. The calculations suggest depth of
Moho at 40.0 km below shot 3 and 51.7 km below shot 4 (dip
angle=2.3 °) which gives an excellent agreement between
calculated and observed Pn arrival times, shot 4 We must
keep in mind, however that these observed Pn arrivals are
coming from a limited portion of the moho discontinuity. The
exact position of the refracting segments which give rise to
the observed first arrivals is shown by the arrows in
fig.33. Subsequently we would like to model the position of
the reflecting segments of the interface. Hence we ray trace
the reflections from the Moho and starting from the SW side
of the profile we notice a clear disagreement between the
calculated and observed times. Calculated reflection times
are significantly greater than observed ones. In particular,
the calculated Xcritical is at 142 km and T'critical is
6.10s, while observed Xcritical is 130 km , T'critical=5.40s
. One might think to remove this discrepancy by increasing
the velocity v(7). This will eliminate the disagreement
between calculated and observed critical times. However, it

will give an even larger value for Xcritical due to the reduced velocity contrast at the base of the crust. Therefore, as the only alternative left, we conclude that the Moho is faulted below line B, the upthrown block being under the SW side of the profile. The throw of the fault is about 2.5 km as shown in fig.4 of the final model. Agreement between theoretical and observed Pm for the SW side of the model is now good. Calculated Xcrit. is 125 km, T'crit is 5.55s . Agreement between calculated and observed Pm is also satisfactory for the NE side of the model although there is some indication that the dip angle of the moho at the subcritical region might be less than 2.3.

The final model in profile form is shown in figure 35 ;figure 36 is the ray diagram, shot 4,while figure 37 shows the travel time calculations;figure 38 and figure 39 show the synthetic seismograms for line B, calculated according to the final model. Agreement between synthetic and observed amplitudes is good.

Finally, we compute the two alternative models B1 and B2 for line B, following the same steps outlined in the interpretation of line A. The results are illustrated in figure 40 and table 4.

TABLE 4

Alternative solutions for line B.Depths of Moho and Pn velocity same as in model B.

| MODEL	SHOT 3	SHOT 4
B1	Vcrust=6.44km/sec	Vcrust=6.38km/sec
B2	$K=0.0372sec^{-1}$ $V_m=7.14km/sec$	$K=0.0286sec^{-1}$ $V_m=6.98km/sec$
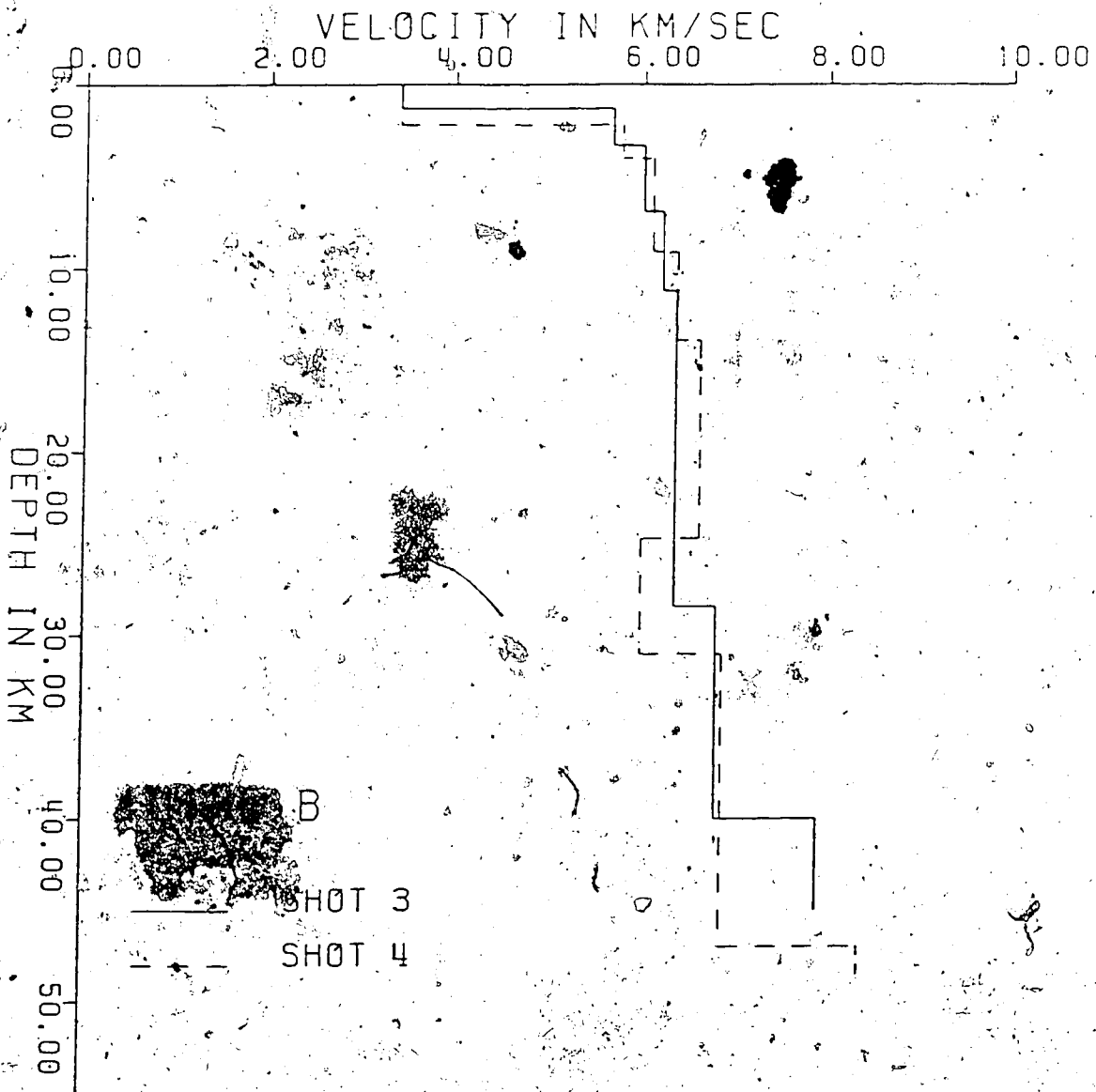
Figure 35.... Final model B in profile form.

RAY TRACING FOR LINE B SHOT 4

M O H O
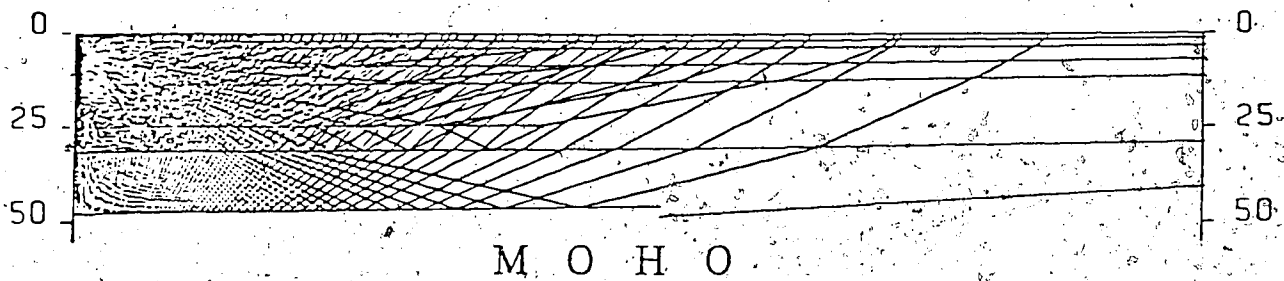
Figure 36.... Ray diagram, line B shot 4.
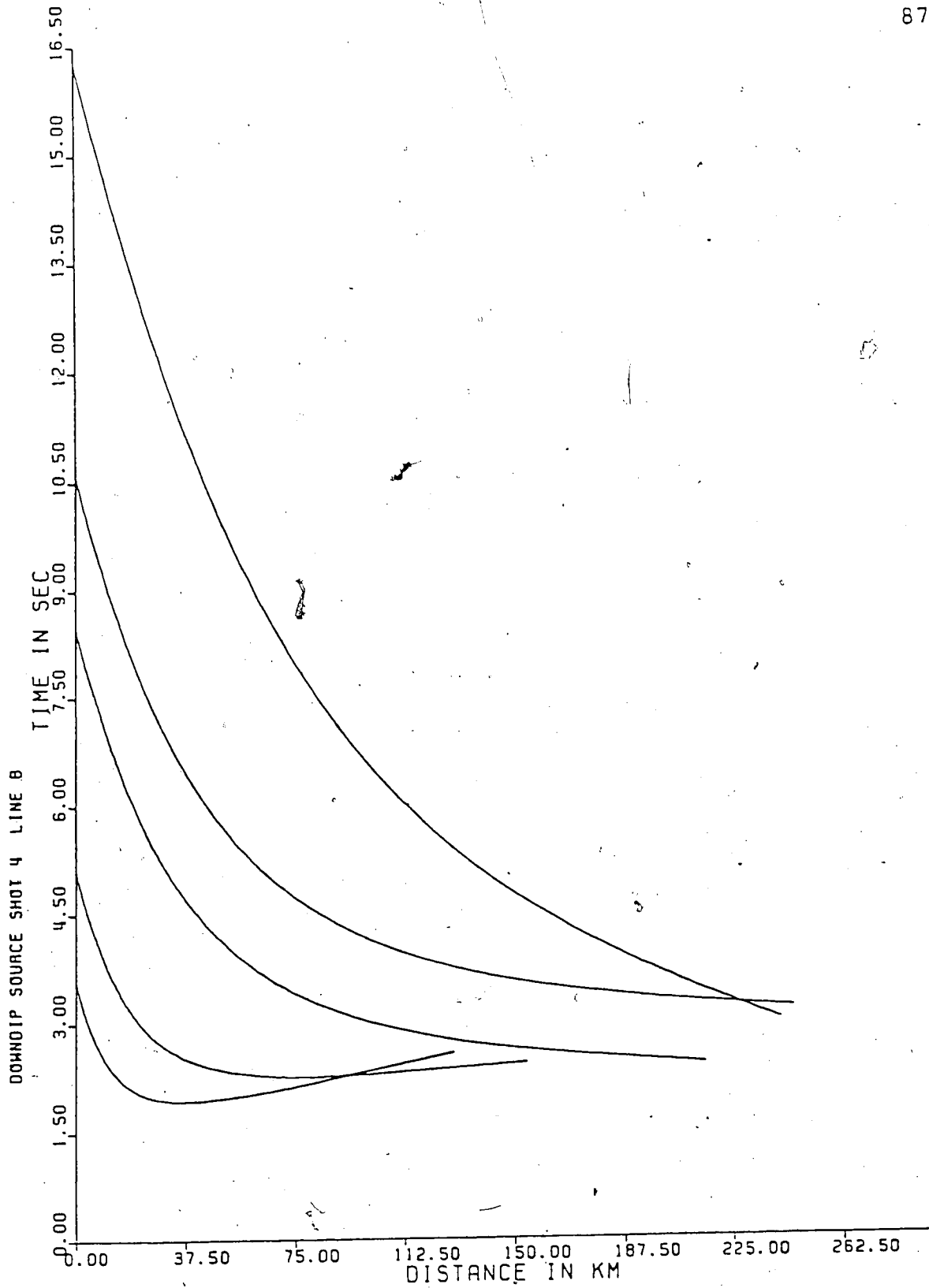
Figure 37.... Theoretical travel time calculations, shot 4.

SHOT 3 LINE B
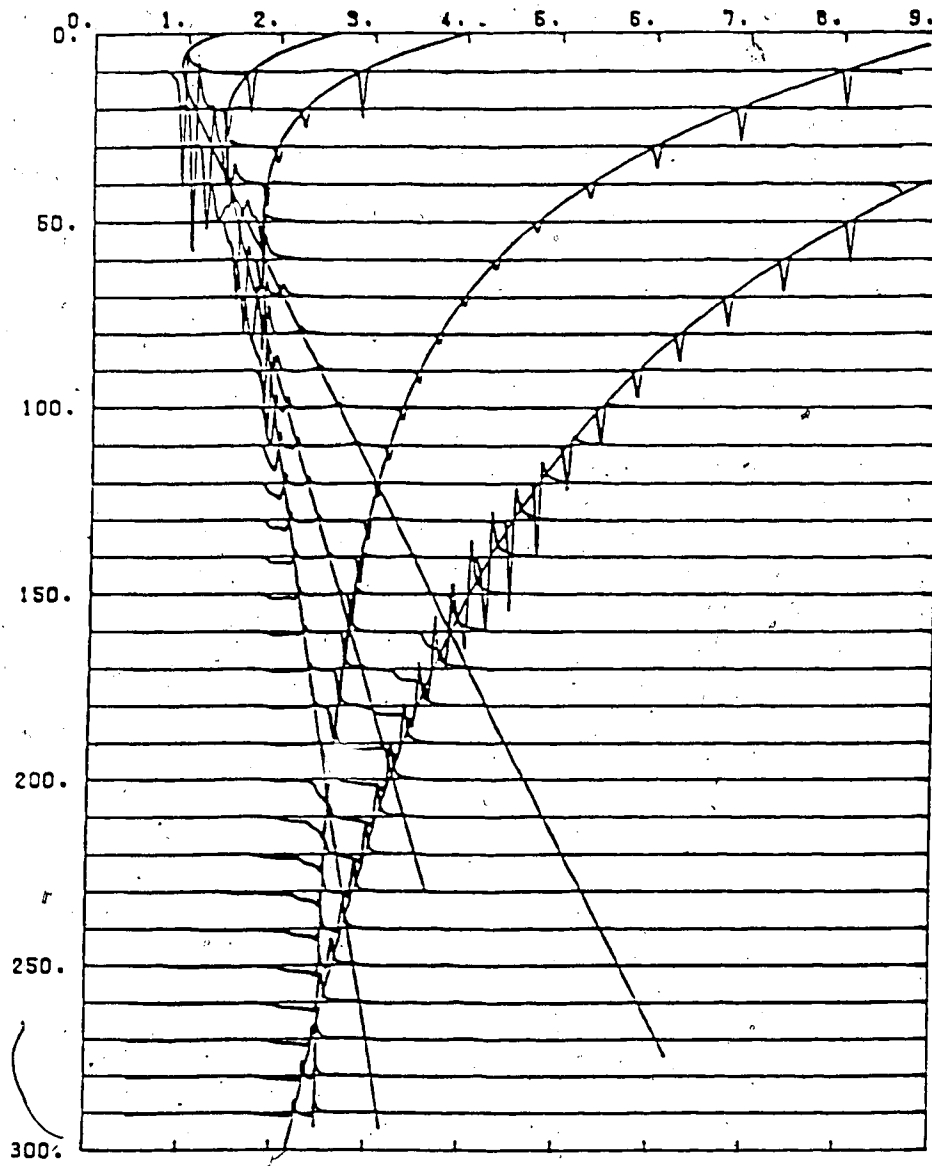
Figure 38..... Synthetic section shot 3

SHOT 4 LINE B
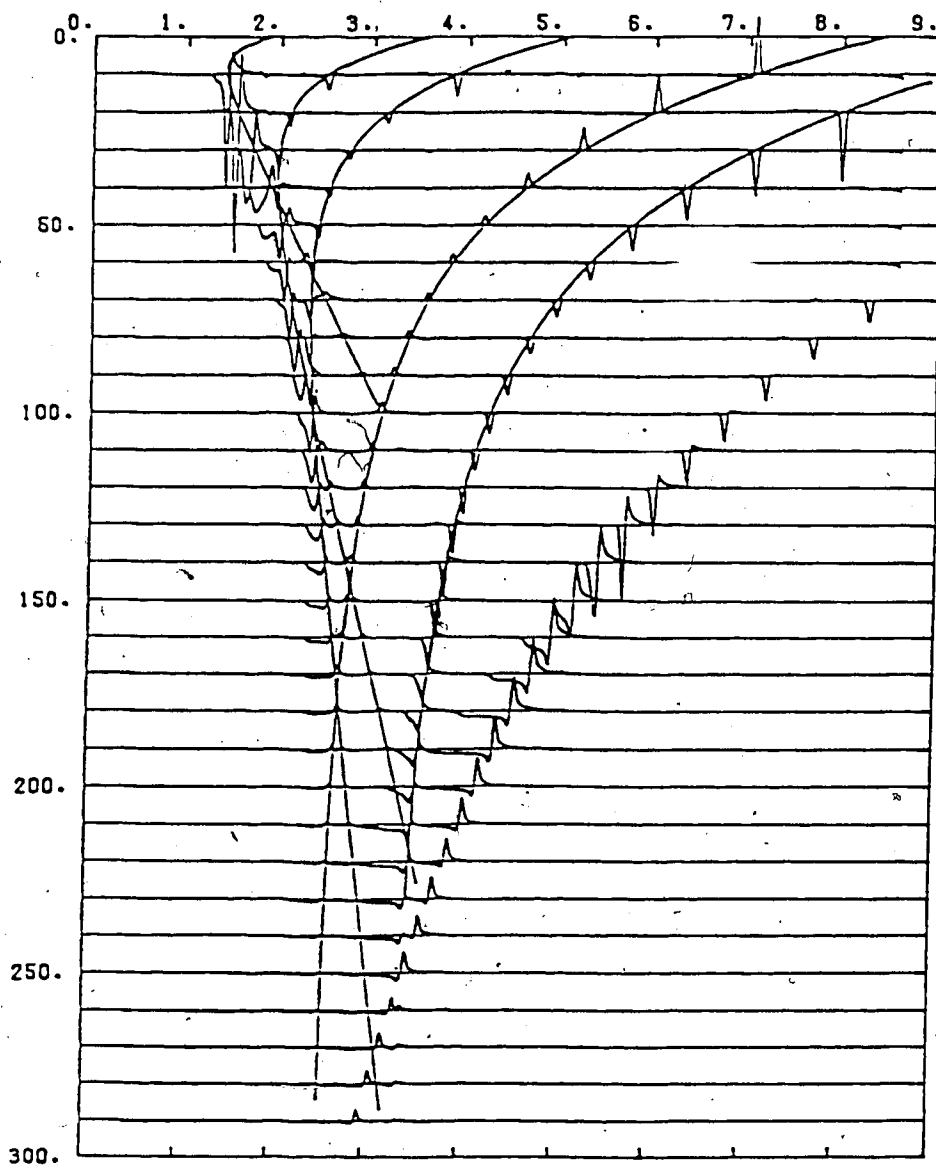

Figure 39.... Synthetic section shot 4.
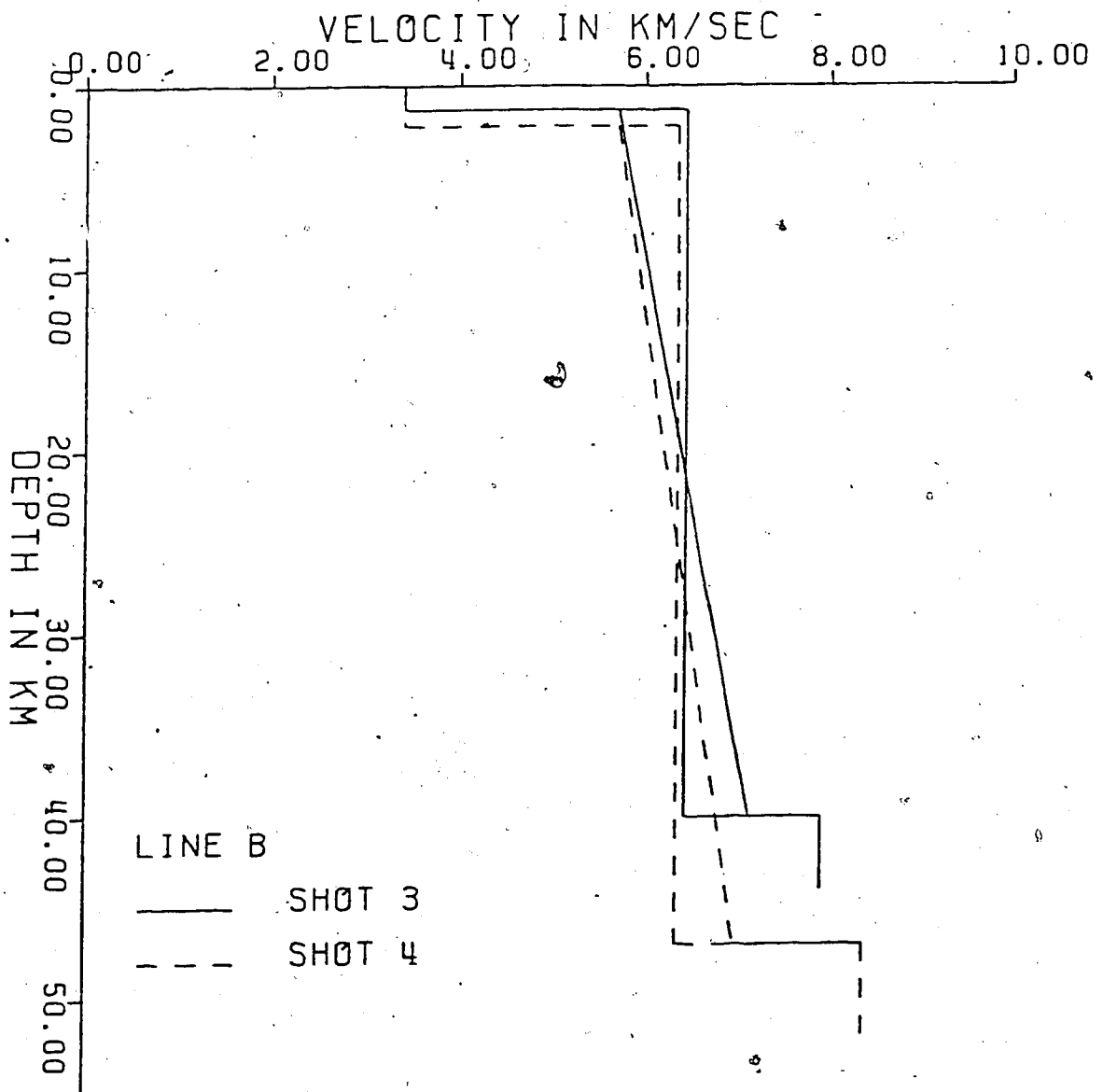
Figure 40.... Two alternative solutions for model B.

5.3 Interpretation of line C

The data for line C are presented in figure 41 and figure 42.First arrival information was reliable for both shots of the profile with the exception of the Pn arrivals of the southeast shot (shot 9) which were rather poor. Careful correlation, of the first, breaks yields four linear travel time segments for each record section.We start our initial inversion assuming an average sedimentary velocity of 3.3 km/s for both sides of the profile. This gives depth of the basement at 2.3 km below shot 6 and 2.5 km below shot 9. However, this latter value is slightly low according to basement wells information, which suggests a depth close to 3 km. This requires an average sedimentary velocity of 3.6 km/s for the SE side of the profile. Then, calculated head wave arrivals for this first layer of our model successfully duplicate the corresponding observed times (table 5).The next set of observed head wave arrivals observed between 30 and 90 km is of a split-nature consisting of two parallel to each other linear travel time segments, displaced with respect to each other by 0.1s . These discontinuities in time could be explained neither by a sudden change in elevation at the corresponding recording sites nor by near surface velocity irregularities since no

TABLE 5

First Inversion Model For Line C.
(V(1)=3.3km/sec under shot 6)
(V(1)=3.6km/sec under shot 9)

.The headers of the columns are defined as follows:
I – Interface.
S – Shot number.
N – Number of records used in least squares.
Rt_0 – Record t_0 (sec).
Mt_0 – Model t_0 (sec).
Depth – Depth of the interface (km).
V app – Apparent velocity (km/sec).
RRT – Record Reciprocal Time (sec).
MRT – Model Reciprocal Time (sec).
Vtr – True velocity (km/sec).
DIP – Dip of interface (degrees).

| I	S	N	Rt_0	Mt_0	DEPTH	V app	RRT	MRT	Vtr	DIP
2	9	3	1.21±0.03	1.23	3.1±0.1	5.67±0.04	52.05	52.30	5.60	0.16
	6	2	1.14±0.03	1.13	2.3±0.1	5.54±0.04	53.15	52.70		
3	9	3	1.59±0.04	1.62	4.7±0.3	6.22±0.04	48.05	47.90	6.19	0.14
	6	3	1.45±0.04	1.44	4.0±0.3	6.14±0.04	48.45	48.20		
4	9	8	2.50±0.06	2.51	13.4±0.4	6.47±0.04	47.06	46.86	6.47	0.00
	6	11	2.65±0.06	2.62	13.4±0.4	6.62±0.04	45.96	45.85	6.62	0.00
5	9	2	8.10±0.04	8.14	38.2±2.7	7.94±0.25	44.20	44.12	8.10	-1.00
	6	4	8.90±0.01	8.91	43.2±1.1	8.27±0.06	43.80	44.12	±15	
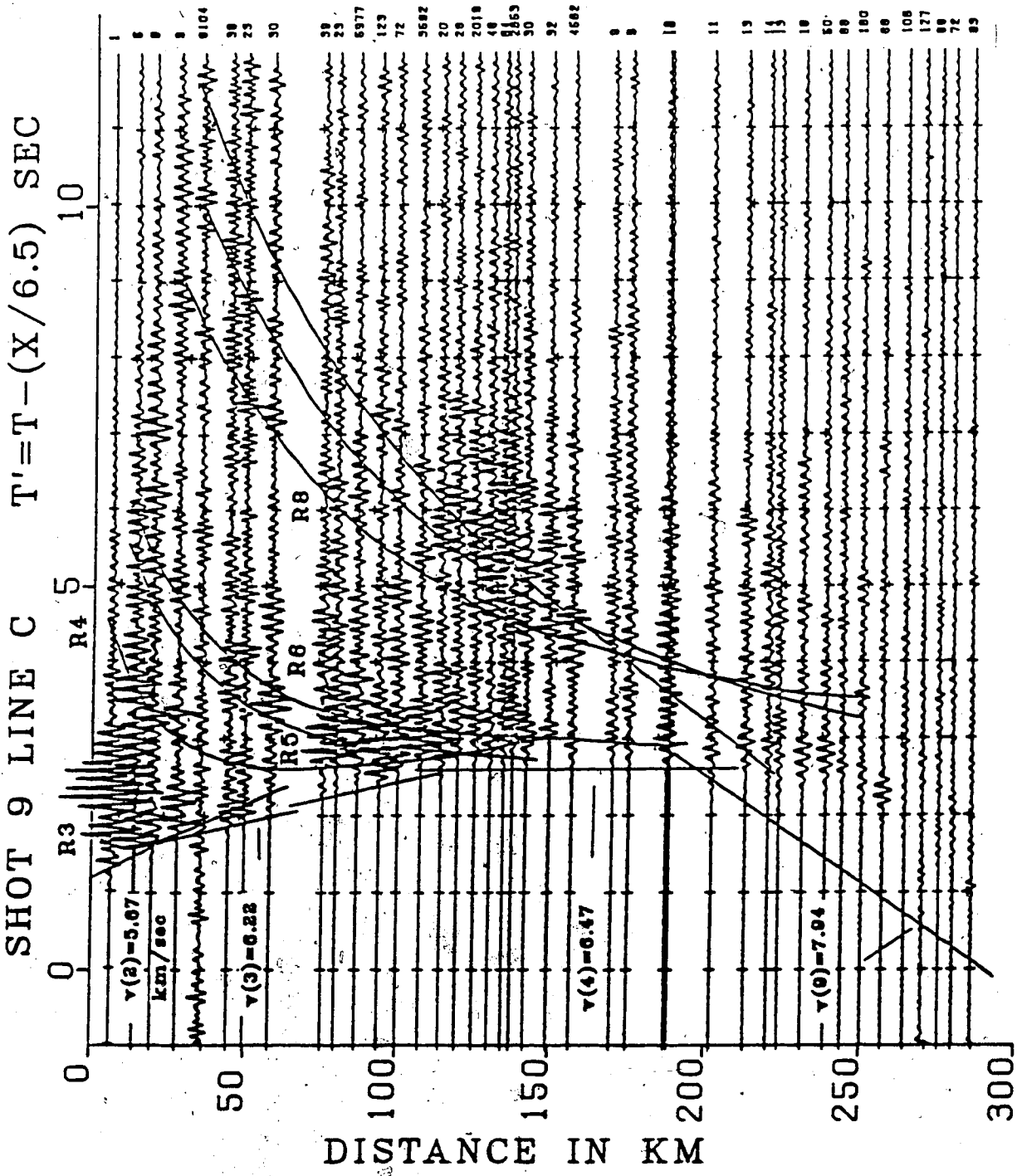
Figure 4.1.... Record section, profile C, shot 9.
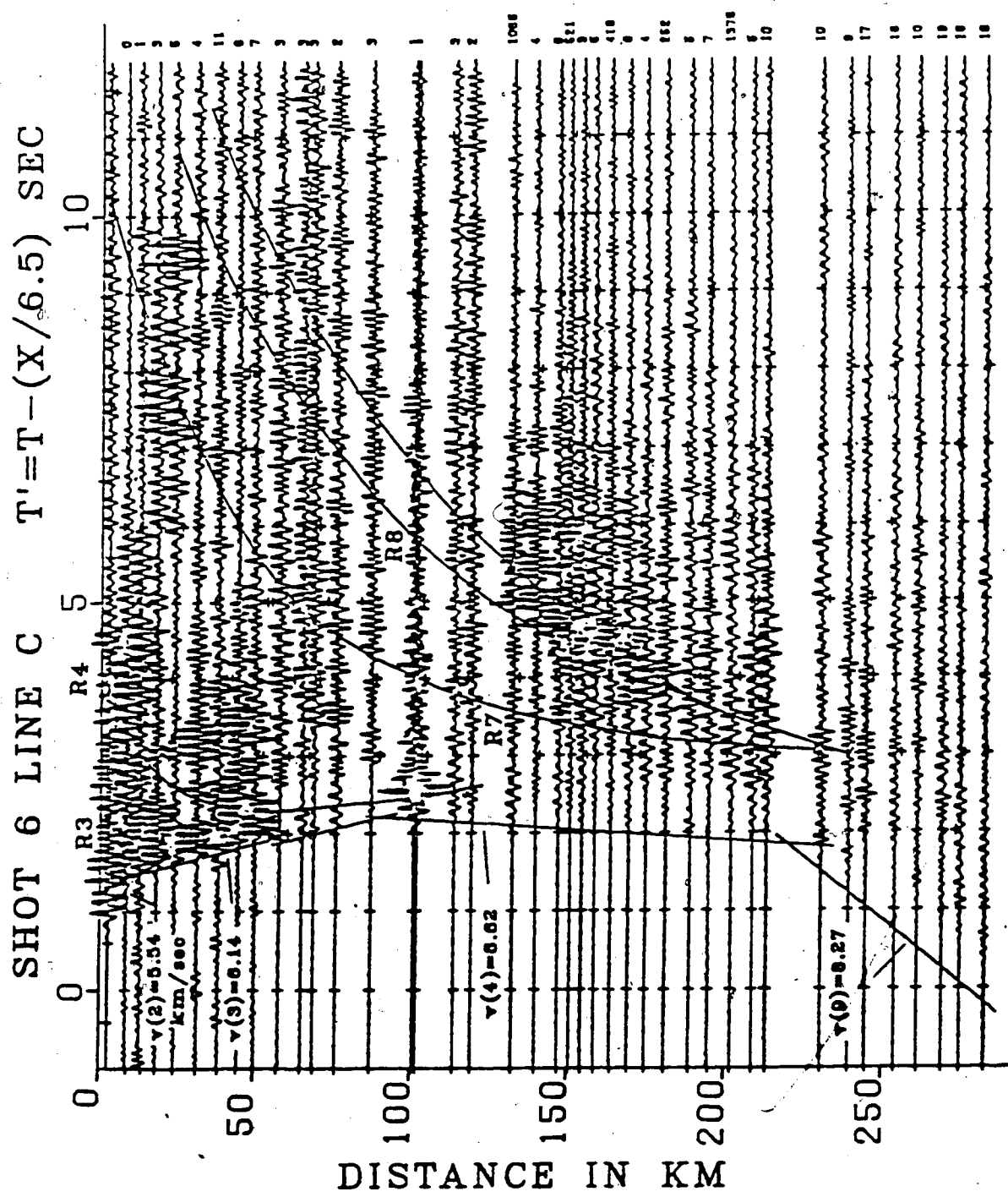
Figure 42.... Record section shot 6.

similar time displacements are observed for the secondary arrivals identified within the same offset range. Hence they must be attributed to the refractor itself and in fact our interpretation is a step-like interface at a depth of 4.5 km below shot 9 and 4.0 km below the reverse shot. Interval velocity is 5.60 km/s. The observed head wave times from this interface, mentioned in table 5, correspond to the near the shot arrivals of the split head head wave travel time segments. The throw of the steps is less than 1 km.

The next travel time segment is very well defined for both shots at offsets between 90 and 190 km. Its apparent velocity is 6.47 km/s for shot 9 and 6.62 km/s for shot 6. It seems however that these differences of the apparent velocities are not associated with the true dip of the refractor but rather with differences in true velocities at the two sides of the profile. This argument is supported by the large discrepancies observed in the reciprocal times of these arrivals-reciprocal time for the shot 6 travel time segment being smaller by 1.1s than that of the reverse shot. Hence, for the purposes of a first inversion based on head wave arrivals we prefer to treat this refractor as horizontal and we invert the data assuming true velocity of 6.62 km/s below the interface, for shot 6, and 6.47 km/s for the reverse shot. This yields a depth of 13.4 km which quite successfully duplicates the observed intercept and reciprocal times, for both shots.

Head wave arrivals from Moho are quite unambiguously identified for shot 6, at distances greater than 200 km from the shotpoint. Correlation of these events yields an apparent velocity of 8.27 km/s and intercept time of 8.9s . Correlation is much more problematic for the reverse shot for which these values can be determined only within a rather large margin of uncertainty (see table 5).In spite of this however, we still believe that a valid correlation can be made[3] and we proceed to invert the data assuming an upper mantle velocity of 8.10 km/s. This yields depth of the moho at 42.4 km below shot 6 and depth of 38.1 km below shot 9, the uncertainty in this latter value being ±2.5 km. The results of our initial model are fully illustrated in table 5.

Quite prominent reflections have been recorded in both record sections of line C.The reflection from the basement could be clearly identified only in the first record of shot 9 (offset=6.4 km) at t'=1.4s . This observed time is in good agreement with the theoretical value (=1.45s) calculated[4] according to the results of our initial model.Analysis of the first reflection branch (R3) of the records gives depths of the reflector in close agreement with the initially derived values. R3 was well defined within the first 40 km.The next retrograde branch (R4) is of considerable length consisting of quite prominent arrivals within the first 130 km.Ray tracing calculations show that the depth of the

---

[3] Giving Vapparent=7.94 km/s, t_i=8.14s .
[4] By use of equation (16) Chapter 4.

reflector must be somewhat different at the two sides of the profile:12.5 km below shot 6 and 14.3 km under the reverse shot. According to our initial inversion, the refracting segments of this interface are positioned horizontally at a depth of 13.4 km, which may suggest the presence of some structural relief associated with this interface, the central part of which may indeed be more or less horizontal. Agreement between synthetic and observed amplitudes , for R4 is very good for both shots.

Continuing our interpretation we notice for shot 9 a quite distinctive pattern of reflections arriving immediately after the R4 branch. These events are particularly strong at distances between 75 and 110 km. Furthermore it is at once noticed that their distinctive character and appearance is strongly similar with the reflections associated with the upper low velocity layer of line A, (compare, for example, with the arrivals at distances between 55 and 90 km of shot 1). Their correlation from trace to trace can in fact be continued without difficulty towards shorter offsets, establishing two additional retrograde branches R5 and R6. These branches are analyzed by the T^2-X^2 method which gives a low interval velocity of 6.11 km/s. Synthetic modelling shows shows that a somewhat lower velocity of 6.00 km/s will probably give a more adequate agreement between the observed and synthetic amplitudes for the top of the LVZ. It is of interest to notice that the R5,R6 reflection branches are not observed

for the NW shot which suggests that the presence of the low velocity layer is justified only for the SE side of the prifile.Probably it is the continuation of the upper low velocity layer identified under line A.

Reflection arrivals from the Moho are designated by quite strong amplitudes in the critical region for both record sections of the line.However, before modelling the Pm arrivals we would like to focus our attention into a well defined set of events appearing in the records of shot 6 at distances around 150 km at t'=3.5s .Although their amplitudes are low, their coherency is adequately good so that we feel that they should not be neglected in our modelling. Their correlation from trace to trace establishes the R7 reflection branch shown in fig.42.No corresponding head waves are identified in the records.For the purposes of our ray tracing modelling we consider the interface as horizontal since no sufficient control of the dip is provided by the data.The calculations suggest a depth of 31 km and an interval velocity between the R4 and R7 reflectors close to 6.58 km/s. The interface is absent under the SE side of the profile since no corresponding reflections or head waves are observed for shot 9. Synthetic amplitudes for R7 are in agreement with the observed ones.

Concluding our interpretation we model the Pm arrivals observed in the records.According to the ray tracing calculations the depth of the Moho is at 39.5 km below shot 9 and 44 km below shot 6.Seismic velocity at the base of the

crust is 6.85 km/sec below shot 6 and 6.65 km/sec below the reverse shot. Agreement between synthetic Pm amplitudes and observed ones is satisfactory as one can see in the synthetic sections figure 43 and figure 44. The final model C is shown in figure 45.

One cannot overlook the presence of quite strong arrivals appearing in the records after the Pm curve. Their correlation is very good .establishing several retrograde curves after the Pm arrivals. The apparent velocity of these arrivals is high and increases with depth. All these branches seem to merge near the critical region giving rise to particularly strong amplitudes and consequently are worthy of further attention. According to the results of our modelling they are interpreted as due to a laminated sub-moho structure consisting of several high and low velocity layers sandwiched between each other, as shown in the final profile model figure 46. Synthetic amplitudes computed fot this sub-moho stucture are shown for shot 9 in figure 47, while the corresponding ray calculations are included in figure 48

The two alternative models C1 and C2 are illustrated in table 6 and in figure 49.

TABLE 6

Alternative solutions for line C. Depths of Moho and Pn velocity same as in model C.

MODEL	SHOT 6	SHOT 9
C1	$V_{crust}=6.52$km/sec	$V_{crust}=6.41$km/sec
C2	$K=0.0414$sec^{-1} $V_m=7.32$km/sec	$K=0.0392$sec^{-1} $V_m=7.02$km/sec

SHOT 6 LINE C
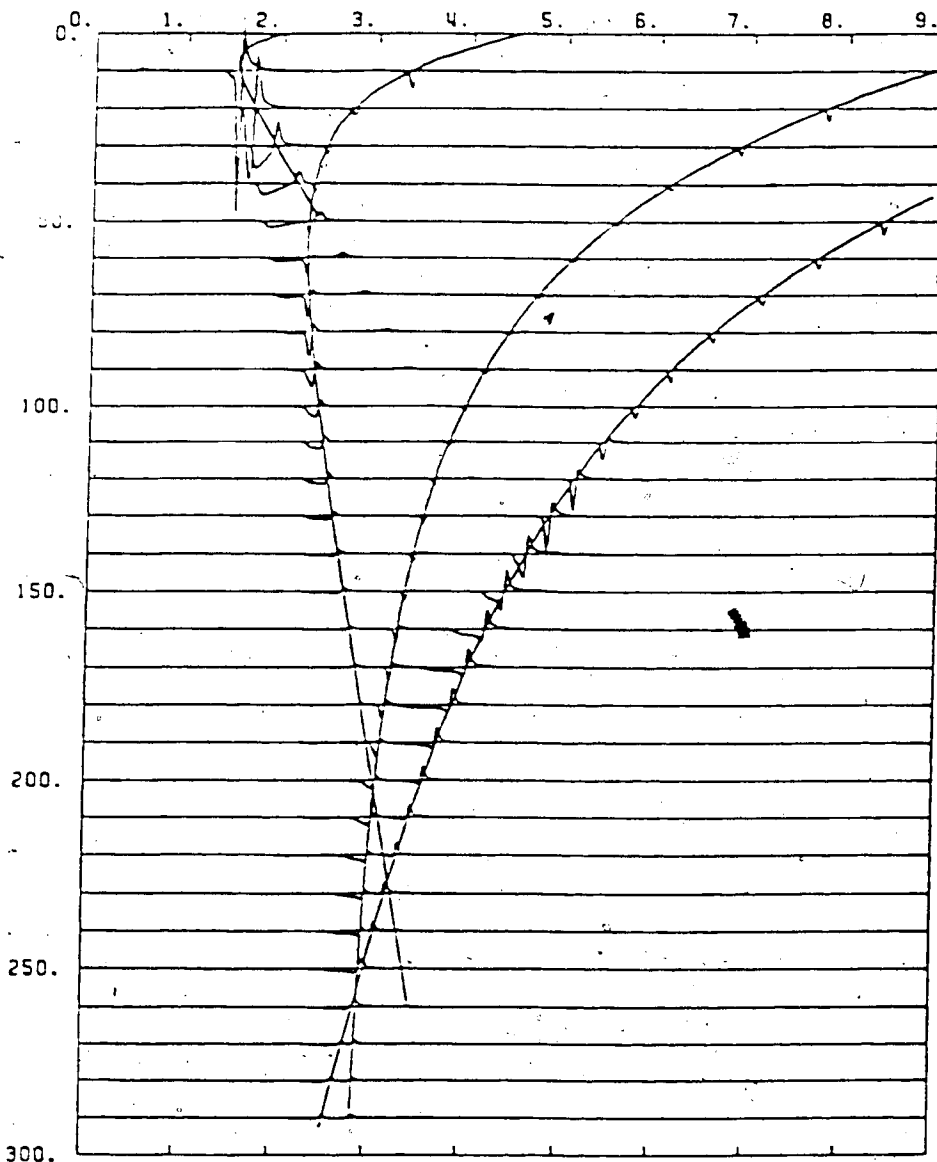
Figure 43.... Synthetic section shot 6.

SHOT 9 LINE C
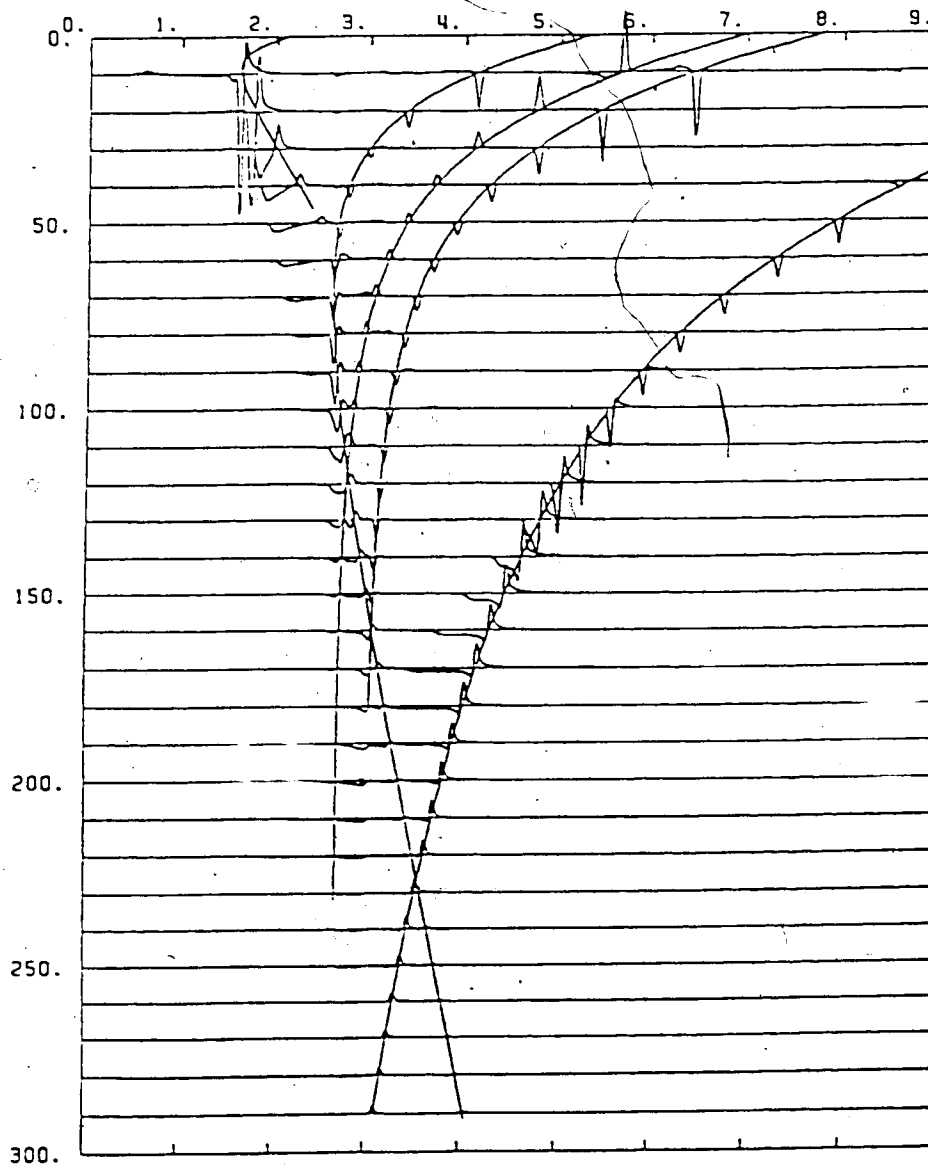
Figure 44 ... Synthetic section shot 9.

LINE C, FINAL MODEL

NW   SE

SHOT6   SHOT9

VERTICAL EXAGGERATION OF FOUR |←——→|——50.000 KM
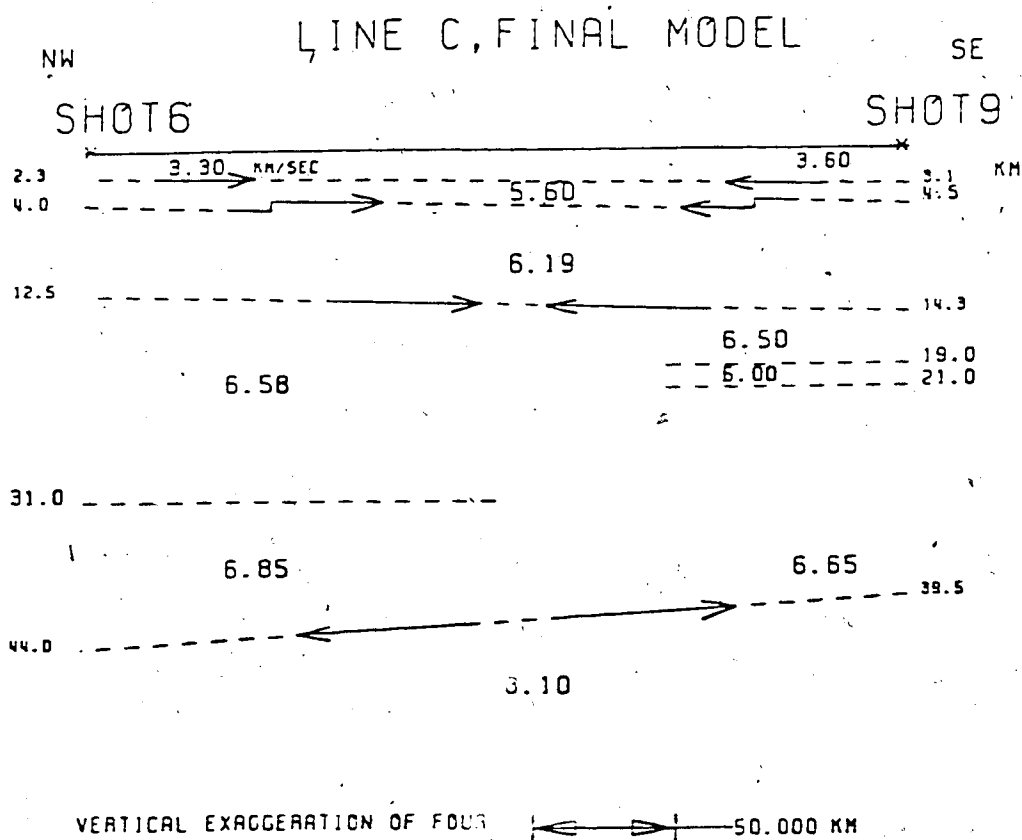
Figure 45.... Final model for line C. Solid lines indicate where head waves provide direct evidence for an interface.
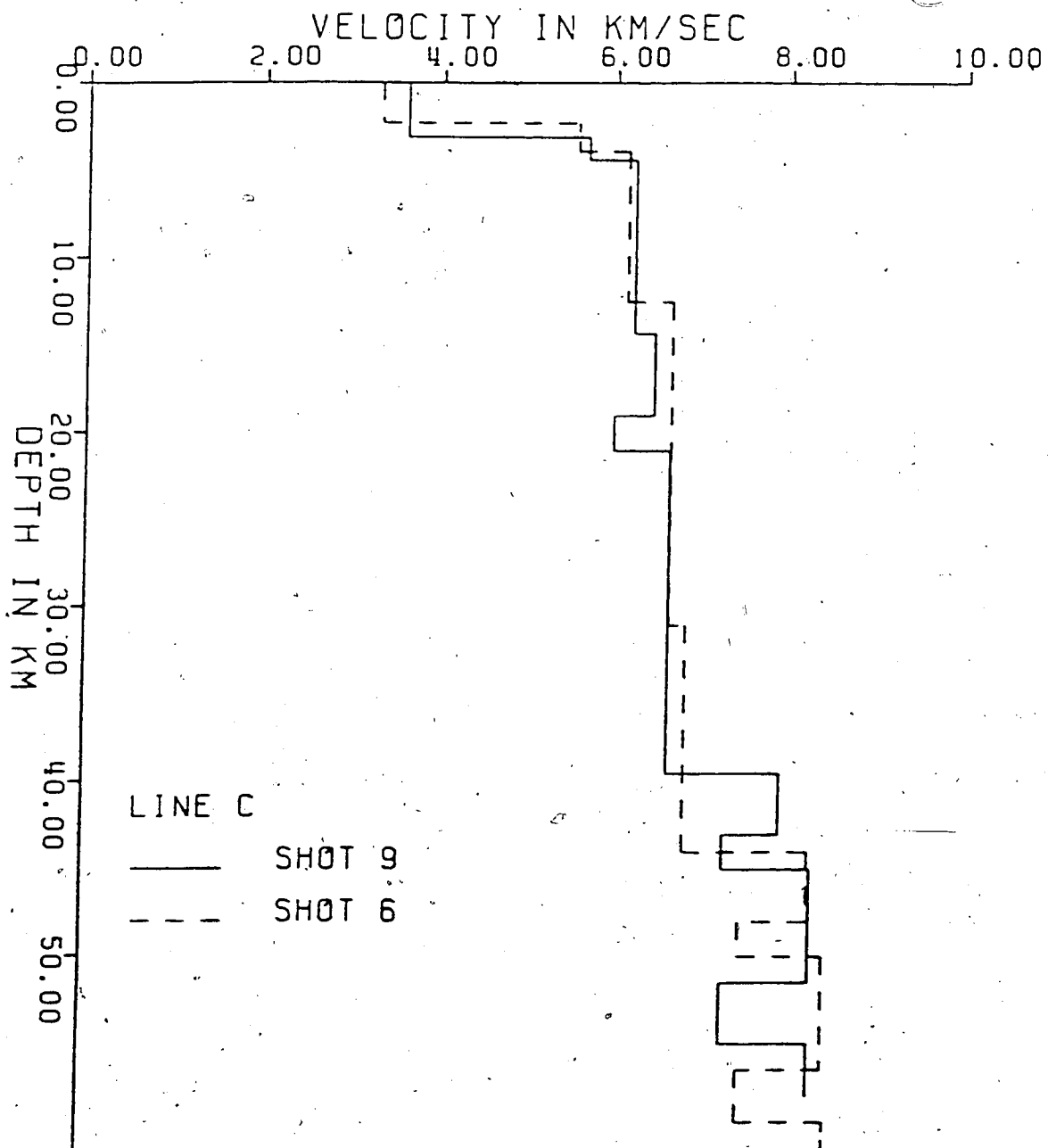
Figure 46.... Final model C in profile form
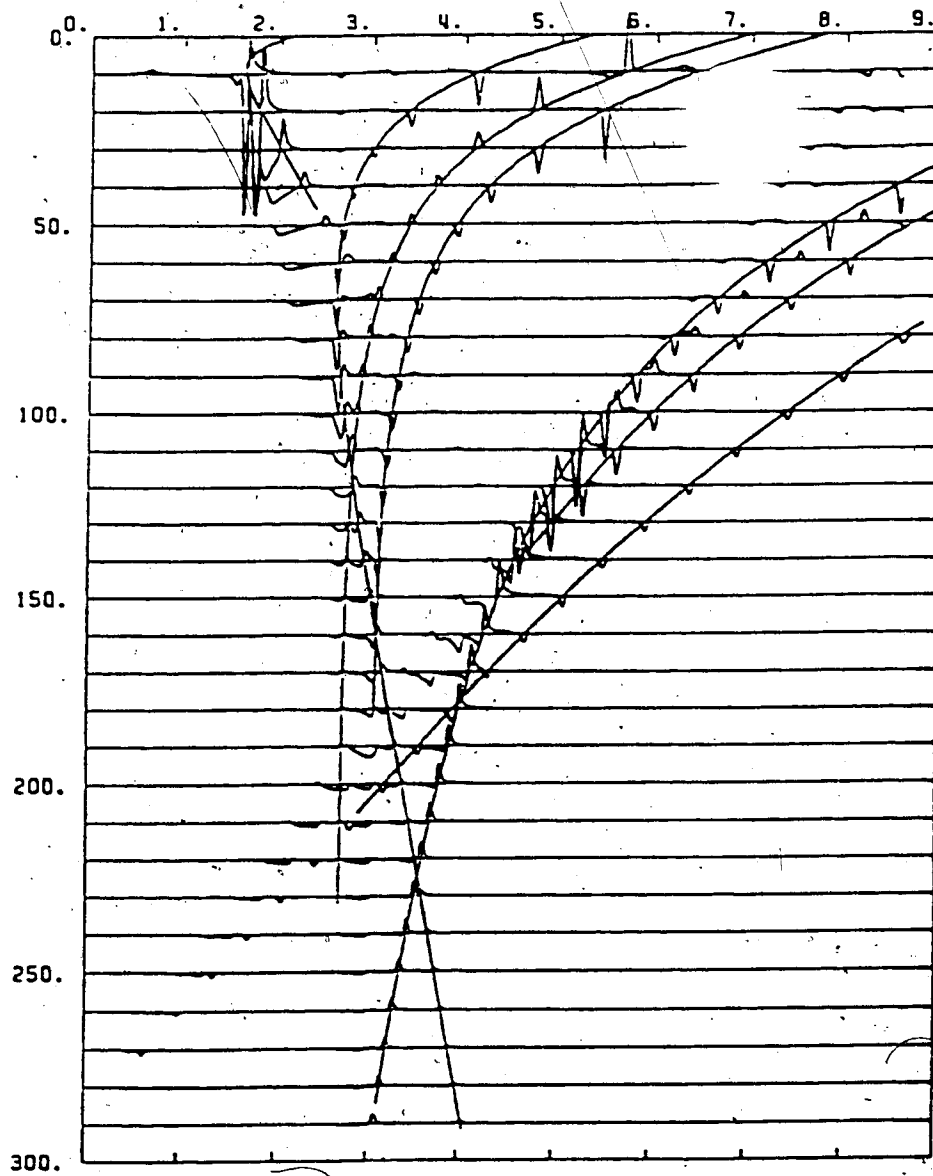
Figure 47.... Synthetic seismograms,shot 9, model C
including a laminated sub-moho structure.Notice the higher
amplitudes of the Pm branch in the critical region.
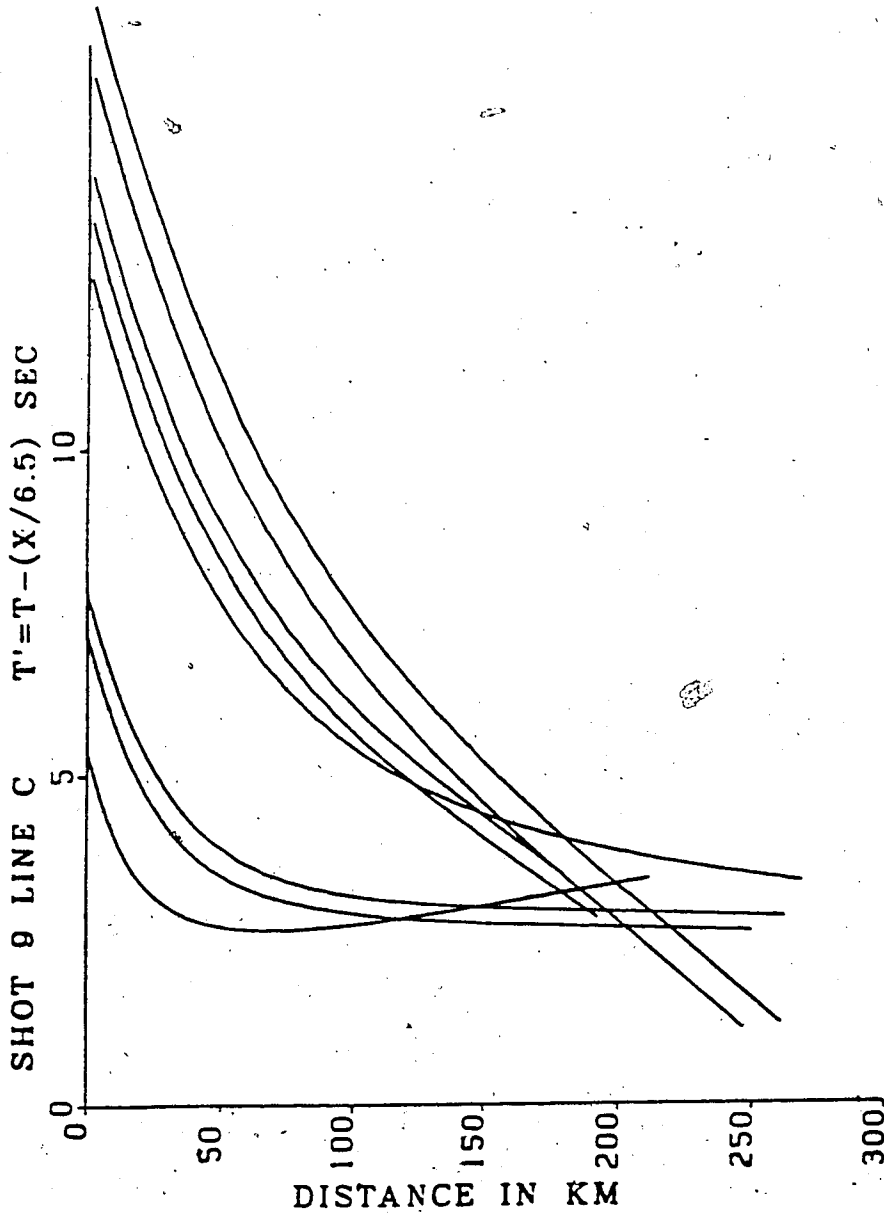
Figure 48.... Ray tracing travel-time calculations,line C
shot 9.
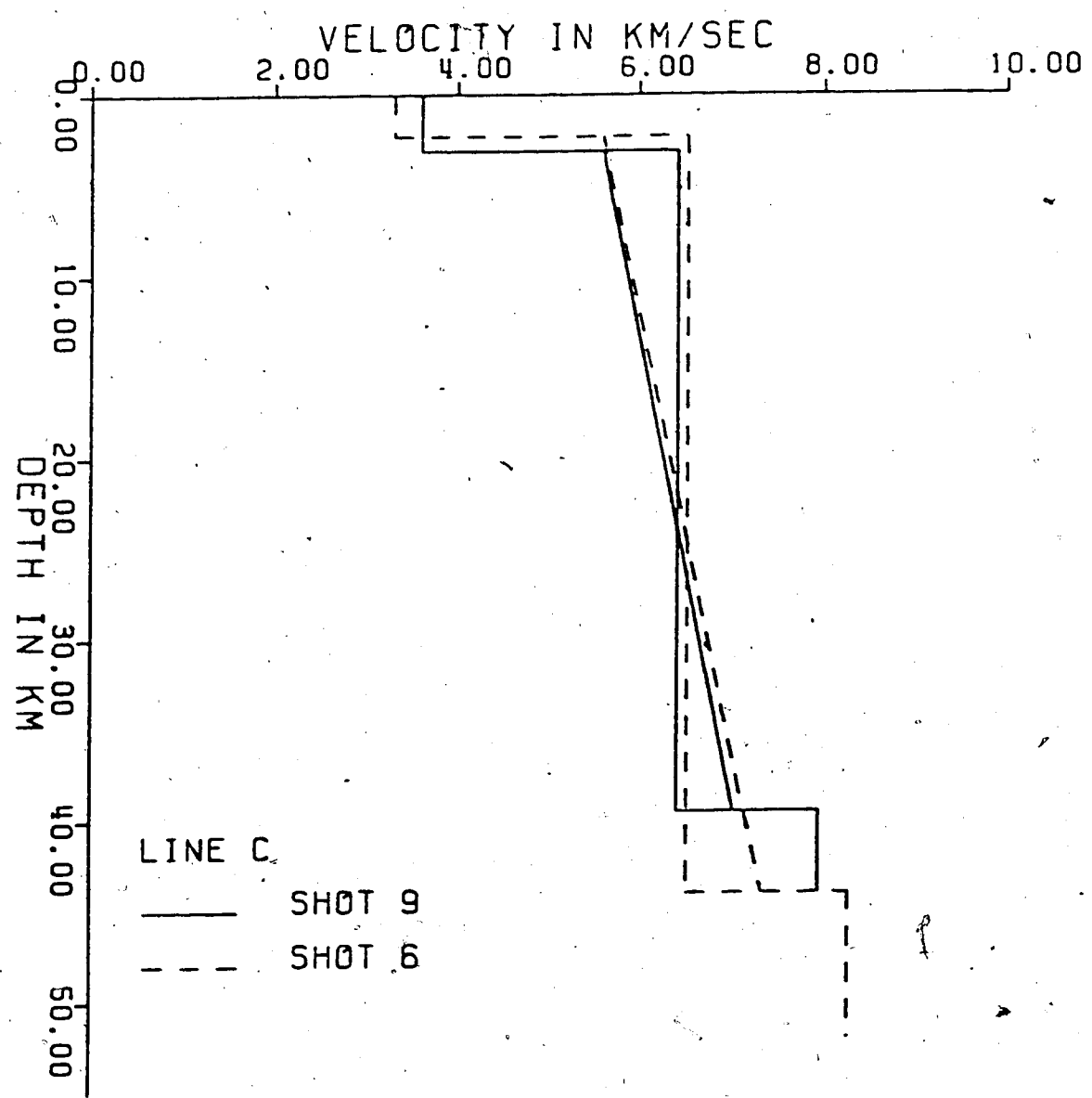
Figure 49.... Two alternative solutions for model C.

6. CONCLUSIONS AND DISCUSSION

The results of the interpretation of lines A,B,C of the 1981 CO-CRUST experiment reveal a very complex structure of the crust below South-Central Saskatchewan.Low velocity layers have been detected below all three profiles.This is a particularly interesting feature of the derived models since no such layers have been identified by previous seismic surveys in Alberta,Manitoba and eastern and western Saskatchwean.It is of interest to speculate on the nature of these low velocity zones and we will return to this matter at the end of this section.The crust thickens southwards and thins eastwards.Crustal thickness below the study area varies from 37 km to 47 km.Depths of Moho below the triangle are shown infigure 50.No evidence of anisotropy or substantial variation of the Pn velocity can be postulated since upper mantle velocity was found to be practically the same below the three profiles where reversed travel times were available.The Pn velocity was close to an average value of 8.13 km/s.This value is in agreement with the results of other seismic studies in Alberta and Saskatchewan.(Substantially lower upper mantle velocities have been reported for Manitoba). This similarity of density values of upper mantle material suggests that the base of the lithosphere below Western Canada is subjected to a uniform thermal regime.There is no evidence of any localized partial melting and thermal alteration of the lower crust.It must be mentioned that such evidence has been reported
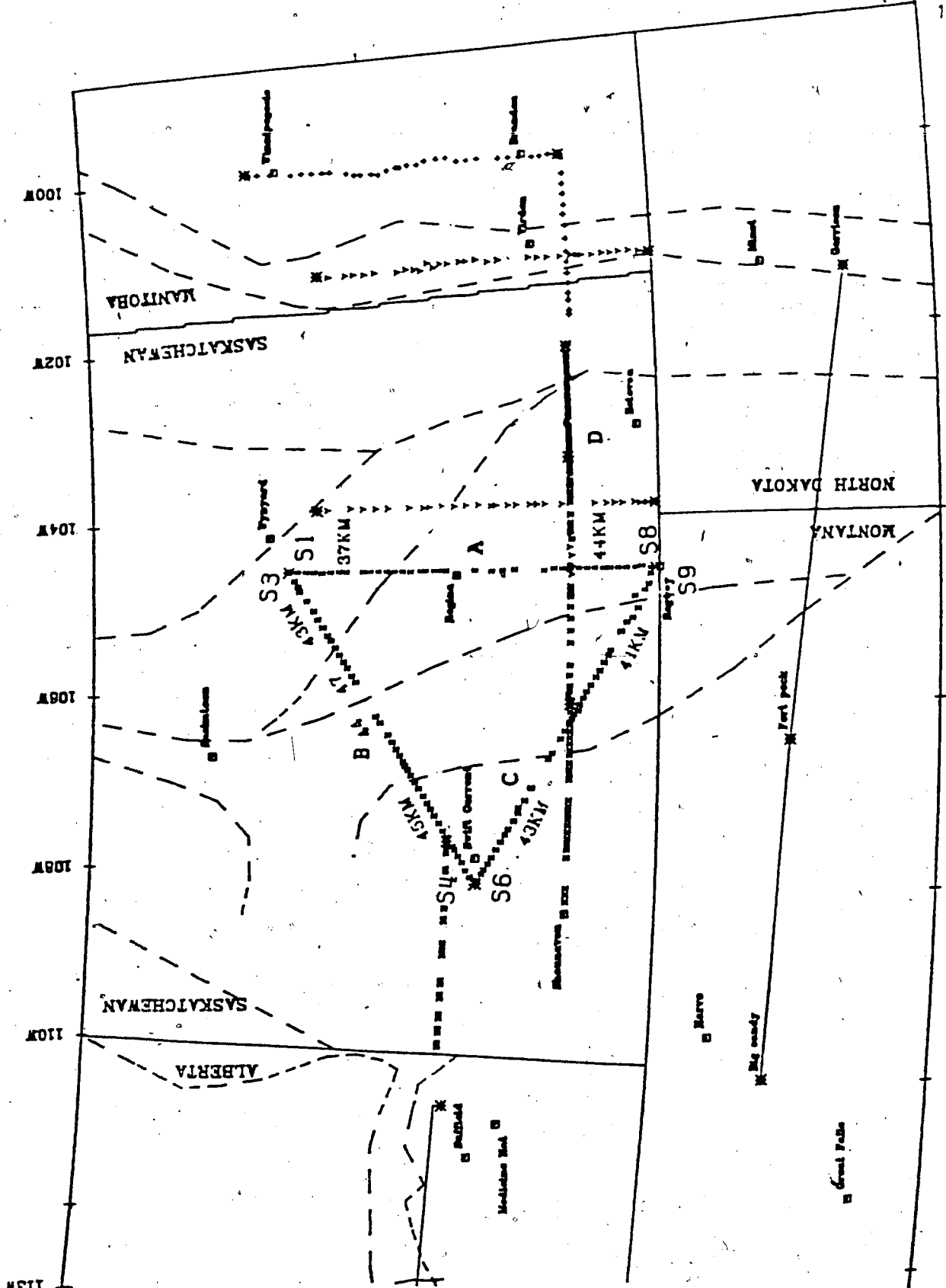
Figure 50.... Depths of Moho under the study area.

previously by seismic studies in U.S.(e.g. in the Basin and Range area,Gish et al.,1981) and was explained as a result of magma intrusion into the base of the lithosphere caused by upward convection within the asthenosphere(Withjack, 1979).However,a slight lateral velocity variation is present in most of the layers of our models B and C showing a consistent westward increase of velocities within the crust.This may be due to a slightly elevated temperature regime within the crust of eastern Saskatchewan.

There is clear evidence that the base of the crust is faulted under line B.The throw of the fault is at least 3 km.A similar structural variation at the intersection of lines A and C shows that the fault is probably continued through southern Saskatchewan,passing through the earthquake prone area of Bengough.The great depth of the Moho near Swift current-below shot 4 of line B can be attributed to the complex N.E-S.W. trends in Saskatchwean intersecting the buried east-west Precambrian rift in Alberta discovered by Kanasewich et al.(1969). Correlation between the various layers of models A,B and C is reasonable both in depth and structure.Considerable effort was spent in attempting to derive other models that would fit the details of the observed seismograms. All these efforts were unsuccessful.A total of about 200 models were tested by synthetic seismograms and ray tracing before concluding the final models appearing in figures 24,34,45. It is noted that a 7 km/s layer is absent in all three models.It is also absent

in the interpretation of the CO-CRUST C-1979 profile which is in very good agreement with our model A.

As mentioned earlier ,line A was located close to the NACP conductivity anomaly as postulated by Alabi. et al.,1975,see figure 51. According to their results the anomaly is a major feature in the lithosphere of Precambrian north America, extending from north-central Saskatchewan to the Black Hills of Wyoming and thence to the northern Southern Rockies.The southern part of the anomaly which is a narrow belt(around 50 km wide) of very high electrical conductivity was modelled by Camfield and Gough(1977) to be in the upper mantle while its maximum depth in Saskatchewan is not more than 35 km. No anomalously high heat flow has been reported for the area of the NACP anomaly in Saskatchewan.Therefore the observed high conductivity must be attributed to different rock type rather than different temperature environment. Whether this is in the form of graphitic sheets, or brines rich in heavy metals transferred into fracture zones ,or high concentration of hydrated minerals in the host rock is a problem which cannot be resolved by the present amount of information.

According to our work,two low velocity zones were identified in the Earth's crust below line A, at depths of 15 and 25 km respectively.It is possible that both of these low velocity layers contribute to the observed conductivity anomaly.There is some indication (see final model C) that the conductor extends itself under the SE side of line C.
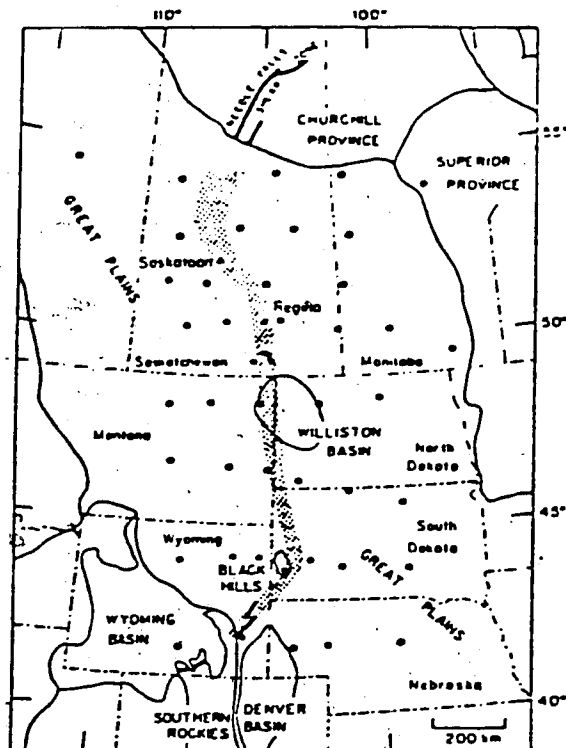
Figure 51.... Location of the conductive body in north american Central plains,after Alabi,Camfield and Gough 1975

Camfield and Gough (1977) postulated that the linear crustal structure may be a major continental fracture zone mapped over a total length of 1800 km.It is in fact quite possible that the fault we have detected in the crust under the triangle ABC(its strike being in alignment with the NACP body) comes in support of this argument.

BIBLIOGRAPHY

Adachi, R. 1954 .On a proof of fundamental formula concerning refraction method of geophysical prospecting and some remarks. Kumamoto Journal of Science, Series A, 18,23.

Alabi,A.O.,Camfield,P.A. and D.I.Gough,1975.The North American Central Plains Conductivity anomaly.Geophys.J.R.Astr.Soc., 43,815-833.

Bell, C. K. 1971. History of the Superior-Churchill boundary in Manitoba, Geological Association of Canada,Special paper,v.9, pp. 5-39.

Birch, F.1964 .Density and composition of the mantle and core, J. Geophys. Res.,69,pp. 4377-4387.

Braile,L.W.,Interpretation of crustal velocity gradients and Q structure using amplitude-corrected seismic refrac n profiles, in the Earth's Crust.Geophys. Monogr. Ser., l 20,edited by J.G.Heacock,AGU,Washington ,D.C.,1977.

Braile , L.W. and Smith, R. B. 1975. Guide to the interpretation of crustal refraction profiles, Geophys. J. R. Astr. Soc., 40, pp.145-176.

Burke,K.C.A., and Dewey, J.F.,1973,An outline of Precambrian plate development, In Tarling and Runvorn,Ed.,Implications of Continental Drift to the Earth Sciences,Academic Press,N.Y.,19351947.

Burwash, R. A. and Culbert, R. R. 1976.Multivariate geochemical and mineral patterns in the Precambrian basement of western Canada,Canadian Journal of Earth Sciences,vol.13,pp.1-18.

Camfield P. A. and Gough, D. I. 1977. A possible Proterozoic plate boundary in North America.Canadian Journal of Earth Sciences, vol 14,pp.1229-1238.

Chandra, N. N. and Cumming G. L. 1972.Seismic refraction studies in western Canada.Canadian Journal of Earth Sciences, 9, p.1099.

Chapman, C. H. 1978.A new method for computing synthetic seismograms. Geophys. J. R. Astr. Soc.,54,pp.481,518.

Clowes, R. M.,Kanasewich E.R. and Cumming G. L.1969.Deep crustal reflections at near-vertical incidence.Geophysics,33,441.

Clowes, R. M. and Kanasewich, E. R. 1970.Seismic attenuation

and the nature of the reflecting horizons within the crust.J Geophys. Res. 75,pp.6693-6705.

Dey-Sarker, S. K. and Chapman, C. H. 1978. A simple method for the computation of body wave seismograms.Bull. Seis. Soc. America.,vol.68, no.6,pp. 1577-1593.

Dix, C. H. 1955. Seismic velocities from surface measurements, Geophysics,20, pp.17-26.

Douglas, R. J. 1970.Geology and Economic Minerals of Canada.

Fuchs, K. 1969. On the properties of deep crustal reflectors, J. Geophys., 35,pp.133-149.

Fuchs, K. and Mueller, G 1971.Computation of synthetic seismograms with the reflectivity method and comparison with observation,Geophys. J., 23,pp.417-433.

Gibb,R. A.and Walcott,R. I.,1971,A Pecambrian suture in the Canadian Shield,Earth Planet.Sci.Lett.,v. 10,p.417-422.

Giese, P. 1976.Calculation of depths, Explosion Seismology in Central Europe.Edited by P. Giese, C.Prodehl and Stein, Springer,New york,pp146-161.

Gish, D.M.,Keller,G.R., and Sbar,M.L.,1981.A refraction Study in the Basin and Range Colorado Plateau of Eastern Arizona.Journal of Geophysical Research,vol.86,no.B7,pp.6029-6038,July 10,1981.

Green, A. G.,Stephenson, O. G.,Mann,G.D. Kanasewich,E.R., Cumming,G.L.,Hajnal,Z.,Mair,J.A.,and West,G.E. 1980.Cooperative seismic survey across the Superior-Churchill boundary zone in Southern Canada,Can.J. Earth Sci.,v. 17 pp.617-632.

Green, A. G.,Cumming, G. L. and Cedarwell D. 1979b.Extension of the Superior-Churchill boundary zone into Southern Canada. Canadian J. Earth Sci.v. 16,pp.1691-1701.

Haller, J.,1958.Probleme der Tiefentektonik Bauformen in migmatitt-Stockwerk der Ostgronlndishen Kalidoniden,Geol: Rundsh, 45,159,1958.

Hess, H. 1964 .Seismic anisotropy of the uppermost mantle under oceans.Nature,203,629.

Hron, F. and Kanasewich, E.R. 1971.Synthetic seismograms for Deep Seismic Sounding Studies using Asymptotic Ray theory.Bull. Seismol. Soc. Am.,vol.61,pp.1169-1200.

Jeffreys, H., 1937. On the materials and density of the Earth' crust.Mon. Not. R. Astr. S. Geophys.Suppl.,4,50.

Kanasewich, E. R., Clowes, R. M. and McClougham, C. H. 1969.A burried Precambrian rift in Western Canada, Tectonophysics,6,pp.513-527.

Kanasewich, E. R., 1981.Time Sequence analysis in Geophysics, 3nd edition, University of Alberta press, Edmonton, Alberta, Canada,pp.237-277.

Kazmierczac, Z. 1980.Seismic crustal studies in Saskatchewan, M.Sc. thesis, University of Alberta, Canada.

Kosminskaya,I.P., and Zverev,S.M.,1968,Abilities of Explosion seismology in oceanic and continental crust and mantle studies;in Symposium on continental margins and island arcs,3rd,Zurich,1967, Can.J.Earth Sci.,v. 5,no 4,pt.2,pp.1091-1100.

Landisman, M. and Mueller S. 1966.Seismic studies of the Earth's crust in continents.Geophys.J.R. Astr.Soc. 10,539-554.

Meissner, R.,The 'Moho' as a transition zone,in Geophysical Surveys, vol.1,pp. 195-216,D.Reidel,Hingham,Mass.,1973.

Moon, W. and de Landro, W. 1981.Detailed interpretation of CO-CRUST 1977 refraction data,Publication of the Center for Precambrian studies, University of Manitoba, Winnipeg,Canada.

Raitt, R.W.,Shor,G.S.,Francis,T.J., and Morris,G.B. 1969. Anisotropy of the Pacific upper mantle.J.Geophys.Res. 74,3095.

Shahriar M. 1982.A detailed interpretation of the 1979 East-West CO-CRUST profile.M.Sc. Thesis,The University of Alberta, Edmonton,Alberta,Canada,pp.47-77.

Smithson,S.B. and Brown,S.K.,1977.A model for lower continental crust,Earth Planet.Sci.Lett.,v.35,p.134-144.

Smithson,S.B.,Shive,P.N.,and Wyckoff,R.,1975.Seismic studies in exposed crystalline basement rocks.Paper presented at 45th Annual international Soc. of Expl. Geophys.Meeting,denver,Colo. Oct.12-16.

Smithson,S.B.,Shive,P.N., and Brown,S.K.1972,Seismic velocity reflections and Structure of the crystalline crust in J.G. Heacock, Ed., The Earth's Crust,Am.Geophys.Union Monograph 20.

Sprenke, K. F. 1982.Potential field inversion, PH.D. thesis, University of Alberta, Edmonton , Alberta,Canada.

Wiggins, R. A. and Helmberger, D. U. 1973. Upper mantle structure of the Western United States, J. Geophys. Res.,78,pp.1870-1880.

Wiggins and Madrid, J. A. 1974.Body wave amplitude calculations, Geophys. J.,37, pp.423-433.

Wiggins, 1976.Body wave amplitude calculations-II,Geophys. J., 46, pp.1-10.

Withjack,M.,A.,A convective heat tranfer model for lithospheric thinning and crustal uplift,J.Geophys.Res.,84 (B6),3008-3022,1979.

APPENDIX

LISTING OF COMPUTER PROGRAMS

1. The despiking program

2. The forward solution for a n-layered system.

3. The inverse solution for a n-layered system.

4. The ray tracing program

```
C     THE DESPIKING PROGRAM
      INTEGER *2 IT(768),ID(768),L1,L2
      CALL READ(ID,L1,0,LA,1)
      ID1=ID(1)
      ID2=ID(2)
      IGRR=ISIGN(1,ID1)
      IGR=ISIGN(1,ID2)
      IG=1
      IGS=1
      IG0=1
      IG1=1
      IG2=1
      IG3=1
      IT(1)=ID(1)
      IT(2)=ID(2)
      IT(3)=ID(3)
      DO 3 J=4,768
      IRJ=ID(J)
      IRJ=IABS(IRJ)
      IF(IRJ.LT.410)GO TO 20
      IDLA=ID(J)-ID(J-1)
      IDLA=IABS(IDLA)
      IF(IDLA.LE.10)GO TO 21
      IF(IDLA.LE.(IRJ+200))GO TO 60
      IF(IG1.LE.0)GO TO 60
      IT(J)=IGS*IRJ
      GO TO 8
   60 IDLZ=ID(J)-IT(J-1)
      IDLZ=IABS(IDLZ)
      IF(IDLZ.LT.IRJ)GO TO 22
      IF(IG1.LT.0)GO TO 24
      IT(J)=IGS*511
      GO TO 8
   20 CONTINUE
      IT(J)=ID(J)
    9 IGRR=IGR
      IGR=IGS
      ITS=IT(J)
      IGS=ISIGN(1,ITS)
      IG3=IG2
      IG2=IG1
      IG1=IG0
      IG0=1
      GO TO 33
   21 CONTINUE
      IT(J)=IGS*511
    8 IGRR=IGR
      IGR=IGS
      ITS=IT(J)
      IGS=ISIGN(1,ITS)
      IG2=IG1
      IG1=IG0
      IG0=(-1)
      GO TO 33
   22 CONTINUE
```

```
      IF(IG2.GT.0)GO TO 23
      IT(J)=IGRR*(-511)
      GO TO 8
   23 CONTINUE
      IT(J)=ID(J)
      GO TO 9
   24 CONTINUE
      IT(J)=IGR*(-511)
      GO TO 8
   33 CONTINUE
C     WRITE(6,200)ID(J),IT(J),IGS,IGR,IGRR,IG0,IG1,IG2,IG3
  200 FORMAT(2I10,7I6)
    3 CONTINUE
    2 CONTINUE
      DO 500 I=4,766
      IF(IT(I).LE.510)GO TO 500
      IF(IT(I+1).NE.(-511))GO TO 500
      IF(IT(I+2).GE.0)GO TO 500
      WRITE(6,503)ID(I),ID(I+1),ID(I+2)
      WRITE(6,504)IT(I),IT(I+1),IT(I+2)
  503 FORMAT(' ID VALUES IN TRAP',3I8)
  504 FORMAT(' IT VALUES IN TRAP',3I8/)
      IT(I+1)=ID(I+1)
      WRITE(6,505)IT(I),IT(I+1),IT(I+2)
  505 FORMAT('  MODIFIED IT VALUES ',3I8/)
  500 CONTINUE
      DO 600 K=4,766
      IF(IT(K).LT.495)GO TO 600
      IF(IT(K+1).NE.(-511))GO TO 600
      IF(IT(K+2).LT.50)GO TO 600
      IT(K+1)=511
  600 CONTINUE
      DO 550 I=1,768,8
      IPP=I+7
      WRITE(6,501)(ID(K),K=I,IPP)
      WRITE(6,502)(IT(K),K=I,IPP)
  550 CONTINUE
  501 FORMAT(8I8)
  502 FORMAT(8I8/)
      STOP
      END
```

```
C     THE FOREWARD SOLUTION OF A MULTILAYERED SYSTEM.
C     THE CALCULATION CAN BE PEFORMED FOR AN ARBITRARILY LARGE NUMBER
C     OF LAYERS.THE LAYERS CAN BE ARBITRARILY DIPPING.NO LOW VELOCITY
C     LAYERS ARE ALLOWED IN THE MODEL.THE SOURCE CAN BE AT ANY DEPTH
C     WITHIN THE FIRST LAYER.THE RESULTS OF THE TRAVEL-TIME
C     CALCULATIONS ARE PLOTTED ON A T-X  AND A T'-X GRAPH.
      DIMENSION A(10),ZU(10),ZD(10),DIP(10),D(10),U(10)
      DIMENSION XSA(32),TSA(32),RSA(32),ASX(32)
      INTEGER VAR1
      READ(5,31)A
 31   FORMAT(10F5.2)
      READ(5,32)ZU
 32   FORMAT(10F6.3)
      READ(5,33)ZD
 33   FORMAT(10F6.3)
      READ(5,34)DIP
 34   FORMAT(10F5.2)
      READ(5,110)PL,PH,PARAM1,PARAM2,MODEL
 110  FORMAT(4F5.1,I4)
      READ(5,120)VAR1
 120  FORMAT(I4)
      READ(5,124)VAR3,OFFSET,RVEL
 124  FORMAT(3F7.2)
C  MODEL IS THE NUMBER OF LAYERS OVER THE HALF SPACE

      DIMENSION RM(10),DI(10),RN(10),UI(10),TU(10),TD(10),RTU(10),F
     R)
      CALL PLOTS
      CALL PLOT(0.5,0.5,-3)
      CALL PLOT(PL,0.0,2)
      CALL PLOT(PL,PH,2)
      CALL PLOT(0.0,0.0,3)
      CALL PLOT(0.0,PH,2)
      CALL PLOT(PL+1.5,0.0,-3)
      CALL PLOT(PL,0.0,2)
      CALL PLOT(PL,PH,2)
      CALL PLOT(0.0,0.0,3)
      CALL PLOT(0.0,PH,2)
      CALL PLOT(-(PL+1.5),0.0,-3)
      NSY=0
      IPL=IFIX(PL)
      IPH=IFIX(PH)
      VAR2=290.-OFFSET
C ALFA IS THE DEPTH OF THE SOURCE
      ALFA=0.0
      ZU(1)=ZU(1)-ALFA
      ZD(1)=ZD(1)-ALFA
C  CONVERT THE ANGLES TO RADIANS
      DO 1 NA=1,10
      DIP(NA)=DIP(NA)*0.01745
 1    CONTINUE
C  CALCULATE ANGLES D(10),U(10)
      DO 42 LEK=1,MODEL
      D(LEK)=ARSIN(A(LEK)/A(LEK+1))+DIP(LEK+1)
      U(LEK)=ARSIN(A(LEK)/A(LEK+1))-DIP(LEK+1)
```

```
   42   CONTINUE
C DIRECT WAVE
        WRITE(6,89)
   89   FORMAT(//,'DIRECT WAVE')
        NCPL=0
        DO 5 IX=10,VAR1,10
        NCPL=NCPL+1
        X=IX-10.
        IF(X.EQ.290.)X=VAR3
        T=(SQRT((ALFA*ALFA)+(X*X)))/A(1)
        REDTDI=T-(X/RVEL)
        WRITE(6,300)X,T,REDTDI
        XSA(NCPL)=X
        ASX(NCPL)=OFFSET-X
        TSA(NCPL)=T
        RSA(NCPL)=REDTDI
  300   FORMAT('0',F10.2,F8.4,F8.4)
    5   CONTINUE
        RMSA=0.0
        TMSA=0.0
        DO 51 K=1,NCPL
        IF(TSA(K).GT.TMSA)TMSA=TSA(K)
        IF(RSA(K).GT.RMSA)RMSA=RSA(K)
   51   CONTINUE
        IF(TMSA.GT.10)GO TO 57
        T2P=(((IFIX(TMSA))/2+1)*2)
        GO TO 59
   57   T2P=(((IFIX(TMSA))/10)+1)*10
   59   CONTINUE
        IF(RMSA.GT.10)GO TO 54
        R2P=(((IFIX(RMSA))/2)+1)*2
        GO TO 58
   54   R2P=(((IFIX(RMSA))/10)+1)*10
   58   CONTINUE
        X2P=OFFSET/PL
        XSA(NCPL+1)=0.0
        XSA(NCPL+2)=X2P
        ASX(NCPL+1)=0.0
        ASX(NCPL+2)=X2P
        TSA(NCPL+1)=0.0
        TSA(NCPL+2)=T2P/PH
        RSA(NCPL+1)=0.0
        RSA(NCPL+2)=R2P/PH
  291 FORMAT(8F10.4)
        CALL LINEP(0.042)
        CALL LINE(XSA,TSA,NCPL,1,1,NSY)
        CALL LINE(ASX,TSA,NCPL,1,1,NSY)
        DO 4 KA=1,IPH
        RL=KA*TSA(NCPL+2)
        RKA=KA
        CALL NUMBER(-0.35,RKA,0.086,RL,0.0,-1)
        CALL SYMBOL(0.0,RKA,0.042,3,0.0,1)
        CALL SYMBOL(PL,RKA,0.042,3,0.0,1)
    4   CONTINUE
        DO 322 KA=1,IPL
        RL=(KA*XSA(NCPL+2))/1000.
        RKA=KA
        CALL NUMBER(RKA-0.12,-0.20,0.087,RL,0.0,1)
        CALL SYMBOL(RKA,0.0,0.042,3,0.0,1)
  322 CONTINUE
```

```
      CALL PLOT(PL+1.5,0.0,-3)
      DO 15 KA=1,IPH
      RL=KA*RSA(NCPL+2)
      RKA=KA
      CALL SYMBOL(0.0,RKA,0.042,3,0.0,1)
      CALL SYMBOL(PL,RKA,0.042,3,0.0,1)
      CALL NUMBER(-0.35,RKA,0.086,RL,0.0,-1)
 15   CONTINUE
      DO 323 KA=1,IPL
      RL=(KA*XSA(NCPL+2))/1000.
      RKA=KA
      CALL NUMBER(RKA-0.12,-0.20,0.087,RL,0.0,1)
      CALL SYMBOL(RKA,0.0,0.042,3,0.0,1)
 323  CONTINUE
      CALL LINE(XSA,RSA,NCPL,1,1,NSY)
      CALL LINE(ASX,RSA,NCPL,1,1,NSY)
      CALL PLOT(-(PL+1.5),0.0,-3)
      NSY=NSY+1
      IF(PARAM1.NE.0.0)GO TO 80
C THE VARIABLE PARAM IS NOT EQUAL TO 0.0 WHEN THE SOURCE
C IS EXACTLY  AT THE SECOND  INTERFACE
C UPDIP SOURCE
C  UPDIP WILL REFFER TO THE SIDE OF THE PROFILE IN WHICH ZU
C  IS DEFINED.(IF ZU>ZD DIP<0.0).
      U12=ARSIN(A(1)/A(2))
      WRITE(6,701)
 701  FORMAT(//,'UPDIP SOURCE  HEAD WAVE FROM INTERFACE 2')
      NCPL=0
      DO 2 IX=10,VAR1,10
      NCPL=NCPL+1
      X=IX-10-(ALFA*TAN(D(1)))
      IF(X.EQ.VAR1-10-(ALFA*TAN(D(1))))X=VAR1-10
     R-(ALFA*TAN(D(1)))-VAR2
      TU2=(X/A(1))*SIN(D(1))+(ZU(1)/A(1))*(COS(D(1)))
     E+(ZU(1)/A(1))*(COS(U(1)))
      TU2=TU2+(ALFA/A(1))*COS(D(1))
      TU2=TU2+(ALFA/A(1))*TAN(D(1))*SIN(D(1))
      REDT=TU2-(X/RVEL)-((ALFA/RVEL)*TAN(D(1)))
      TT1=X+(ALFA*TAN(D(1)))
      WRITE(6,100)TT1,TU2,REDT
 100  FORMAT('0',F10.2,F8.4,F8.4)
      XSA(NCPL)=TT1
      TSA(NCPL)=TU2
      RSA(NCPL)=REDT
 2    CONTINUE
      CALL LINE(XSA,TSA,NCPL,1,1,NSY)
      CALL PLOT(PL+1.5,0.0,-3)
      CALL LINE(XSA,RSA,NCPL,1,1,NSY)
      CALL PLOT(-(PL+1.5),0.0,-3)
      NSY=NSY+1
C DOWN DIP SOURCE
      NCPL=0
      WRITE(6,702)
 702  FORMAT(//,'DOWNDIP SOURCE  HEAD WAVE FROM INTERFACE 2')
      DO 3 IX=10,VAR1,10
      NCPL=NCPL+1
      X=IX-10.-(ALFA*TAN(U(1)))
      IF(X.EQ.VAR1-10-(ALFA*TAN(U(1))))X=VAR1-10
     E-(ALFA*TAN(U(1)))-VAR2
      TD2=(X/A(1))*SIN(U(1))+(ZD(1)/A(1))*(COS(D(1)))+
```

```
      E(ZD(1)/A(1))*(COS(U(1)))
       TD2=TD2+(ALFA/A(1))*COS(U(1))
       TD2=TD2+(ALFA/A(1))*TAN(U(1))*SIN(U(1))
       REDTD=TD2-(X/RVEL)-((ALFA/RVEL)*TAN(U(1)))
       TT1=X+(ALFA*TAN(U(1)))
       WRITE(6,200)TT1,TD2,REDTD
       XSA(NCPL)=TT1
       TSA(NCPL)=TD2
       RSA(NCPL)=REDTD
  200  FORMAT('0',F10.2,F8.4,F8.4)
  3    CONTINUE
       CALL LINE(ASX,TSA,NCPL,1,1,NSY)
       CALL PLOT(PL+1.5,0.0,-3)
       CALL LINE(ASX,RSA,NCPL,1,1,NSY)
       CALL PLOT(-(PL+1.5),0.0,-3)
C THREE LAYERS
C UPDIP SOURCE
  80   U23=ARSIN(A(2)/A(3))
       B1=(A(1)/A(2))*SIN(D(2)-DIP(2))
       D13=ARSIN(B1)
       C1=(A(1)/A(2))*SIN(U(2)+DIP(2))
       U13=ARSIN(C1)
       REAL NEWD1
       REAL NEWU1
       NEWD1=D13+DIP(2)
       NEWU1=U13-DIP(2)
       WRITE(6,90)
  90   FORMAT(//,'UPDIP SOURCE  HEAD WAVE FROM INTERFACE 3')
       NCPL=0
       DO 645 IX=10,VAR1,10
       NCPL=NCPL+1
      .X=IX-10.-(ALFA*TAN(NEWD1))
       IF(X.EQ.VAR1-10-(ALFA*TAN(NEWD1)))X=VAR1-10
      F-(ALFA*TAN(NEWD1))-VAR2
       TU3=(X/A(1))*SIN(NEWD1)+(ZU(1)/A(1))*(COS(NEWD1)+COS(NEWU1))
      M+(ZU(2)/A(2))*(COS(D(2))+COS(U(2)))
       TU3=TU3+(ALFA/A(1))*COS(NEWD1)
       TU3=TU3+((ALFA/A(1))*TAN(NEWD1)*SIN(NEWD1))
       RTU3=TU3-(X/RVEL)-((ALFA/RVEL)*TAN(NEWD1))
       TT1=X+(ALFA*TAN(NEWD1))
       WRITE(6,400)TT1,TU3,RTU3
       XSA(NCPL)=TT1
       TSA(NCPL)=TU3
       RSA(NCPL)=RTU3
  400  FORMAT('0',F10.2,F8.4,F8.4)
  645    CONTINUE
       CALL LINE(XSA,TSA,NCPL,1,1,NSY)
       CALL PLOT(PL+1.5,0.0,-3)
       CALL LINE(XSA,RSA,NCPL,1,1,NSY)
       CALL PLOT(-(PL+1.5),0.0,-3)
       NSY=NSY+1
C DOWNDIP SOURCE
       WRITE(6,91)
  91   FORMAT(//,'DOWNDIP SOURCE HEAD WAVE FROM INTERFACE 3')
       NCPL=0
       DO 7 IX=10,VAR1,10
       NCPL=NCPL+1
       X=IX-10.-(ALFA*TAN(NEWU1))
       IF(X.EQ.VAR1-10-(ALFA*TAN(NEWU1)))X=VAR1-10
      G-(ALFA*TAN(NEWU1))-VAR2
```

```
       TD3=(X/A(1))*SIN(NEWU1)+(ZD(1)/A(1))*(COS(NEWD1)+COS(NEWU1))
      N+(ZD(2)/A(2))*(COS(D(2))+COS(U(2)))
       TD3=TD3+(ALFA/A(1))*COS(NEWU1)
       TD3=TD3+((ALFA/A(1))*TAN(NEWU1)*SIN(NEWU1))
       RTD3=TD3-(X/RVEL)-((ALFA/RVEL)*TAN(NEWU1))
       TT1=X+(ALFA*TAN(NEWU1))
       WRITE(6,500)TT1,TD3,RTD3
       XSA(NCPL)=TT1
       TSA(NCPL)=TD3
       RSA(NCPL)=RTD3
  500  FORMAT('0',F10.2,F8.4,F8.4)
     7 CONTINUE
       CALL LINE(ASX,TSA,NCPL,1,1,NSY)
       CALL PLOT(PL+1.5,0.0,-3)
       CALL LINE(ASX,RSA,NCPL,1,1,NSY)
       CALL PLOT(-(PL+1.5),0.0,-3)
       NSY=NSY+1
C PARAM2 ISNOT EQUAL TO 0.0 WHEN THE MODEL CONSISTS ONLY OF
C THREE LAYERS
       IF(PARAM2.NE.0.0)GO TO 22
C GENERALIZATION FOR ANY NUMBER OF LAYERS
       DO 20 J=3,MODEL
C IN ITS GENERAL FORM,THE PREVIOUS STATEMENT IS
C DO 20 J=3,N WHERE N=(TOTAL NUMB. OF LAYERS-1)
       IVAL=J+1
       RM(1)=0.
       RM(2)=ARSIN(A(J-1)/A(J)*SIN(D(J)-DIP(J)))
       INDEX1=1
       DI(1)=0.
       DI(J-INDEX1)=RM(2)+DIP(J)
       INDEX=1
       DO 40 K=3,J
       RM(K)=ARSIN(A(J-1-INDEX)/A(J-INDEX)*SIN(DI(J-INDEX)
      M-DIP(J-INDEX)))
       INDEX1=INDEX1+1
       IF(J-INDEX1.LT.2)GO TO 40
       DI(J-INDEX1)=RM(K)+DIP(J-INDEX)
       INDEX=INDEX+1
   40  CONTINUE
       RN(1)=0.
       RN(2)=ARSIN(A(J-1)/A(J)*SIN(U(J)+DIP(J)))
       IND1=1
       UI(1)=0.
       UI(J-IND1)=RN(2)-DIP(J)
       IND=1
       DO 60 K=3,J
       RN(K)=ARSIN(A(J-1-IND)/A(J-IND)*SIN(UI(J-IND)
      N+DIP(J-IND)))
       IND1=IND1+1
       IF(J-IND1.LT.2)GO TO 60
       UI(J-IND1)=RN(K)-DIP(J-IND)
       IND=IND+1
   60  CONTINUE
       WRITE(6,92)IVAL
   92  FORMAT(//,'UPDIP SOURCE, HEAD WAVE FROM INTERFACE',I4)
       NCPL=0
       DO 53 IX=10,VAR1,10
       NCPL=NCPL+1
       X=IX-10.-(ALFA*TAN(RM(J)+DIP(2)))
       IF(X.EQ.VAR1-10-(ALFA*TAN(RM(J)+DIP(2))))X=VAR1-10
```

```
 125

      E-(ALFA*TAN(RM(J)+DIP(2)))-VAR2
       TU(1)=0.
       TU(2)=0.
       TU(3)=0.
       K=J+1
       TU(K)=(X/A(1))*SIN(RM(J)+DIP(2))
       TU(K)=TU(K)+(ALFA*COS(RM(J)+DIP(2)))/A(1)
       TU(K)=TU(K)+(ZU(1)/A(1))*(COS(RM(J)+DIP(2))+COS(RN(J)
      F-DIP(2)))
       TU(K)=TU(K)+((ALFA/A(1))*TAN(RM(J)+DIP(2))*SIN(RM(J)
      E+DIP(2)))
       TU(K)=TU(K)+(ZU(J)/A(J))*(COS(D(J))+COS(U(J)))
       INTEGER R
       R=J-1
       DO 52 I=2,R
       TU(K)=TU(K)+(ZU(I)/A(I))*(COS(DI(I))+COS(UI(I)))
 52    CONTINUE
       RTU(K)=TU(K)-(X/RVEL)-((ALFA/RVEL)*TAN(RM(J)+DIP(2)))
       TT1=X+(ALFA*TAN(RM(J)+DIP(2)))
       XSA(NCPL)=TT1
       TSA(NCPL)=TU(K)
       RSA(NCPL)=RTU(K)
       WRITE(6,71)TT1,TU(K),RTU(K)
 71    FORMAT('0',F10.2,F8.4,F8.4)
 53    CONTINUE
       CALL LINE(XSA,TSA,NCPL,1,1,NSY)
       CALL PLOT(PL+1.5,0.0,-3)
       CALL LINE(XSA,RSA,NCPL,1,1,NSY)
       CALL PLOT(-(PL+1.5),0.0,-3)
       NSY=NSY+1
C DOWNDIP SOURCE
       WRITE(6,93)IVAL
 93    FORMAT(//,'DOWNDIP SOURCE ,HEAD WAVE FROM INTERFACE',I4)
       NCPL=0
       DO 63 IX=10,VAR1,10
       NCPL=NCPL+1
       X=IX-10.-(ALFA*TAN(RN(J)-DIP(2)))
       IF(X.EQ.VAR1-10-(ALFA*TAN(RN(J)-DIP(2))))X=VAR1
      K-10-(ALFA*TAN(RN(J)-DIP(2)))-VAR2
       TD(1)=0.
       TD(2)=0.
       TD(3)=0.
       K=J+1
       TD(K)=(X/A(1))*SIN(RN(J)-DIP(2))
       TD(K)=TD(K)+(ZD(1)/A(1))*(COS(RM(J)+DIP(2))+COS(RN(J)
      U-DIP(2)))
       TD(K)=TD(K)+((ALFA/A(1))*TAN(RN(J)-DIP(2))*SIN(RN(J)
      E-DIP(2)))
       TD(K)=TD(K)+(ZD(J)/A(J))*(COS(D(J))+COS(U(J)))
       INTEGER P
       P=J-1
       DO 62 I=2,P
       TD(K)=TD(K)+(ZD(I)/A(I))*(COS(DI(I))+COS(UI(I)))
       TD(K)=TD(K)+(ALFA*COS(RN(J)-DIP(2)))/A(1)
 62    CONTINUE
       RTD(K)=TD(K)-(X/RVEL)-((ALFA/RVEL)*TAN(RN(J)-DIP(2)))
       TT1=X+(ALFA*TAN(RN(J)-DIP(2)))
       WRITE(6,43)TT1,TD(K),RTD(K)
       XSA(NCPL)=TT1
       TSA(NCPL)=TD(K)
```

```
      RSA(NCPL)=RTD(K)
43    FORMAT('0',F10.2,F8.4,F8.4)
63    CONTINUE
      CALL LINE(ASX,TSA,NCPL,1,1,NSY)
      CALL PLOT(PL+1.5,0.0,-3)
      CALL LINE(ASX,RSA,NCPL,1,1,NSY)
      CALL PLOT(-(PL+1.5),0.0,-3)
      NSY=NSY+1
20    CONTINUE
22    CONTINUE
21    CALL PLOT(0.0,0.0,999)
24    STOP
      END
```

```
      THE INVERSE SOLUTION OF A MULTILAYER SYSTEM.
   THE PROGRAM CALCULATES DIPS,VELOCITIES AND UPDIP AND
   DOWNDIP DEPTHS FROM INTERCEPT TIMES AND APPARENT VELOCITIES
   NTOTAL IS THE NUMBER OF LAYERS INCLUDING THE HALF SPACE

         DIMENSION VD(10),VU(10),RID(10),RIU(10),A(10),DIP(10)
         DIMENSION D(10),U(10),DD(10),UU(10),ZD(10),ZU(10)
         DIMENSION DL(10),UL(10),ANGLE(10)
         READ(5,1)DVEL,NTOTAL
    1    FORMAT(F6.2,I3)
         A(1)=DVEL
         READ(5,2)(VD(K),K=1,7)
    2    FORMAT(7F6.2)
         READ(5,2)(VU(KK),KK=1,7)
         READ(5,2)(RID(L),L=1,7)
         READ(5,2)(RIU(LL),LL=1,7)
         D12=0.5*(ARSIN(A(1)/VD(2))+ARSIN(A(1)/VU(2)))
         DIP(2)=0.5*(ARSIN(A(1)/VD(2))-ARSIN(A(1)/VU(2)))
         ANGLE(2)=57.2958*DIP(2)
         WRITE(6,3)ANGLE(2)
    3    FORMAT('0','DIP(2)=',F6.3,'DEGREES'/)
         D(1)=D12+DIP(2)
         U(1)=D12-DIP(2)
         A(2)=A(1)/SIN(D12)
         WRITE(6,4)A(2)
    4    FORMAT('0','A(2)=',F6.2,'KM/SEC'/)
         ZD(1)=(A(1)*RID(2))/(COS(D(1))+COS(U(1)))
         ZU(1)=(A(1)*RIU(2))/(COS(D(1))+COS(U(1)))
         WRITE(6,5)ZD(1)
    5    FORMAT('0','ZD(1)=',F8.3,'KM'/)
         WRITE(6,6)ZU(1)
    6    FORMAT('0','ZU(1)=',F8.3,'KM'/)
      THREE LAYERS
         D13=(-1)*DIP(2)+ARSIN(A(1)/VD(3))
         U13=DIP(2)+ARSIN(A(1)/VU(3))
         DD(1)=D13+DIP(2)
         UU(1)=U13-DIP(2)
         D23=0.5*(ARSIN(A(2)*SIN(D13)/A(1))+
        EARSIN(A(2)*SIN(U13)/A(1)))
         DIP(3)=DIP(2)+0.5*(ARSIN(A(2)*SIN(D13)/A(1))
        E-ARSIN(A(2)*SIN(U13)/A(1)))
         ANGLE(3)=57.2958*DIP(3)
         WRITE(6,7)ANGLE(3)
    7    FORMAT('0','DIP(3)=',F6.3/)
         A(3)=A(2)/SIN(D23)
         WRITE(6,8)A(3)
    8    FORMAT('0','A(3)=',F6.2/)
         DD(2)=D23+DIP(3)
         UU(2)=D23-DIP(3)
         ZD(2)=(A(2)/(COS(DD(2))+COS(UU(2)))
        E*(RID(3)-(ZD(1)/A(1)*(COS(DD(1))+COS(UU(1)))))
         WRITE(6,9)ZD(2)
    9 FORMAT('0','ZD(2)=',F6.3,'KM'/)
         ZU(2)=(A(2)/(COS(DD(2))+COS(UU(2))))
        E*(RIU(3)-(ZU(1)/A(1)*(COS(DD(1))+COS(UU(1)))))
```

```fortran
      WRITE(6,10)ZU(2)
   10 FORMAT('0','ZU(2)=',F6.3,'KM'/)
C  GENERALIZATION FOR N LAYERS
      DO 100 N=4,NTOTAL
      D(1)=(-1)*DIP(2)+ARSIN(A(1)/VD(N))
      U(1)=DIP(2)+ARSIN(A(1)/VU(N))
      INDEX=N-2
      DO 200 J=2,INDEX
      DL(J-1)=ARSIN(A(J)/A(J-1)*SIN(D(J-1)))-
      UL(J-1)=ARSIN(A(J)/A(J-1)*SIN(U(J-1)))
      D(J)=DIP(J)-DIP(J+1)+DL(J-1)
      U(J)=DIP(J+1)-DIP(J)+UL(J-1)
  200 CONTINUE
      D(N-1)=0.5*(ARSIN(A(N-1)/A(N-2)*SIN(D(N-2)))
     E+ARSIN(A(N-1)/A(N-2)*SIN(U(N-2))))
      DIP(N)=DIP(N-1)+0.5*(ARSIN(A(N-1)/A(N-2)*SIN(D(N-2)))
     E-ARSIN(A(N-1)/A(N-2)*SIN(U(N-2))))
      ANGLE(N)=57.2958*DIP(N)
      A(N)=A(N-1)/SIN(D(N-1))
      WRITE(6,11)ANGLE(N),A(N)
   11 FORMAT('0','DIP=',F6.3,'   VELOCITY=',F6.2,'KM/SEC'//)
      SUMD=0.0
      SUMU=0.0
      DO 300 JJ=1,INDEX
      DD(JJ)=D(JJ)+DIP(JJ+1)
      UU(JJ)=U(JJ)-DIP(JJ+1)
      SUMD=SUMD+ZD(JJ)/A(JJ)*(COS(DD(JJ))+COS(UU(JJ)))
      SUMU=SUMU+ZU(JJ)/A(JJ)*(COS(DD(JJ))+COS(UU(JJ)))
  300 CONTINUE
      ZD(N-1)=(A(N-1)*(RID(N)-SUMD))/
     E(COS(D(N-1)+DIP(N))+COS(D(N-1)-DIP(N)))
      ZU(N-1)=(A(N-1)*(RIU(N)-SUMU))/
     E(COS(D(N-1)+DIP(N))+COS(D(N-1)-DIP(N)))
      WRITE(6,13)ZD(N-1),ZU(N-1)
   13 FORMAT('0','ZD=',F6.3,'KM   ZU=',F6.3,'KM'//)
  100 CONTINUE
      STOP
      END
```

```
C    THE RAY TRACING PROGRAM.
      DIMENSION THETA(46),H(46),V(46),PHI(46),PPHI(46),UP(46)
      DIMENSION LABEL(10),FFDIST(300),FRTSUM(300),LABEL1(9),TITLE(2
      DIMENSION FDIST(300),RRTSUM(300),TTSUM(300),HH(46)
C  FDIST,RRTSUM,TTSUM ARE THE FINAL OUTPUT ARRAYS
      DIMENSION CHI(46),CCHI(46),ZETA(1),A(46),B(46),C(46)
      DIMENSION D(46),CC(46),DD(46),X(46),Y(46),XX(46),YY(46)
      DIMENSION FYY(1),PATH(46),TPATH(46),PPATH(46),TPPATH(46)
C NSURF IS THE NUMBER OF INTERFACES IN THE MODEL INCLUDING
C THE FREE SURFACE.OFFSET IS THE SHOT TO SHOT DISTANCE.
C THE CONVENIENT SYSTEM OF COORDINATES IS:POSITIVE X AXIS
C  POINTING DOWNWARDS AND POSITIVE Y AXIS POINTING AT THE
C  SHOT.THE ORIGIN IS AWAY FROM THE SHOT AT THE OTHER END
C  OF THE PROFILE.
C  IF THE SHALLOW PART OF AN INTERFACE IS UNDER THE SHOT
C  THE DIP ANGLE OF THE INTERFACE IS POSITIVE,OTHERWHISE
C  IT IS NEGATIVE.
C  SHOT=1.0 FOR THE RIGHT SIDE SHOT OF THE PROFILE.SHOT=-1.0
C  FOR THE LEFT SHOT.
   41 FORMAT(9A4)
      READ(5,12)TITLE
   12 FORMAT(2A4)
      READ(5,3)NSURF,OFFSET,RVEL,SHOT
      READ(5,47)LABEL
   47 FORMAT(10A4)
      READ(5,41)LABEL1
C  ONE INCH IS TEN KM IN THE RAY PLOT
      SCALE=10.0
C  LEFT SIDE DEPTHS,HH USED ONLY FOR PLOTING THE MODEL
    3 FORMAT(I3,3F7.2)
      READ(5,331)(THETA(J),J=1,17)
      READ(5,331)(V(I),I=1,17)
      READ(5,331)(UP(IE),IE=1,17)
      READ(5,331)(H(IT),IT=1,17)
      READ(5,331)(HH(ITR),ITR=1,17)
  331 FORMAT(17F5.2)
C CONVERT THE DIP ANGLES THETA TO RADIANS
      DO 2 NX=1,17
      THETA(NX)=THETA(NX)*0.017453
    2 CONTINUE
      CALL PLOTS
C  PLOT THE MODEL
      CALL PLOT(2.0,7.5,-3)
      CALL PLOT(0.0,-6.0,2)
      CALL PLOT(0.0,0.0,3)
      CALL PLOT(OFFSET/SCALE,0.0,3)
      CALL PLOT(OFFSET/SCALE,-6.0,2)
      CALL PLOT(0.0,0.0,3)
      CALL SYMBOL(6.7,0.7,0.4,LABEL1,0.0,36)
      CALL SYMBOL(9.5,-6.1,0.4,TITLE,0.0,8)
      CALL AXIS2(0.0,0.0,'DEPTH IN KM',-11,5.5,270.0,0.0,10.,1.00)
      CALL AXIS2(OFFSET/SCALE,0.0,' ',0,5.5,270.0,0.0,10.,1.00)
      CALL PLOT(0.0,0.0,3)
C  LINE A
      DO 600 IB=2,9
```

```
      IF(IB.EQ.6)GO TO 600
      IF(IB.EQ.7)GO TO 600
      CALL PLOT(OFFSET/SCALE,0.0,2)
      CALL PLOT(OFFSET/SCALE,-(UP(IB)/SCALE),3)
      CALL PLOT(0.0,-(HH(IB)/SCALE),2)
      CALL PLOT(0.0,0.0,3)
  600 CONTINUE
      CALL PLOT(OFFSET/SCALE,0.0,2)
      CALL PLOT(OFFSET/SCALE,-(UP(12)/SCALE),3)
      CALL PLOT(0.0,-(HH(12)/SCALE),2)
      CALL PLOT(0.0,0.0,3)
      CALL PLOT(OFFSET/SCALE,0.0,2)
      CALL PLOT(OFFSET/SCALE,-(UP(17)/SCALE),3)
      CALL PLOT(0.0,-(HH(17)/SCALE),2)
      CALL PLOT(0.0,0.0,3)
      IF(SHOT.LT.0.)CALL PLOT(OFFSET/SCALE,0.0,-3)
C PLOT THE TRAVELTIME FRAME
      CALL PLOT(0.5,9.0,-3)
      CALL AXIS(0.0,0.0,'DISTANCE IN KM',-14,8.0,270.0,
     E0.0,37.5)
C FOR THE DOWNDIP SOURCE MAKE  THE T AXIS FOUR INCHES LONGER
      CALL AXIS(0.0,0.0,'TIME IN SEC',11,8.5,0.0,0.0,1.5)
      CALL SYMBOL(1.5,0.5,0.14,LABEL,0.0,40)
      N1=4
      N2=NSURF
  301 CONTINUE
      DO 900 N=N1,N2
      IF(N.EQ.6)GO TO 900
      IF(N.EQ.7)GO TO 900
C FACTOR CONTROLS THE DENSITY OF THE TRACING.FOR N=4
C YOU NEED HIGH DENSITY.FOR THE OTHER INTERFACES THE
C DENSITY IS LOWERED.
      FACTOR=0.20
      IF(N.NE.4)FACTOR=0.3
      IF(N.EQ.17.)FACTOR=0.4
      WRITE (6,44)N,LABEL
   44 FORMAT(' ','INTERFACE',I5,9A4/)
   45 FORMAT(' ','          OFFSET    REDTIME   TIME'/)
   49 FORMAT(' ','           KM        SEC       SEC'/)
      X(1)=0.0
      Y(1)=OFFSET
      A(1)=0.0
      B(1)=0.0
      C(1)=0.0
      D(1)=0.0
C DEFINE THE EQUATIONS OF THE INTERFACES.
C NOTICE THAT EVEN IF THE INTERFACE IS NOT PLOTTED IN THE
C RAY DIAGRAM,OR THE TRAVEL TIME PLOT, THE CORRESPONDING LAYER
C IS TAKEN INTO PROPER ACCOUNT IN THE CALCULATIONS.
      DO 1000 I=2,N
      A(I)=-(1/TAN(THETA(I)))
      B(I)=OFFSET+(H(I)/TAN(THETA(I)))
 1000 CONTINUE
C CALCULATE THE MINIMUM TAKEOFF ANGLE ZETA(1) MEASURED WITH
C RESPECT TO THE VERTICAL TO THE FREE SURFACE.
C THE CALCULATION IS NEEDED IN ORDER TO AVOID ANY UNDEFINED
C ANGLES ALONG THE PATH OF THE RAY.
      DO 444 IVXX=2,10
      RATIO=V(N-IVXX)/V(N-IVXX+1)
      WRITE(6,778)V(N-IVXX),V(N-IVXX+1),RATIO
```

```
  778 FORMAT(3F6.2)
      IF(RATIO.LT.1.) GO TO 314
  444 CONTINUE
  314 CONTINUE
      ANGLE=ARSIN(RATIO)
      WRITE(6,688)IVXX
  688 FORMAT(I5)
      DO 333 IAEK=1,50
      IF(N.NE.8) GO TO 894
      ANGLE=ANGLE+ABS(THETA(N-IVXX+1-IAEK))-ABS(THETA(N-IVXX
     D+2-IAEK))
      GO TO 895
  894 ANGLE=ANGLE+(THETA(N-IVXX+1-IAEK))-(THETA(N-IVXX+2-IAEK))
  895 ANGLE=ARSIN(SIN(ANGLE)*V(N-IVXX-IAEK)/V(N-IVXX+1-IAEK))
      IF((N-IVXX-IAEK).EQ.1)GO TO 278
  333 CONTINUE
  278 ZETA(1)=90.15*0.01745-ANGLE+THETA(2)
      TEST1=ZETA(1)*57.296
      WRITE(6,8)TEST1
      ZETA(1)=ZETA(1)-(FACTOR*0.01745)
      WRITE(6,45)
      WRITE(6,49)
    8 FORMAT(' ','ZETA(1) IS',F7.2,' DEGREES'/)
      IR=0
      DO 100 JJ=1,285
      ZETA(1)=ZETA(1)+(FACTOR*0.01745)
      TEST=ZETA(1)*57.296
C     WRITE(6,26)TEST
      IF(TEST.GE.90.)GO TO 999
  26  FORMAT(F7.3)
C DEFINE THE PAIRS OF REFLECTION AND REFRACTION ANGLES
C     (PHI,CHI),(PPHI,CCHI)  BY USE OF SNELL'S LAW.
      PHI(1)=90.*0.01745-ZETA(1)+THETA(2)
      CHI(1)=ARSIN(SIN(PHI(1))*V(2)/V(1))
      INDEX1=N-1
      DO 220 K=2,INDEX1
      PHI(K)=CHI(K-1)+THETA(K+1)-THETA(K)
C  AVOID CHI(N-1) WHICH IS NOT DEFINED FOR OVERCRITICAL
C  PHI(N-1).SINCE ZETA(1) IS CALCULATED,ONLY PHI(N-1)
C  IS ALLOWED TO BE OVERCRITICAL.
C  THERE IS NO OVERCRITICAL ANGLE FOR A RAY INDIDENT AT THE
C  TOP OF A LVZ
      IF(K.EQ.INDEX1)GO TO 220
      CHI(K)=ARSIN(SIN(PHI(K))*V(K+1)/V(K))
  220 CONTINUE
      PPHI(INDEX1)=PHI(INDEX1)
      L=N
      INDEX2=N-2
      DO 320 KK=1,INDEX2
      L=L-1
      CCHI(L-1)=PPHI(L)+THETA(L+1)-THETA(L)
      PPHI(L-1)=ARSIN(SIN(CCHI(L-1))*V(L-1)/V(L))
  320 CONTINUE
C DEFINE THE EQUATIONS OF THE INCIDENT AND REFLECTED RAYS
C   C,D ARE FOR THE INCIDENT, CC,DD FOR THE REFLECTED RAYS.
C   ALSO CALCULATE THE COORDINATES OF THE POINTS AT WHICH
C   THE INCIDENT AND REFLECTED RAYS INTERSECT THE INTERFACES.
C   BY SOLVING THE SYSTEM OF THE LINEAR EQUATIONS.
      C(2)=(-1)*(1/TAN(ZETA(1)))
      D(2)=OFFSET
```

```
      X(2)=(B(2)-D(2))/(C(2)-A(2))
     .Y(2)=(C(2)*B(2)-(A(2)*D(2)))/(C(2)-A(2))
      DO 420 LM=3,N
      C(LM)=-(1/TAN(90.*0.01745-CHI(LM-2)+THETA(LM-1)))
      D(LM)=Y(LM-1)+(X(LM-1)*TAN(CHI(LM-2)-THETA(LM-1)))
      X(LM)=(B(LM)-D(LM))/(C(LM)-A(LM))
      Y(LM)=(C(LM)*B(LM)-(A(LM)*D(LM)))/(C(LM)-A(LM))
  420 CONTINUE
      LL=N
      INDEX1=N-1
      XX(N)=X(N)
      YY(N)=Y(N)
      DO 50 M=1,INDEX1
      LL=LL-1
      CC(LL)=TAN(PPHI(LL)+THETA(LL+1))
      DD(LL)=YY(LL+1)-(XX(LL+1)*TAN(PPHI(LL)+THETA(LL+1)))
      IF(LL.EQ.1)GO TO 50
      XX(LL)=(B(LL)-DD(LL))/(CC(LL)-A(LL))
      YY(LL)=(CC(LL)*B(LL)-(A(LL)*DD(LL)))/(CC(LL)-A(LL))
   50 CONTINUE
      XX(1)=0.0
      YY(1)=DD(1)
C  FYY IS THE OFFSET OF THE RAY WITH TAKEOFF ANGLE ZETA(1)
C  THE LAST REFLECTING HORIZON OF THE RAY IS INTERFACE N
C  FDIST HAS TO BE AN ARRAY .ALSO RRTSUM,TTSUM
      FYY(1)=OFFSET-YY(1)
C  INCREASE ZETA(1) TO DECREASE THE OFFSET
      IF(ABS(FYY(1)).GT.OFFSET)GO TO 100
      IF(FYY(1).LT.0.)GO TO 999
      IR=IR+1
      FDIST(IR)=FYY(1)
C  CALCULATE THE TRAVEL TIME OF THE RAY
      INDEX1=N-1
      DO 60 NA=1,INDEX1
      PATH(NA)=SQRT((X(NA+1)-X(NA))**2+(Y(NA+1)-Y(NA))**2)
      TPATH(NA)=PATH(NA)/V(NA)
   60 CONTINUE
      DO 70 NN=1,INDEX1
      PPATH(NN)=SQRT((XX(NN+1)-XX(NN))**2+(YY(NN+1)-YY(NN))**2)
      TPPATH(NN)=PPATH(NN)/V(NN)
   70 CONTINUE
      TSUM=0.0
      DO 80 IP=1,INDEX1
      TSUM=TSUM+TPATH(IP)+TPPATH(IP)
      TTSUM(IR)=TSUM
   80 CONTINUE
      RTSUM=TSUM-(FYY(1)/RVEL)
      RRTSUM(IR)=RTSUM
      CONST=1.0*0.01745
C  FIND OUT THE CRITICAL OFFSET OF THE HORIZON N
      IF(V(N-1).GT.V(N))GO TO 19
      IF(ABS(PHI(N-1)-ARSIN(V(N-1)/V(N))).LE.CONST)GO TO 52
   19 WRITE(6,22)FYY(1),RTSUM,TSUM
   22 FORMAT('             ',3F7.2)
      GO TO 66
   52 WRITE(6,23)FYY(1),RTSUM,TSUM
   23 FORMAT('CRITICAL',3F7.2)
   66 CONTINUE
   77 FORMAT('0','NUMBER OF RAYS TRACED',I5//)
C  PLOT THE RAYS
```

```
      CALL PLOT(SHOT*OFFSET/SCALE,0.0,3)
      DO 601 IA=2,N
      CALL PLOT(SHOT*Y(IA)/SCALE,-X(IA)/SCALE,2)
  601 CONTINUE
      LX=N
      DO 602 ID=1,INDEX1
      LX=LX-1
      CALL PLOT(SHOT*YY(LX)/SCALE,-XX(LX)/SCALE,2)
  602 CONTINUE
  100 CONTINUE
  999 CONTINUE
      WRITE(6,77)IR
      DO 800 IL=1,IR
      FFDIST(IL)=FDIST(IR-IL+1)
  800 CONTINUE
      DO 801 ILL=1,IR
      FRTSUM(ILL)=RRTSUM(IR-ILL+1)
  801 CONTINUE
      FFDIST(IR+1)=0.0
      FFDIST(IR+2)=-37.5
      FRTSUM(IR+1)=0.0
      FRTSUM(IR+2)=1.5
      CALL LINE(FRTSUM,FFDIST,IR,1,0,0)
  900 CONTINUE
      CALL PLOT(0.0,0.0,999)
      STOP
      END
```